Spatial Control of Ligand Presentation on Biomaterial Surfaces

by

Gillian L. Brown

S.B., Materials Science and Engineering
Massachusetts Institute of Technology, 1988

M.S., Materials Science and Engineering
University of California, Berkeley, 1991

Submitted to the Department of Materials Science and Engineering
in partial fulfillment of the requirements for the degree of

Doctor of Philosophy

at the

Massachusetts Institute of Technology

May, 1999

Signature of Author.....
Department of Materials Science and Engineering
April 30, 1999

Certified by.....
Linda G. Griffith
Associate Professor of Chemical Engineering
Thesis Supervisor

Certified by.....
Michael F. Rubner
Professor of Materials Science and Engineering
Thesis Reader

Certified by.....
Linn Hobbs
Chairman, Departmental Committee on Graduate Students

SPATIAL CONTROL OF LIGAND PRESENTATION ON BIOMATERIAL SURFACES

by

Gillian L. Brown

Submitted to the Department of Materials Science and Engineering on April 30, 1999
in partial fulfillment of the requirements for the degree of
Doctor of Philosophy in Materials Science and Engineering

Abstract

Adhesion of many cell types to the extracellular matrix or to synthetic bioactive surfaces is mediated by transmembrane integrin receptors. Integrin clustering is believed to be closely associated with focal contact formation and signaling, as assessed by the behavior of cells on surfaces presenting relatively uniform ligand distributions. It has therefore been hypothesized that controlled clustering of *2, 3.....n* integrins might be achieved by controlling the spatial distribution of adhesion ligands on biomaterial surfaces.

Substrates were prepared on which cell-surface interactions are controlled by modifying non-adhesive poly(ethylene oxide) (PEO) hydrogels with the minimal cell-adhesion peptide sequence GRGDY (RGD). The peptide is tethered to the hydrogel surfaces via star PEO molecules, producing surfaces on which the ligands are presented to cells in "clusters", or domains of high concentration. The substrates are compared with others on which the RGD peptide is uniformly distributed. Control of the RGD cluster size was achieved by varying the relative concentrations of reactants in solution. The binding of RGD-modified stars to surfaces was found to be a non-linear function of its concentration in solution and degree of modification, and is reasonably explained by a Langmuir model of competitive adsorption.

Quantitative techniques for visualizing the ligand distribution on the surface were developed, and indicated that surfaces to which ligands had been tethered via star molecules showed a significant deviation from normal, random distribution. Thus, control of the ligand spatial distribution was achieved. In addition, preliminary biological testing suggests that substrates on which adhesion ligands are presented to cells in a clustered format produces more physiological behaviour than those on which ligands are uniformly distributed *at the same average ligand density.*

Thus, we have fabricated surfaces which, because of their resistance to non-specific cell interactions and the control of specific interactions at the molecular level, can serve as a model for artificial matrix development and can be used for fundamental *in vitro* studies.

Thesis supervisor: Linda G. Griffith
Title: Associate Professor of Chemical Engineering

This thesis is dedicated

to the memory of my grandmother

Minna Louise Dexter (1906-1995)

I miss you and think about you every day

Acknowledgments

Before I take my leave of MIT for the last time, I wish to express my deep appreciation to several people and organizations whose contributions were invaluable as I worked on my thesis. First, I am grateful to my thesis advisor, Professor Linda Griffith, for her support and guidance throughout my thesis research, especially towards the end, in the writing of this document. I would like to thank my thesis committee, Professors Rubner, Mayes and Laibinis, whose insight at key moments in my research truly helped to direct my thinking. I also consider myself very fortunate to have been a member of the Griffith/Lauffenburger research group, which was a stimulating and fun place to be for four years. In particular, the many biology discussions with Gargi Maheshwari and chemistry discussions with Jeff Sperinde were very helpful and greatly appreciated.

Many thanks to the following individuals and organizations, whose assistance was crucial in the completion of this work: Patricia Reilly (Department of Biology), Yuan Lu (McKay Characterization Facility, Harvard University), Catherine Bambenek and Professor Edwin Thomas (Department of Materials Science and Engineering), Dr. Kenneth Wright (High Voltage Research Lab, MIT), Seok-Won Lee and Diane Rintzler Yen (Department of Chemical Engineering) and Digital Instruments, who provided Atomic Force Microscopy training. The assistance of two very talented undergraduates, Carmen Patrick and Julie Ji was also essential for the completion of the project.

I wish to thank several individuals at Corning Incorporated, whose moral and financial support. My former managers, Joe Antos and Rob Vandewoestine patiently provided financial support while I worked on this Ph.D., for which I am extremely grateful. I am also deeply indebted to Mark Taylor and Keith Horn, who provided funding for my research in response to my pleas for help when I was having difficulty in finding a suitable project. Finally, I am very appreciative of the many career-planning discussions with David Root, Mark Taylor and Tyrone Mitchell.

Thanks also to the many friends, especially Toni King, Michelle Johnson, Deborah-Anne Spence, the Clarke family, Michael Owu and John Ofori-Tenkorang, who made themselves available when I needed an escape, and were very understanding during the times when I failed to return phone calls and e-mail messages. My family in Kingston, Jamaica has always provided encouragement and a listening ear; of course I cannot begin to thank you for the countless things you've done for me over the years. And finally, my deepest gratitude goes to my best friend, Steven Isabelle, whose daily doses of "tough love" proved truly motivational, especially while I struggled to finish this work.

TABLE OF CONTENTS

CHAPTER 1. INTRODUCTION

1.1 Background

Biomaterials may be defined as "substances other than food or drugs contained in therapeutic or diagnostic systems that are in contact with tissue or biological fluids" [1]. Their uses are many and varied, including *in vitro* (for example, tissue culture substrates and diagnostic products), *in vivo* (for example, contact lenses, hard and soft tissue replacements and drug delivery materials) and *ex vivo* (for example, kidney dialysis machines) applications. Regardless of the application, however, it is the surface of the biomaterial which first comes into contact with blood or other biological media, and to a large degree, the ability of those media to take advantage of the properties of the material without eliciting an unfavourable response, or its "biocompatibility" [2], is very strongly dependent on the surface properties of the material.

Most existing materials do not have both the bulk (mechanical) properties and the surface properties required to make them suitable for biomaterials applications. The materials used in such applications are often selected for their mechanical properties, and then subjected to a surface treatment to make them biocompatible. Earlier approaches to implantable biomaterials design involved the selection of a material not originally intended for use in a biological environment, but which appeared to have the desired mechanical properties. These materials were used on a trial-and-error basis, sometimes with catastrophic results. The implantation of such unmodified materials typically induces non-specific adsorption of the proteins present in biological fluids (note that there are over 200 proteins present in blood plasma), in a distribution of conformations and orientations. Thus, a wide variety of cellular attachment processes may be induced, depending on which proteins are adsorbed, and in which conformations [3]. The cell or tissue response to the biomaterial is therefore

characterized by non-specificity, slow kinetics and an unpredictable outcome to the interaction [2]. Biological interactions at these non-engineered fluid-biomaterial interfaces can introduce the complication of platelet deposition and clot formation at the interface; under the shear force of blood flow, these clots may detach from the surface of an implant, and may cause a stroke. Alternatively, the surface may become overgrown with connective tissue, due to the non-specificity of the interactions between the surface of the material and its biological environment. The non-specific nature of the interactions also impairs the ability to obtain the controlled cell growth and function crucial to *in vitro* culture systems. Modern approaches to biomaterials therefore require an increased understanding of cell-biopolymer-surface interactions, and how they can be manipulated to produce a desired outcome. This is achieved by combining principles from materials science, molecular cell biology, nanofabrication and surface science. The key to modern biomaterials design, then, is to engineer materials used in implants or tissue culture to ensure that, at the material surface, the cells of interest encounter precisely the environment they need in order to attach, grow and perform their specific functions.

1.2. Integrin Receptors and Adhesion to the Extracellular Matrix

The adhesion of cells to natural or synthetic surfaces is controlled by the recognition of specific molecules on the surface by transmembrane adhesion receptors at the surface of the cell. Adhesion is required for survival of most cell types, and the nature of the adhesive interaction mediates many important cell functions, including migration, growth and differentiation [4]. In living systems, cells tend to adhere to each other [5], or to the extracellular matrix (ECM), a complex, insoluble meshwork of polymers proteins and polysaccharides, secreted by cells, which fills the extracellular space [6], as can be seen in Figure 1.1 below.

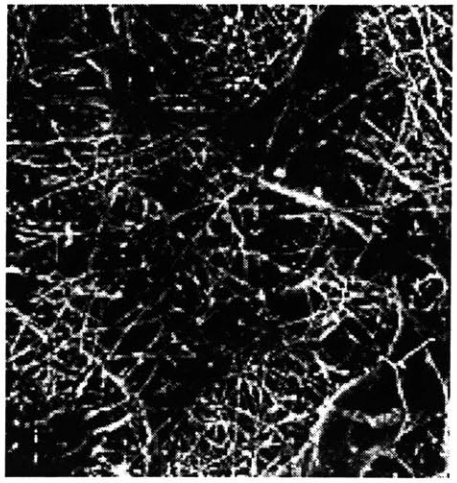

Figure 1.1: Scanning electron micrograph of fibroblasts (connective tissue cells) in extracellular matrix (Nishida et al. *Invest. Ophthalmol. Vis. Sci.* 29: 1887 (1988))

Several families of adhesion receptors have been identified. The best characterized are the integrins, which bind cells to specific extracellular matrix proteins, for example, fibronectin, fibrinogen and laminin, and also to other cells [7], [8]. Integrin receptors are "dimeric", they consist of two different glycoprotein chains (designated α and β). A schematic representation is given in Figure 1.2.

Adhesion of cells to synthetic materials takes place by the same mechanism as adhesion to the extracellular matrix, as it is mediated by extracellular matrix proteins at the surface. Fibronectin, for example, is a glycoprotein which is capable of participating in receptor-mediated adhesion processes via several binding domains [8]. When adsorbed on a synthetic surface, fibronectin mediates cell attachment through specific interactions with integrins.

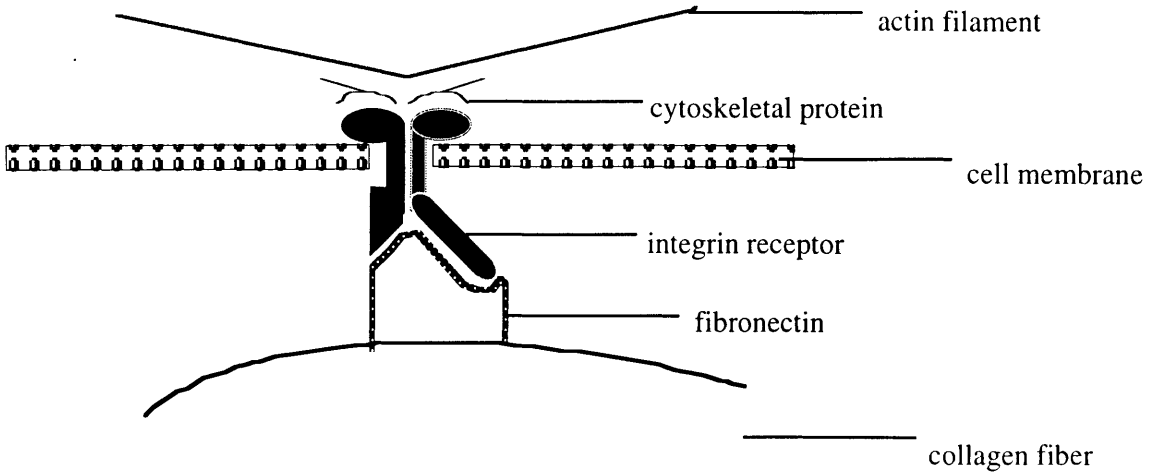

Figure 1.2 Anchoring of cells to ECM is mediated by integrins (Redrawn from [6]).

1.2.1 Binding of Integrins to ECM Protein Fragments

Rigorous study of integrin receptors and their ECM interactions has enabled the identification of the amino acid sequence of Arg-Gly-Asp (RGD), a common cell-attachment domain of fibronectin and several other matrix proteins [9]. [10], [11], [12]. Some of the proteins containing the RGD sequence are listed in Table 1.1 (from [13]).

The discovery has enabled many investigations of specific adhesive interactions between cells and synthetic surfaces. For example, Massia and Singer have studied the interactions between fibroblasts and RGD-containing peptides of 5 residues [14], or 15 residues [15].

Sequence	Protein	Cell type, function
RGDN	Laminin A	Endothelial, adhesion
RGDS	Fibronectin	Many cell types, adhesion
RGDV	Vitronectin	Many cell types, adhesion
RGD	Thrombospondin	Platelets, aggregation
RGDTP	Collagen	Fibroblasts, adhesion
FRGDS	Entactin	Mammary tumor cells

Table 1.1 RGD-containing sequences in ECM proteins (from [13])

Both found that RGD alone was sufficient to promote cell attachment and spreading. Massia and coworkers [16] have shown that the sequence Gly-Arg-Gly-Asp-Tyr, when grafted to glycophase glass substrates (usually non-adhesive), allowed cell attachment and spreading, but only at an inter-ligand spacing of 440 nm or lower, and the formation of focal contacts at a spacing of 140 nm. It therefore seems that not only are cell receptors able to recognize the presence or absence of the relevant ligands, but that they are also sensitive to the *density* of ligand present.

The affinity of RGD peptides for integrins is believed to be low relative to fibronectin: Hautanen [17] reported a difference of a factor of 10-1000. The peptide was found to be very specific in its action, however, similar peptides in which the RAD or RGE sequence was substituted for RGD showed negligible cell-binding activity. Ward and Hammer showed theoretically that in such cases the critical ligand density, above which focal contact formation occurs, is higher for the peptide of lower affinity [18], supported by the findings of Massia and Hubbell mentioned above [16].

1.2.2 Clustering of receptors improves adhesion and function

Many studies suggest that integrins provide more than a simple physical connection between the cell and its surroundings. For example, integrin receptors serve to bind anchorage-dependent cells to their support, but integrin clustering has been shown to be a crucial event in the development of strong adhesive contacts, known as focal contacts [19]. A focal contact is a region in which the cell approaches its substrate very closely (separation $\approx$ 15 nm), estimated at approximately 1 μm^2 in cross-sectional area [20]. Within the focal contact, clusters of integrins have been identified [19], closely associated with cytoskeletal proteins and other bioactive molecules. This phenomenon of receptor clustering is of great interest to cell biologists and tissue engineers, as it has been observed to be a key event in a variety of cell processes, accompanying such cell processes as receptor-mediated endocytosis, anchorage and signal trafficking.

Both mechanical and biochemical explanations for this clustering behaviour have been offered. It has been suggested [21] that the integrins first bind their extracellular ligands by molecular recognition processes, but remain bound to the substrate because of reorganization within the cytoskeleton, involving receptor clustering and assembly of stiff cytoskeletal structures which change the rheology of the cell. The formation of these improved load-bearing structures thereby increases the strength of adhesion, because applied stresses are distributed over a larger cross-section. That the cytoskeletal stiffening which accompanies focal contact formation is an integrin-specific response was shown by Wang et al., who used a model system to apply controlled mechanical stresses to specific cell surface receptors, and measured the resulting strains [22]. They suggested that integrins can act as mechanotransducers, transferring forces to the cytoskeleton which creates a series of intracellular mechanical signals and causes significant reorganization of

the cytoskeleton. Ezzell et al. [23] found that cells lacking the focal adhesion protein vinculin lack the mechanical stiffness that comes from actin stress fiber assembly and did not spread efficiently on fibronectin substrates, and concluded that vinculin serves as a mechanical link between the cytoplasmic domain of the integrin receptor and the actin network within focal contacts. Other experiments in which cell-cell and cell-surface adhesion were investigated indicate that integrin-ligand binding is also responsible for significant intracellular changes due to the transduction of biochemical signals from the matrix or surrounding cells, using processes similar to those used by growth factors [24]. Kornberg et al. [25] studied the behaviour of tyrosine, a non-integrin amino acid, during adhesion. They observed increased tyrosine phosphorylation, known to regulate a variety of metabolic pathways, in the 130 kDa protein pp130 when integrins were made to cluster by incubating human carcinoma cells with anti α_1 antibody followed by anti IgG. Later it was shown that 125^{fak}, a 125 kDa tyrosine kinase also showed an increase in tyrosine phosphorylation when cells were allowed to attach to fibronectin, laminin and collagen type IV, and that this protein was concentrated in focal contacts [26]. They suggested that ligand binding, followed by integrin clustering, induces the phosphorylation of tyrosine, which in turn mediates cell spreading.

1.3 Tissue Engineering

Tissue engineering is an emerging, interdisciplinary field, which combines biological and engineering principles towards the creation of biologically derived substitute tissues, designed to restore, maintain or improve existing tissue function. The field is very broad, and encompasses a variety of technologies from genetic engineering to hormone and growth factor development to the use of mechanical forces to affect cell behaviour. The aim of tissue engineering is to provide functioning tissue by removing of a small piece of healthy donor tissue, separating of that tissue into smaller groups of cells, attaching of

those cells to a supporting structure on which they may be cultured, and even modified *in vitro*, and finally implanting the cells, supported by the biocompatible support into the patient.

1.3.1 Bioactive Surfaces for Tissue Engineering

The field of tissue engineering relies heavily on the use of cell culture substrates for fundamental studies of all aspects of cell physiology. The precise characterization of cell behaviour on synthetic surfaces has traditionally been difficult, however, because of the "remodeling", or "fouling" of cell culture substrates by the cells under study; within hours cells are able to secrete a layer of protein which adsorbs to the surface, confounding the results of such studies. The development of synthetic substrates for *in vitro* cell and tissue culture, which target specific cells for attachment is essential to tissue engineering so that precise, well-defined biological responses can be achieved. One approach to the problem is to create a substrate which is inert towards protein adsorption, thus eliminating non-specific cell interactions, then immobilizing ligands which prompt highly specific interactions with cells, and therefore precise control of their behaviour.

Coating of substrates with a hydrophilic, non-ionic polymer, especially poly(ethylene oxide) (PEO) has been extensively investigated as a means of achieving a "bioinert" surface [27], [28], [29], while the hydroxyl chain ends of the polymer provide sites for the immobilization of the appropriate ligands. In many fundamental studies of cell adhesion, the fibronectin fragment RGD, rather than the entire fibronectin molecule is used, due mainly to their robustness and simplicity of structure compared with fibronectin.

1.4 Hypothesis

Using the PEO-RGD system, it has been shown that cells bind specifically to RGD via their integrin receptors, and in a density-dependent fashion [30], [31]. For tissue engineering applications, however, we are interested in the optimization of a cell's response to RGD, or to other ligands, and in using this insight in tissue engineering. We hypothesize that if we can control not only the surface density, but also the spatial organization of ligands, we can achieve control over receptor clustering, and ultimately achieve improved control over such aspects of cell behaviour as adhesion, migration, differentiation and proliferation. To facilitate this, we have designed, fabricated and tested a series of surfaces, on which the ligands to which receptors may bind are presented to the cells in a spatially controlled fashion where cluster sizes and spacings can be varied over a wide range of values.

The two surfaces represented in Figure 1.3 have same overall surface density of adhesion ligands. Using surfaces such as those in the figure, the effects of spatial distribution on adhesion and focal contact formation may be examined at constant surface density.

The direct application of this research is the development of improved cell culture substrates. The insight obtained from this research will be applied towards the design of coatings for the petri dishes to be used in *in vitro* cell and tissue culture. Experimental evidence of the ability to control cell behaviour via clustered ligand surfaces may mean that it is not necessary to coat cell culture substrates with a uniformly high density of RGD peptide, as was done by Massia [16], but rather that it is possible to create surfaces on which RGD is immobilized in domains of high concentration, thereby using lower amounts of RGD per substrate. In addition, the clustering of adhesion ligands in this was may enable us to observe new physiological behaviours, previously inaccessible because of a

lack of control of cell function. For example, presenting RGD ligands to cells in high-density clusters may result in previously unseen levels of receptor occupancy, which result in changes in adhesion, migration and cytoskeletal organization.

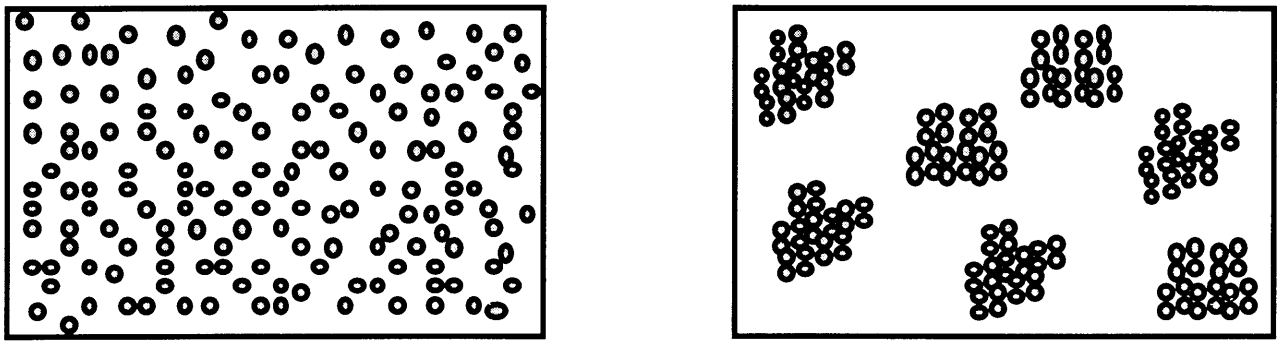

Figure 1.3: Schematic representation of intended ligand distributions on RGD surfaces. (i) evenly distributed ligands (ii) clustered ligands

1.5 Objectives

The first objective of this thesis was the creation of a system of model surfaces for use in fundamental studies of cell behaviour. In particular, surfaces on which ligands are distributed in aggregates of 1 nm to 50 nm in size (corresponding to clusters containing between 1 and 10 ligands) with spacings of 20 nm to 500 nm between clusters, are expected to span the range of conditions, from poorly cell-adhesive to highly adhesive. Testing the hypothesis required extensive work in preparing and characterizing model surfaces with known properties. The model surfaces used in this study presented clusters of adhesion ligands against a protein-resistant background. A single type of adhesion ligand, a pentapeptide containing the RGD sequence, was presented by the surface which

interacted with specific cell-surface receptors, to simplify the interpretation of cell adhesion studies.

The cells used for the biological testing of these surfaces are NR6 cells, a fibroblast cell line. It is estimated that there are approximately 100 integrin receptors per μm^2 in contact with the surface. The RGD-binding domain of the integrin receptor is estimated to be approximately 15 nm in diameter, however the number of integrins present in a focal contact, and indeed the dimensions of a focal contact are unknown. It is therefore difficult to estimate *a priori* the number of ligands that will be required per cluster, hence surfaces having a broad range of cluster sizes, spacings and average surface densities were prepared and tested.

While the diameter of a ligand cluster is on the order of 30 nm (see Chapter 4), the size of a focal contact has been speculated to be on the order of 1 μm^2. Hence, while focal contacts may be imaged by optical microscopy of stained specimens, visualization of PEO molecules linked with RGD ligands requires techniques which afford higher resolution, in particular electron microscopy. Thus, the second contribution from this thesis was the development of characterization techniques which could be used to visualize ligand distribution at this scale.

1.6 Overview of the thesis

The approach taken in this work is to begin with substrates which completely resist non-specific cell and protein attachment, and then to provide sites for specific interaction by tethering a peptide containing the minimal adhesive sequence Arg-Gly-Asp to these substrates. In order to achieve the desired spatial control, ligands are tethered to this

substrate via star poly(ethylene oxide) molecules. Star molecules are highly branched, each molecule having several arms emanating from a central core, which affords us a high density of chain ends per molecule, and therefore a high local ligand density when used as a tether. Thus, one novel achievement of this project is the molecular-level control of RGD cluster size; variation in the number of arms modified per star molecule has, in this case yielded clusters containing from 1 to 10 RGD molecules. The diameter of the RGD "islands" is therefore roughly 30 nm. To our knowledge, no one has yet prepared a bioactive surface on which ligand domains are so small; most work cited in the literature describes preparation of RGD domains on the order of several microns in size, or approximately the size of a focal contact [20]. Because we would like to be able to manipulate adhesion and focal contact formation at the molecular level, we are using star molecules as tethers, rather than creating our RGD domains by lithographic techniques. This approach is also unique because of the time scale of the experiment, and because of the size of the RGD domains. We imposed the requirement that substrates should be cell resistant for at least 24 hours, whereas experiments of this sort are typically carried out for 2-4 hours [32], [14], [15].

Chapter 2 of this thesis examines many of the conventional synthetic routes to preparing a "bioinert" surface, and the failure of typical surfaces, prepared by covalent grafting of PEO, to resist non-specific attachment of cells under the experimental conditions required for this thesis. The preparation of a crosslinked PEO hydrogel which meets our requirements in terms of non-adhesiveness to a variety of cell types, is described in Chapter 3. Chapter 4 details the chosen synthetic route to clustered ligand surfaces, and the quantitative characterization of the prepared surfaces. Chapter 5 contains descriptions of the ligand visualization techniques employed, their limitations and the results obtained. Chapter 6 outlines a number of cell studies which were performed, demonstrating the

validity of the central hypothesis. Finally, Chapter 7 summarizes the accomplishments of the thesis and makes some recommendations for future research.

CHAPTER 2. GRAFTED PEO SUBSTRATES AND THEIR ADHESION RESISTANCE

2.1 Background

PEO has generated a great deal of interest in the biomaterials field, due to its unique physical and chemical properties. Surfaces to which PEO has been physically or chemically attached generally exhibit significantly reduced adsorption of proteins and thus resist cell adhesion [33]. The protein-repelling nature of PEO has been attributed to excluded volume effects [34], its strong enthalpic interactions with water [35], and its high water solubility and low interfacial energy [33].

The literature on creating cell- and protein-resistant surfaces with PEO is relatively substantial. In some key studies, summarized in Tables 2.1 and 2.2, a variety of substrates, protein adsorbates and concentrations, cell types and experimental conditions are used. It is therefore difficult to compare the results of these experiments, and further, to generalize those results such that specific rules can be laid down regarding the preparation of a surface which is "bioinert" to any particular cell type, or one which is universally cell- and protein resistant for the desired period of time.

Theoretical models have been used extensively to predict the PEO coverage required for optimum protein resistance [36], [37], [38]. When PEO chains are end-grafted to a surface, the most common mode of preparation, it is generally agreed that the adsorption resistance of a surface increases with increasing PEO density on the surface, where density is modulated by both the number and the length of the chains. However, there are many other factors which may affect the performance of a

TABLE 2.1: SUMMARY OF PROTEIN ADSORPTION STUDIES

PEO SURFACE	AUTHOR	PROTEIN	CONC. (mg/ml)	TIME (hr)	TEMP. (C)	% REDUCTION vs. CONTROLS
BLOCK COPOLYMER:						
(i) on glass beads	Maechlin-Strasser, 1989	Fibrinogen	0.05	4	25	95 -98
(ii) on LDPE	Lee, 1989	Albumin	1	0.5	25	40 - 60
(iii) on glass tubes	Mc Pherson, 1995, 1998	Fibrinogen,	0.1	1	25	96
		Lysozyme	0.15	1	25	90
(iv) pyrolytic carbon,	McPherson, 1997	Fibrinogen	0.1	1	25	34
nitinol		Fibrinogen	0.1	1	25	88
COVALENTLY GRAFTED:						
(i) on PET	Gombotz, 1991	Fibrinogen,	0.2	2	37	80-85
		Albumin	0.2	2	37	
(ii) on silicon	Sofia, 1998	Fibronectin,	0.1	24	25	100
		Albumin,	2	24	25	100
		Cytochrome-*c*	2	24	25	50
(iii) on PS beads	Van Delden, 1996	Albumin	12.5	1	37	85
		Plasma	90%	1	37	40
SELF-ASSEMBLED MONOLAYERS:						
(i) on gold/silicon	Prime, 1993	Fibrinogen	1	2	25	100
		Lysozyme	1	2	25	100
		Pyruvate kinase	1	2	4, 25, 37	100
		RNAse A	1	2	25	100
(ii) on silicon	Zhang, 1998	Albumin,	2	2	37	75
		Fibrionogen,	2	2	37	80
		IgG	2	2	37	65

TABLE 2.2: SUMMARY OF CELL ADHESION STUDIES

PEO SURFACE	AUTHOR	CELL TYPE	TIME	% REDUCTION vs. CONTROLS
BLOCK COPOLYMER:				
(i) on glass, nitinol, pyrolytic carbon	McPherson, 1997	Human Platelets/Plasma	1 hour	100% (glass), > 90% (nitinol), > 50 % (PC)
COVALENTLY GRAFTED:				
(i) on PET	Desai, 1991	Fibroblasts/serum	up to 26.4 days	80-95
		Platelets/whole blood	10 min	85-90
(ii) on LDPE	Lee, 1997	Platelets/plasma	30 min	50-90
(iii) on glass	Tseng, 1992	Platelets/plasma	1 hour	95
SELF-ASSEMBLED MONOLAYERS:				
(i) on silicon	Zhang, 1998	Fibroblasts/serum	5 hours	50
		Epithelial/serum	5 hours	60
(ii) on Au/silicon	Singhvi, 1994	Hepatocytes/serum-free	24 hours	100
	Chen, 1998	Endothelial/serum	24 hours	100

specific substrate. For example, Gombotz et al [27] observed a reduction in adsorption of protein with increasing buffer ionic strength (and with increasing PEO molecular weight), from which they inferred that the interaction between protein and substrate may be ionic in nature. In addition, using grafted PEO surfaces, Van Delden et al. [39] achieved an 85% reduction in adsorption of a single protein relative to unmodified controls (after one hour); however, in a solution containing a variety of proteins at high concentrations, a reduction in adsorption of less than 40% was achieved. This, they suggested, was evidence that PEO surfaces are not generally "protein resistant"; the complexity of the protein adsorption process requires that both the *concentration* of each protein and its *affinity* for the surface be taken into account.

The studies outlined in Tables 2.1 and 2.2, therefore, cannot easily be generalized to recommend a *specific* PEO surface suitable for the requirements of this thesis. Most of the investigations described above were of relatively short duration (2 - 4 hours), and showed significant reduction, but not elimination of cell adhesion. For our studies, however, the complete elimination of non-specific cell-substrate interactions was desired, so that specific receptor-ligand interactions could be studied quantitatively. While non-specific cell attachment at up to 5 to 15% confluency, as typically seen on control substrates [40], may be perfectly acceptable for biomaterials for *in vivo* applications, the quantitative *in vitro* studies planned in this investigation impose far more restrictive constraints.

2.2 Experimental Design

The preparation of a substrate able to completely resist non-specific cell and protein interactions for at least 24 hours was considered a key requirement for this thesis. One approach which has been taken by several investigators is to suppress endogenous protein secretion, using such inhibitors as cycloheximide [41], [42] and emetine [43]. This

solution was deemed inappropriate for our investigation for the following reasons. First, there have been concerns expressed [43] regarding the ability to of cells to replace those receptors damaged by the trypsinization process, when protein secretion is prevented. Second, many such inhibitors are toxic to cells; while their effects may not be seen during 1 - 2 hour experiment, an experiment conducted over a 24 hour period would almost certainly be confounded by their adverse effects.

Results of both theoretical [38] and experimental [44] studies indicate that the cell-resistance of a PEO-modified surface increases with increasing PEO density on the surface, where the attainable density is affected by the length of the PEO chains. The simplest routes to preparing PEO-rich surfaces are formation of a PEO brush via chemical grafting or adsorption of amphiphilic molecules. Despite the reported excellent performance of adsorbed PEO-bearing molecules, such as PEG-alkanethiols on gold [29] or PEO-containing block copolymers [31], we limited our investigation to chemical grafting approaches for the following reasons. First, concerns have been expressed regarding the stability of adsorbed coatings in aqueous environments. For this project especially, it has been observed that the attachment of ligands to adsorbed block copolymers via a high molecular weight PEO tether renders the copolymer molecules soluble, allowing them to detach from the surface (unpublished data). Second, it is known that cells exert a contractile force on their substrate via their adhesion receptors. The extent to which cells may disrupt an adsorbed coating is unclear; to eliminate concerns about the possibility of the coating's integrity being compromised by cells, it was therefore considered best to prepare substrates on which the PEO was covalently attached.

The objective of this investigation was to determine whether a PEO surface which met our requirements of complete cell resistance for 24 hours could be achieved by standard covalent grafting techniques. Studies of the effects of PEO molecular weight and

architecture on adhesion of different cell types were undertaken, using previous results from the literature as a guide to the best approaches. The PEO architectures investigated are depicted in Figure 2.1. To observe the effects of PEO molecular weight on adhesion resistance, linear PEGs of two different molecular weights (3,000 and 20,000) were grafted to glass substrates. Desai et al. [45] found an improvement in the protein-repelling ability of grafted PEO surfaces with increasing PEG molecular weight up to 18,500 Daltons. They suggested that at a molecular weight of 18,500, an optimum chain length is achieved: polymer molecules are long enough to provide effective surface coverage, yet small enough to have appreciable diffusivities and chain end reactivities in the coupling solution, so that sufficient grafting densities may be obtained.

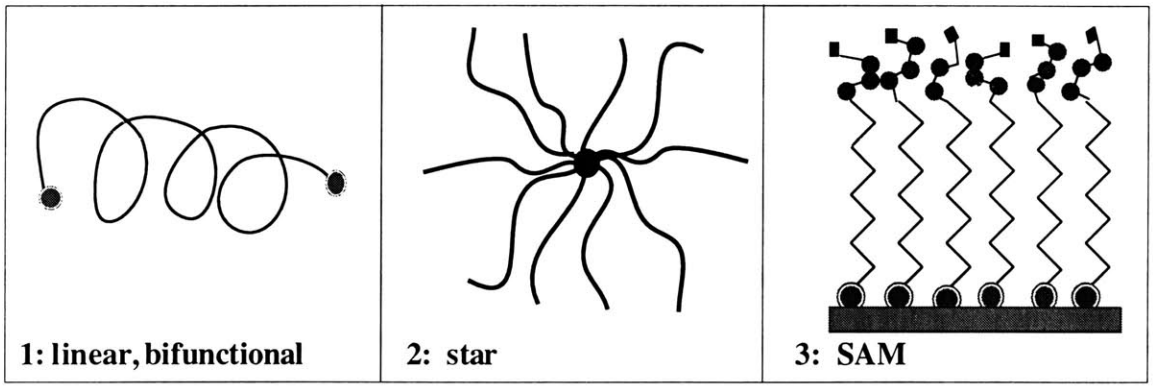

Figure 2.1 PEO architectures used in cell adhesion experiments

To observe the effect of PEO segment density on cell resistance, star PEO coatings and oligo(ethylene oxide) (OEO)-terminated self-assembled monolayers (SAMs) were also prepared. Star polymers have highly branched molecules with several arms emanating from a central multifunctional core. Because of the joining of the arms at the centre of the molecule, the segment density in the core region is very high and decreases radially outward, to the density of a single, linear arm at the surface of the molecule [46]. Star

molecules have therefore been investigated as a means of increasing polymer segment densities above those achievable using linear molecules. Irvine et al. examined the structure of star and linear PEO grafted surfaces using neutron reflectivity [47], and found that grafted star polymers achieved the swollen layer thicknesses and volume fraction maxima that were the same as or higher than those seen in comparable linear systems, but were achieved at significantly lower graft densities. However, Irvine [47] and Sofia [48] have both reported that star PEO layers allow the adsorption of relatively small protein molecules, where grafted linear PEO layers do not.

OEO-terminated SAMs are believed to present a dense, but disordered OEO surface to cells and proteins in solution, forming a close-packed layer on substrates because of hydrophobic interactions between the alkyl chains [49]. Such SAMs have been shown, by ellipsometry and by *in situ* surface plasmon resonance to effectively resist the adsorption of certain model proteins, even when mixed with as much as 50 % of methyl-terminated alkanethiolate [50], [29]. Mixed SAMs containing OEO have been used to control the adhesion, shape and function of cells [30], [51], [52]. The SAMs used in this study are OEO-terminated alkylsiloxanes, which have been observed to allow the adsorption of relatively large protein molecules [53], and have been shown to form monolayers less reproducible, and more prone to defects on average than the oligoethylene glycol terminated alkanethiolates [54]. However, these siloxane-based SAMs were investigated, because of their superior thermal and chemical stability compared with alkanethiolates [55].

The SAMs used in this work had their OEO segments terminated by methoxy groups. While a surface consisting purely of a methoxy OEO-terminated SAM would not permit the necessary immobilization of bioactive ligands for the planned studies, the surfaces were investigated with the intent that if these SAMs provided the required cell resistance, substrates which allowed the covalent attachment of bioactive ligands could later be

achieved by preparing SAMs consisting of a mixture of methoxy-OEO-terminated and an alkylsiloxane terminated by amine or other reactive functionality.

Typical analysis of grafted PEO surfaces involves the acquisition of XPS spectra; reduction of the carbon-1s peak to its components can verify the presence of ether units [45], [56], [57]. Alternatively, the contact angles of PEO surfaces have been measured by some investigators [27], [58], [45]. In both techniques, the substrate to which the PEO is grafted can have a significant effect on the measurement. Therefore, only qualitative comparisons are usually made between data obtained from different grafted PEO substrates, with direct, quantitative comparisons possible only when the underlying substrates are similar. In this study, the XPS technique for characterization of PEO surfaces was preferred for two reasons. First, the analysis of high-resolution scans of the carbon 1s peak from XPS measurements gives the intensity of the ether (C-O) signal, directly correlated with the amount of PEO grafted to the surface, provided the underlying substrate does not contribute to the ether signal. Second, the acquisition of XPS data would enable direct comparisons to be made between grafting densities obtained on glass surfaces prepared for this investigation and those prepared on oxidised silicon substrates by other investigators [47], [48].

2.3 Materials and Methods

The specific PEGs used for this study are listed in Table 2.3. Star PEO 460 is a highly branched PEO molecule, having an average of 35 arms emanating from a crosslinked divinylbenzene core, M_{arm}= 9,100 (Shearwater Polymers, see Chapter 4 for details of molecular weight determination). EG_3-OMe denotes a SAM prepared from a methoxy oligo(ethylene glycol)-terminated alkyltrichlorosilane, having a C_{11} hydrocarbon chain

[53]. All other PEGs were linear molecules. Typical end-grafting protocol involved the conversion of the PEO chain ends from hydroxyl to a more reactive entity; in a separate step the substrates were also activated for reaction with the PEO. Then the polymer was coupled with the substrate from an aqueous solution.

DESIGNATION	SUPPLIER	MOLECULAR WEIGHT	TERMINAL GROUP
PEG-3k-COOH	Sigma	3,000	carboxyl-carboxyl
PEO-20k	Fluka	20,000	hydroxyl-hydroxyl
Star PEO 460	Shearwater	320,000	hydroxyl
EG_3-OMe	S. Lee (MIT)	132	Methoxy-OEO-terminated alkylsiloxane

Table 2.3: Summary of PEGs used for surface modification

2.3.1 Activation of PEO

The hydroxyl end groups of PEO-20k and star PEO 460 were converted to carboxylic acid groups by a modification of the method of Royer et al. [59]. Details of the carboxylation procedure are given in Appendix A. Briefly, conversion of hydroxyl end-groups to carboxyl was accomplished by deprotonation in a solution of potassium *t*-butoxide in *t*-butyl alcohol, followed by reaction with bromoethyl acetate, hydrolysis at pH = 10, then acidification to a pH of 3.

2.3.2 Preparation of glass substrates for grafting of PEO brushes

Substrates were prepared for PEG grafting using a modification of the method of Stenger et. al. [60]. Glass coverslips, 18 mm in diameter, #1 thickness (VWR Scientific) were cleaned by immersion, first in 50% hydrochloric acid in methanol, then in 50% sulfuric acid in water, for 30 minutes each and rinsed thoroughly in deionized distilled water after each step. The coverslips were briefly rinsed in methanol to remove adsorbed water, which could lead to inhomogeneities in the silane film. Then the cleaned coverslips were immersed in a freshly-mixed solution containing 5 vol% water, 1 vol% trimethoxysilylpropyl diethylenetriamine (aminosilane, Huls America, Inc.) in anhydrous methanol for 15 minutes. Coverslips were rinsed three times in methanol, then cured at 120 °C for 10 minutes. XPS analysis indicated 4 to 6 atomic % nitrogen on these surfaces.

2.3.3 Grafting of PEO to aminated substrates

Carboxylated PEGs were grafted to aminated coverslips from a 15 % (w/v) solution in a buffer containing 0.1 M N-(morpholino ethanesulfonic acid) (MES), 0.5 M NaCl (pH = 6.1, Sigma). The carboxyl PEGs were activated for coupling by the addition of a 2-fold molar excess of 1-ethyl-3-(3-dimethylaminopropyl)carbodiimide hydrochloride (EDC) (Pierce Chemical) and a 3-fold molar excess of N-hydroxysulfosuccinimide (sulfo-NHS) (Pierce Chemical) over total chain ends in solution. Aminosilane-treated coverslips were immersed in the activated PEO solution and allowed to react for 16 hours at room temperature in a humid chamber. Coverslips were rinsed several times in deionized distilled water, then immersed in a 0.05 M solution of Tris-HCl, pH = 6 for four hours, to terminate any remaining active chain ends. Coverslips were then rinsed again in water, and stored under PBS until use.

2.3.4 Preparation of OEO-terminated Self-Assembled Monolayers

Methoxy-OEO-terminated siloxane SAMs (3 ethylene oxide units, methoxy-terminated) on microscope slides were kindly supplied by Seok-Won Lee of the Department of Chemical Engineering at MIT. Details of the synthesis of the OEO-terminated alkyltrichlorosilane and the preparation of the SAM are described in detail elsewhere [53].

2.3.5 Characterization of grafted PEO surfaces

Grafted PEG surfaces were analyzed using X-Ray Photoelectron Spectroscopy (Surface Sciences model SSX-100 spectrometer, with a monochromatized aluminum Kα X-Ray source, Harvard University). High resolution scans of the carbon 1s photoelectron peak (spot size = 600 μm) at a takeoff angle of 35 degrees were used to compare the relative intensities of the ether (C-O) and hydrocarbon (C-C) peaks. Carbon 1s peaks were fitted using instrument software. The flood gun setting was 5 eV and a nickel mesh was positioned a few mm above the samples to prevent charging. Two specimens were analysed for each PEG architecture.

In addition, PEO surfaces were examined using a Nanoscope III Atomic Force Microscope (Digital Instruments). The instrument was operated in "tapping mode", in ambient air using a silicon tip, and topographical images of the dried PEO layers were obtained. A standard silicon probe of length 125 μm, tip radius between 5 and 10 nm and a spring constant between 20 and 100 N/m was used for imaging. The resonant frequency of the cantilever was found at 300-350 Hz. 1 μm x 1 μm areas were imaged at a scan rate of 2

Hz. Two surfaces were prepared at each molecular weight for AFM studies, and a 1 μm x 1 μm area was examined at various points on each substrate.

2.3.6 Cell adhesion assays

In preparation for adhesion assays, grafted PEO surfaces were glued into the wells of a 12-well culture dish (Corning) using a small amount of a 5-minute epoxy (Devcon). Five cell types were used in two adhesion studies: the NR-6 (murine) fibroblast cell line (derived from NIH 3T3 cells and lacking endogenous epidermal growth factor receptors, received from Professor Alan Wells, University of Alabama, Birmingham), rat lung microvascular endothelial cells (RLMEC, received from Vascular Endothelial Cell Technologies), Chinese hamster ovary cells (CHO-LA), bovine aortic endothelial cells (BAE) and a murine stem cell line, (BAF/3). Cells were maintained in culture under the conditions described in Appendix C.

Most cell types were removed from culture dishes by trypsinization, then the action of the trypsin was stopped by the addition of a small amount of the culture medium containing serum. CHO cells were removed from culture dishes by the action of EDTA.

The investigation was carried out in two phases. In a first assay, NR6, BAF/3, BAE, and CHO cells were seeded on aminated glass coverslips to which linear PEO (M.W. = 20,000) had been covalently grafted as described above. In this first set of experiments,

cells were seeded in their respective growth (serum-containing) media, as the presence of serum, as well as endogenous proteins is expected to provide the most challenging of conditions to the grafted PEO layer. A PEO surface which could resist cell attachment for

24 hours under these conditions would therefore be a very promising candidate for a substrate against which bioactive ligands could be presented. All cells were seeded at a density of 8,000 cells per cm^2, then incubated at 37 °C for 24 hours. Then the culture medium was removed from each well, surfaces were rinsed gently in PBS and remaining adherent cells were fixed using 3.7% paraformaldehyde in PBS. Cells were photographed under a phase contrast microscope.

In a second set of experiments, the NR6 and RLMEC cells seeded at 8,000 cells per cm^2 in serum-free medium on all of the PEO surfaces described above. The two cell types were also seeded at the same density on tissue culture-treated polystyrene (TCPS) as a control. Cells were examined at intervals using a phase contrast microscope and photographed, and the projected cell spread areas measured by obtaining outlines for at least 30 cells using image analysis software (Scion Image 1.49). Serum-free medium was used in this set of experiments, as this would presumably allow us to observe the way in which cells control their own rate of attachment and spreading, that is by secretion of matrix proteins. Furthermore, the detailed studies for which these surfaces were intended are carried out in the absence of serum; serum-free conditions were therefore the most representative of the environment the cells would encounter in the desired application. For each PEG architecture and cell type, three surfaces were tested.

2.4 Results

2.4.1 Measurement of relative PEO surface coverage

PEO coverage on grafted surfaces has typically been characterized using XPS and contact angle measurements [48], [45], [27]. The thickness of the PEO layer may be estimated from XPS data, shown in Table 2.4. Using the technique of Sofia [48], ether intensities

may be converted to PEO layer thicknesses, by comparing the intensity, I, of the ether peak with that of an "infinitely thick" (that is, > 50 Å) PEO layer, I_o, using the following formula:

$$\frac{I}{I_0} = 1 - \exp\left[\frac{-d}{\lambda \sin(\theta)}\right] \qquad (1)$$

where d is the thickness of the PEO layer in angstroms

λ is the attenuation length for hydrocarbon films, given by

λ = 9.0 + 0.022(K.E.) [61]

θ is the takeoff angle for the instrument (= 35°)

The thickness of the OEO segment of the SAM on silicon surfaces has been measured independently by ellipsometry as 10 Å [53]; this thickness was combined with the intensity of the ether peak in XPS and the value of I_o calculated using equation (1). Then the values of I for the remaining PEG surfaces were inserted, and equation (1) was solved for the thicknesses, d, of the PEO coatings. Results are given in Table 2.4.

The cell- and protein-resistance of PEO surfaces clearly depend on their surface coverage, typically described in terms of a grafting density, σ, the number of grafted molecules per unit area. The grafting density is derived from the measured layer thickness and known molecular weight (M.W.), according to:

TABLE 2.4: SUMMARY OF C-O:C-C RATIOS ON GRAFTED PEO SURFACES

PEO M.W.	ARCHITECTURE	TERMINAL GROUPS	SOLUTION CONC.(mg/ml)	RATIO, C-O/C-C	AV. ETHER INTENSITY, I	PEO LAYER THICKNESS, Å	THICKNESS, Å (Sofia, 1998)
3,000	Linear	carboxyl	150 (MES)	1.06 +/- 0.54	6451	11	11
20,000	Linear	carboxyl	150 (MES)	2.35 +/- 0.26	5979	10	12
560,000	Star 460	carboxyl	150 (MES)	4.74 +/- 0.52	8208	20	22 **
132	EG3-terminated siloxane SAM	silane	2 mM (toluene)	0.92	7404	15	n/a

** Thickness of layer of Star PEO 3510: f = 70, M(arm) = 5,200, M.W. = 350,000

Synthesized by P. Lutz, Institut Charles Sadron, Strasbourg, France

$$\sigma = \frac{\rho d N_A}{M.W.} \tag{2}$$

where d is the thickness of the grafted layer (in cm), N_A is Avogadro's number, ρ is the density, in g/cm^3, and σ is the grafting density in molecules/cm^3. Graft densities for star and linear PEGs on silicon have been estimated in this way by Irvine et al. from ellipsometric measurements of PEO layer thickness [47]. Alternatively, Sofia used the de Gennes definition of grafting density as the fraction of grafted sites on a solid substrate, given by the ratio of the number of grafted chains per unit area to the number of surface sites (of area a^2) per unit area [62], and obtained:

$$\sigma = \frac{\rho d N_A a^2}{M.W.} \tag{3}$$

for linear polymers, where a is the size of a monomer unit (for PEO, $a \approx 3$ Å) [48].

For star molecules, Sofia defined the grafting density as the ratio of the number of grafted star molecules per unit area to a characteristic size of the star, or:

$$\sigma = \frac{\rho d N_A R_g^2}{M.W.} \tag{4}$$

Consequently, in order to compare the graft densities of Sofia et al. with those obtained in this study, their results were divided by a factor of a^2 for linear PEGs and by R_g^2 for star molecules. However, it is also well known that the surface coverage of PEO is controlled, not only by the number of grafted molecules per unit area, but also by the length of the grafted PEO chains [38]. Longer PEO chains have been shown to slow the protein adsorption process compared with shorter chains grafted at the same density, but may not be able to achieve the same graft densities due to their increased cross-sectional areas. For example, the triethylene glycol layer, presented at the surface of OEG-terminated SAMs should be able to pack more densely than a linear polymer of molecular weight 3,000 or 20,000 (which have 68 and 455 ethylene glycol units per molecule, respectively), based on its size alone. It is therefore somewhat misleading to attempt to predict the effectiveness of a PEO surface based solely on the number of grafted molecules per unit area. A better parameter for comparing surface coverage across surfaces of different PEO architectures is therefore the density of ether (monomer) units, given by:

$$\omega = \sigma\left(\frac{\text{M.W.}}{M_r}\right) \tag{5}$$

where M_r is the molecular weight of the repeat unit (= 44 for PEO).

Results of those calculations for ether unit density are shown in Table 2.5, and compared with ether unit densities obtained by Sofia and Irvine. The star polymer used by Sofia and Irvine (f = 70 arms and M(arm) = 5200) had different dimensions from that used for this investigation (characterized as f = 35, M(arm) = 9,100, see Chapter 4 for details). The radius of gyration of the star PEO used in previous investigations was measured at 10 nm [47], while that of the star molecules used in these experiments was estimated to be 14 nm (see Chapter 4). Thus, the area of cross section of a star PEO 460 molecule may be

TABLE 2.5: SUMMARY OF PEO GRAFT DENSITIES ON GRAFTED SURFACES

PEO M.W.	ARCHITECTURE	PEO LAYER THICKNESS, Å	MONOMER DENSITY (ether units/Å^2)	MONOMER DENSITY (Sofia, 1998)	MONOMER DENSITY (Irvine, 1998)
3,000	Linear	11	0.161	0.155	n/a
20,000	Linear	10	0.147	0.126	0.256
320,000	Star 460	20	0.293	0.286**	0.412**
132	EG3-terminated siloxane SAM	15	0.220	n/a	n/a

** Density of ether units in layer of Star PEO 3510: f = 70, M(arm) = 5,200, M.W. = 350,000
Synthesized by P. Lutz, Institut Charles Sadron,
Strasbourg, France

expected to be roughly twice that of a star 3510 molecule. Calculating the density of ether units for each architecture provides a way to eliminate the specifics of star molecular weight and functionality, and normalize the graft density results respect to the size of the star molecule; the densities obtained using star 460 are thus comparable to those obtained in the other studies. Hence, in all cases the grafting densities obtained by grafting carboxyl-terminated PEO from MES buffer using EDC/Sulfo NHS as a crosslinker, were between those obtained by Sofia and those obtained by Irvine, who coupled tresyl-activated PEGs from PBS buffer (in the presence or absence of K_2SO_4).

2.4.2 Nanotopography

Surface topography was examined in 3 - 4 locations on each substrate to ensure that the images obtained were reproducible. Representative AFM images are shown in Figure 2.2. The figure shows, for each substrate, a 3-dimensional image 500 nm x 500 nm, of the surface, and a 2-dimensional section through that image, from which the film thickness and uniformity may be inferred. A typical AFM image of an aminated glass coverslip is shown in Figure 2.2 (a), and shows the relative smoothness of the coverslips, aside from some pitting, which facilitates the visualization of the grafted PEO molecules in the AFM.

The morphology observed was typical of polymers grafted at a high density in a poor solvent. The chains appear to have collapsed together, forming "haystack" structures or pinned micelles, connected to the surface via the covalently grafted ends [63]. No significant defects were observed in the grafted PEO coatings.

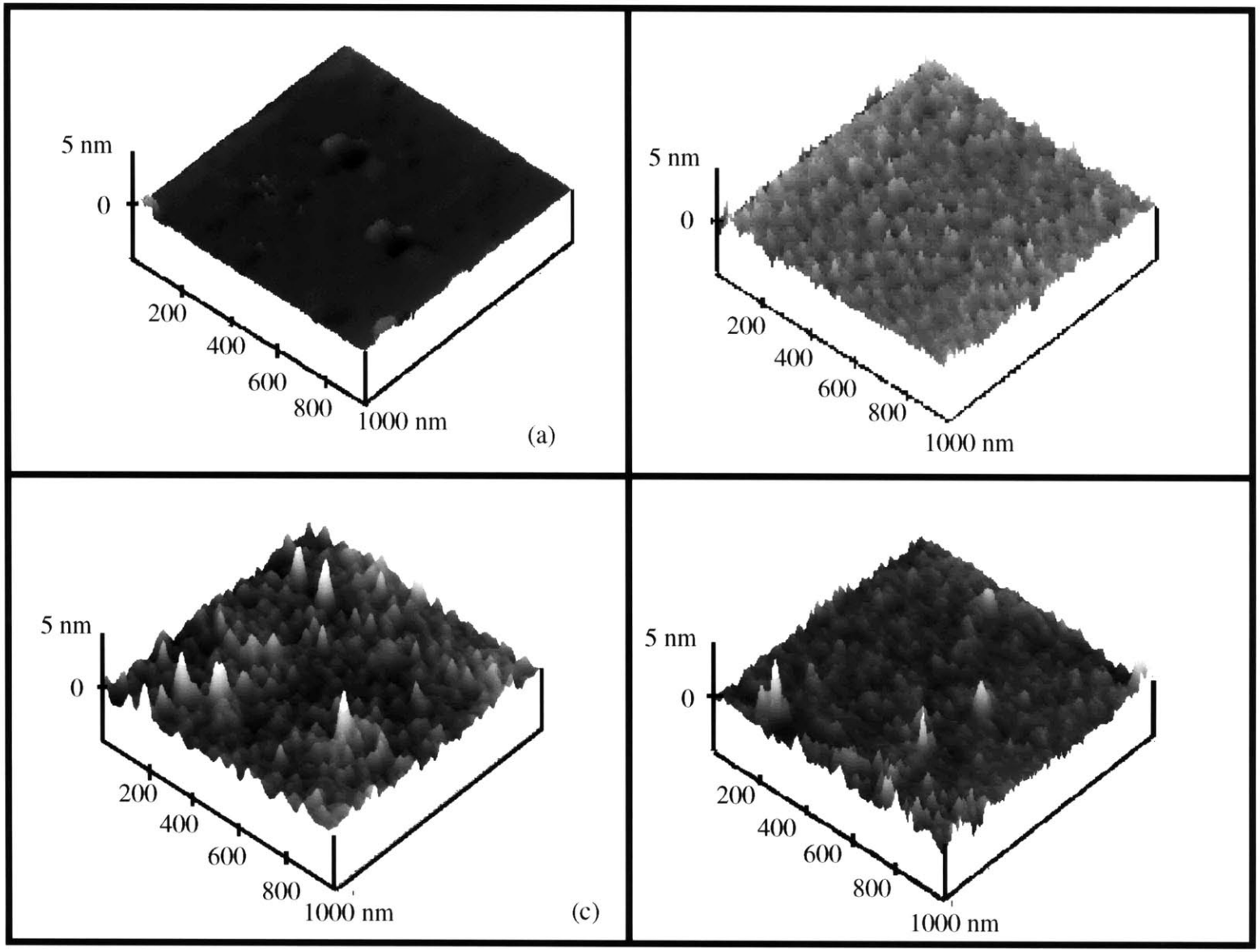

Figure 2.2 TM-AFM images of (a) aminosilane-treated coverslip (b) PEO-COOH-3k, (c) PEO-COOH-20k, (d) Star PEO 460

2.4.3 Adhesion studies

Photographs of the four cell types (NR6, CHO, BAE, BAF/3) on linear PEO surfaces (M.W. = 20,000), taken 24 hours post-seeding are given in Figure 2.3(a). As can be seen from the figure, these grafted surfaces were unable to resist attachment of most of the cell types under investigation; with the exception of the stem (BAF/3) cells, all of the cell types studied were able to attach and spread after 24 hours. Even in the presence of serum, the stem cells showed no adhesion after 24 hours.

More detailed studies were performed using only the NR6 and RLMEC cells. BAF/3 cells showed no attachment to grafted PEO substrates even under serum-containing conditions, and were therefore not studied more extensively. The CHO cells showed significant attachment and spreading, achieving near-confluency after 24 hours. The high cell densities achieved by CHO cells made obtaining accurate cell outlines difficult, as many of the cells were in contact with each other, hence these were not subjected to detailed investigation of the increase in cell spread area with time. Photographs of NR6 and RLMEC cells, taken at regular intervals post-seeding are given in Figures 2.3(b) and 2.3(c). In most cases, the cells adhered and spread on PEO surfaces within four hours. An exception was seen in the case of star PEO surfaces, which remained completely non-adhesive to the RLMECs for the duration of the experiment, although the NR6 cells were able to attach and spread.

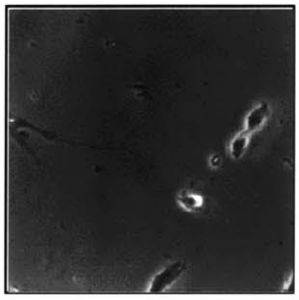

Fibroblasts (NR6)

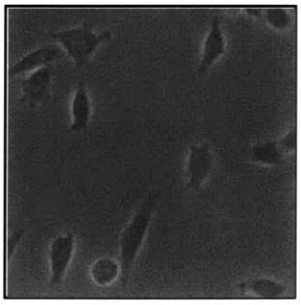

Chinese Hamster Ovary

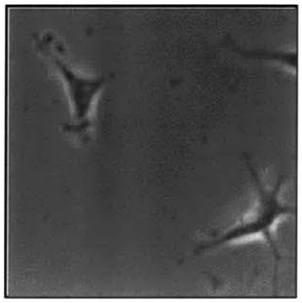

Endothelial (BAE)

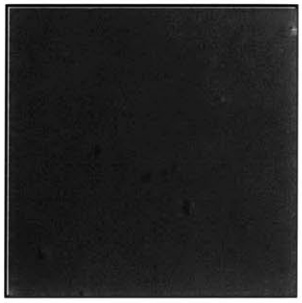

Stem (BAF3)

Figure 2.3(a): Attachment and spreading of four cells types on grafted PEO surfaces (linear, M.W. = 20,000) after 24 hours in serum-containing media

Figure 2.3 (b): RLMEC cell adhesion on PEO surfaces

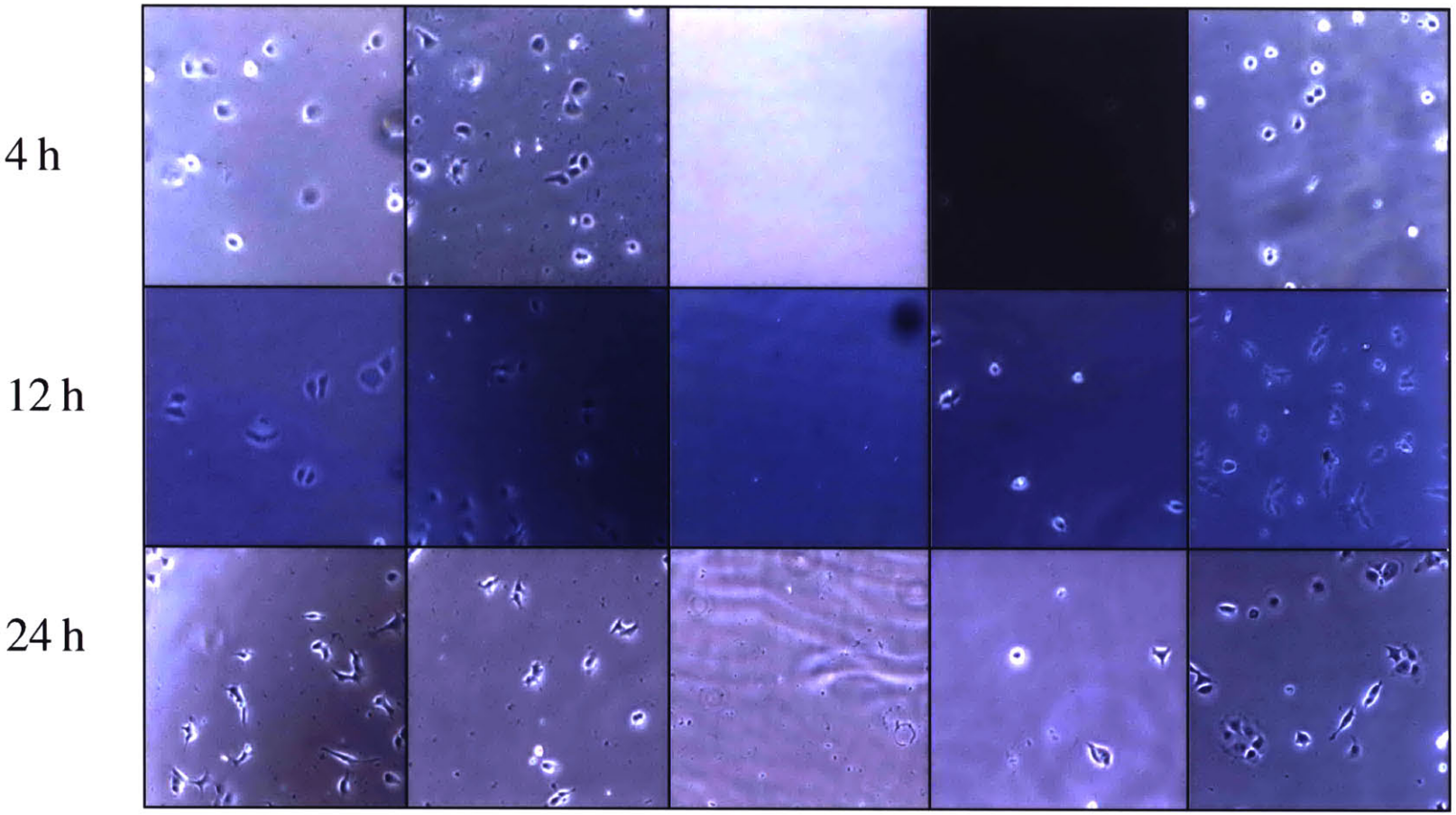

Figure 2.3 (c): NR-6 cell adhesion on PEO surfaces

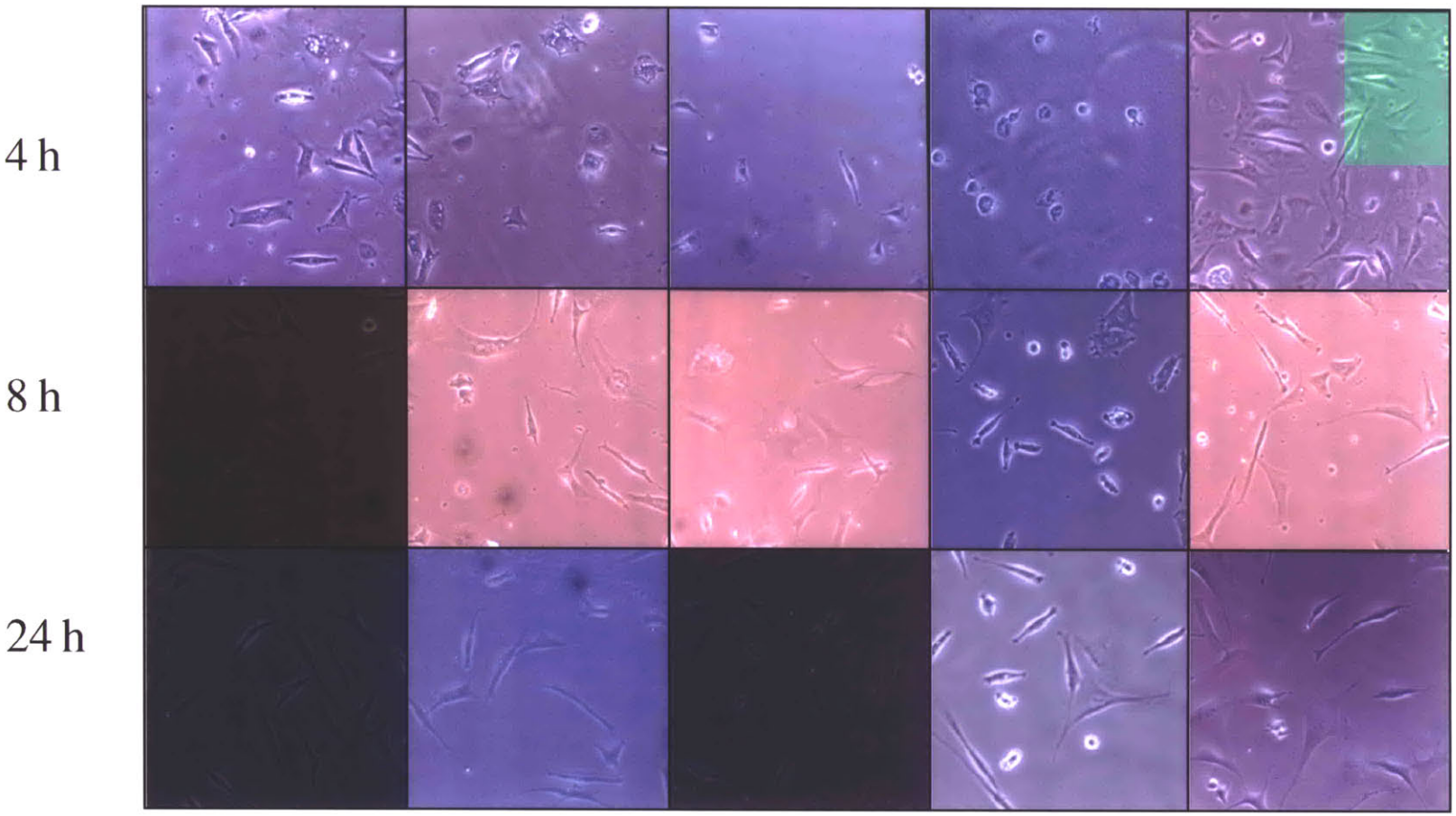

The evolution of cell spread areas with time was obtained by tracing the outlines of cell images and computing the enclosed area, and is shown in Figures 2.4(a) and 2.4(b). The figures seem to indicate somewhat different responses of each cell type to each substrate. In the case of the NR-6 fibroblasts, cells achieve the same spread areas on all substrates except the SAMs after 24 hours; the spread areas after a day are the same as those seen on tissue-culture polystyrene (within standard error). After 4 hours, NR-6 spread areas were roughly the same on the 3k, 20k, star and tissue-culture polystyrene surfaces. Average NR-6 spread area on the SAM was significantly lower (approximately 50%). On all PEO surfaces, except the star PEO substrates, the RLMECs spread at the same rates, and achieved the same final spread areas. No adhesion of endothelial cells was observed on the star 460 substrates.

2.5 Discussion

In an attempt to meet the stringent requirements of (i) complete adhesion resistance (0 % confluency) for 24 hours in serum-containing media and (ii) stability of the PEO coating toward potential rearrangement by cells, a number of approaches previously examined in the literature were tested. Specifically, glass substrates to which PEO had been covalently grafted in a variety of molecular weights and densities were extensively examined. The covalent grafting of linear and star PEO to oxidised silicon surfaces was investigated quantitatively by Sofia [48] and Irvine [47]; these studies provided a basis for comparison for the PEO layers prepared in this work. The grafting densities reported by Sofia and Irvine are among the highest reported, as both investigators attempted to maximise PEO graft density by varying such grafting conditions as coupling

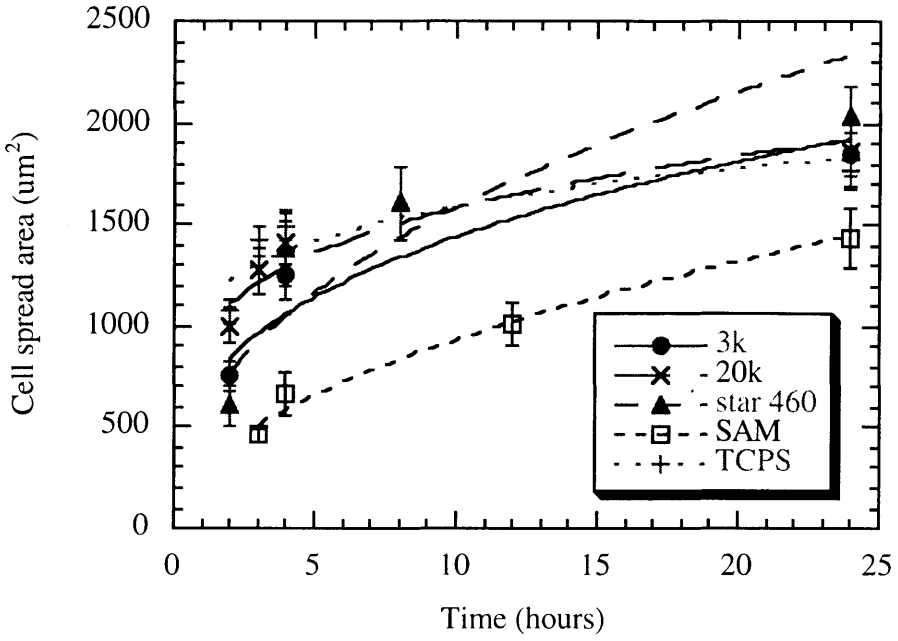

(a)

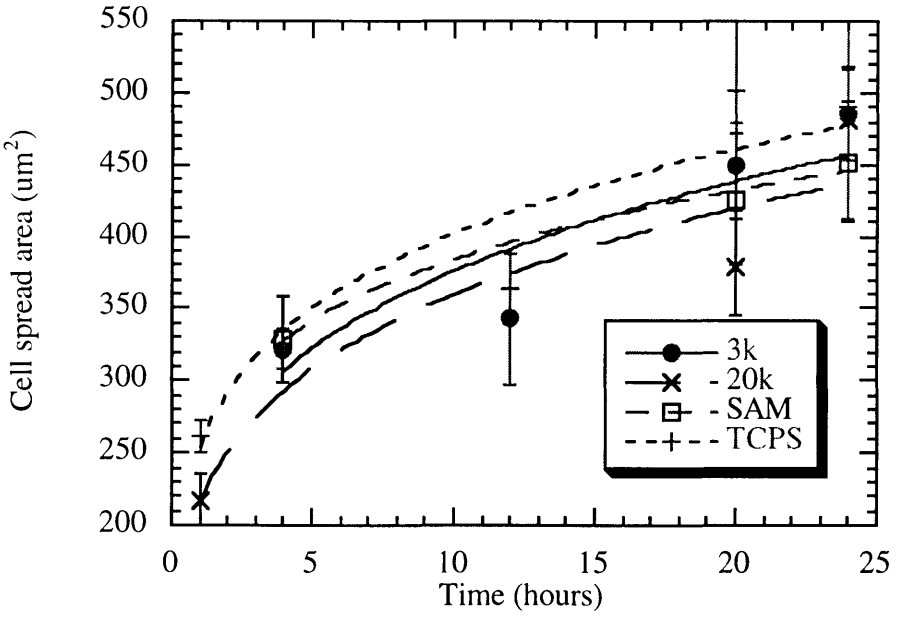

(b)

Figure 2.4: Increase in spread area of (a) NR-6 cells (b) RLMECs with time on grafted PEO surfaces (mean ± standard error).

solution concentration and solvent quality. Since PEO grafting density is considered a key parameter for obtaining effective cell and protein resistance, techniques used in those studies were used here as well. Although different coupling chemistries were used, the underlying substrates were very similar (aminosilane-treated glass or oxidised silicon substrates), and the thicknesses, graft densities and densities of ether units of linear and star PEO achieved were comparable to those seen earlier by Sofia and Irvine.

The most important conclusion which can be reached from this study is that the results of model protein-adsorption experiments, such as were performed by Sofia and Irvine, while useful for discerning adsorption mechanisms and kinetics, cannot easily be extrapolated to select a substrate of universal cell resistance. Although Sofia [48] observed negligible adsorption of fibronectin and albumin on grafted star and linear PEO surfaces after 24 hours at room temperature, this study revealed that many cell types are able to attach and spread on PEO surfaces of similar (or higher) PEO coverage. In spite of the relatively high graft densities achieved by covalent grafting techniques, none of the surfaces prepared by covalent grafting of PEO were able to meet our requirement of complete resistance to non-specific attachment of a variety of cell types for 24 hours.

In a preliminary set of experiments, various cell types were seeded on linear PEO surfaces (M.W. = 20,000, approximately the PEG chain length deemed optimum for protein resistance, [45]) in serum-containing media, and examined after 24 hours. These are considered relatively challenging conditions for substrates, as there is the possibility of adsorption of serum as well as endogenous proteins. With the exception of the stem cells, surfaces allowed the attachment of all of the cell types under study. Stem cells have also been shown previously to be poorly adhesive on tissue culture plastic, showing significant adhesion only to adsorbed fibronectin, and are typically cultured in suspension. Therefore,

the observation that these cells did not also adhere to grafted PEO surfaces is not surprising.

The failure of these PEO substrates to resist the non-specific adhesion of most of the cell types studied underscores the importance of testing grafted PEO layers in the environment for which they are intended. Grafted PEO surfaces, of roughly the "optimum" molecular weight, and high grafting density showed excellent resistance to the adsorption of single proteins in the model studies of Sofia, Irvine and others. When tested under more physiological conditions, that is, in the presence of cells, seeded in a buffer containing a variety of proteins and secreting their own matrix proteins, over a period of 24 hours, the surfaces were unable to resist the non-specific attachment of most of the cell types tested. This has significant implications for the typical investigations of the interactions between cell surface receptors and ligands immobilized on glass or polymer substrates. Although cell adhesion to the tripeptide motif of Arg-Gly-Asp has been studied extensively [64], [32], [65], [14], [41], the peptide is usually presented against a substrate which itself supports matrix deposition, substrate remodeling, and therefore cell adhesion in the long term (up to 24 hours). It is therefore likely that such model surfaces present to cells not only the immobilized ligand of interest, but other adsorbed proteins as well [30].

In the second set of experiments, the effects of PEO architecture on the spreading kinetics of NR6 and RLMEC cells was examined. Cells were seeded in serum-free media, so it is assumed that the adhesion and spreading observed is due to the adsorption of matrix proteins secreted by the cell. Even under these less severe conditions, however, no substrate was able to universally resist cell adhesion and spreading for 24 hours. There were some cell type-specific exceptions, however. Endothelial cell attachment was entirely prevented on the star PEO surfaces, and the SAMs served to slow the spreading rate of the fibroblasts dramatically, such that after 24 hours their average spread area was significantly

lower than on the other substrates. This points to a second possibility: it is likely that over a period of 24 hours, the degree of non-specific adhesion will be cell-type dependent. For example, cells which secrete relatively large quantities of matrix proteins, or which have relatively high expression of adhesion receptors might be better able to remodel the substrate and adhere than others which secrete smaller amounts or have fewer receptors. Alternatively, two cell lines may express different types of integrin receptors, or different levels of other, non-integrin adhesion receptors, which may have an effect on their adhesion behaviour. At present, the exact reasons for these cell type-dependent variations in response to the PEO substrates are unclear.

Whereas it was previously assumed that the process of protein adsorption reached an equilibrium after 1-2 hours, it has more recently been suggested that there is a kinetic effect of PEO density and chain length on adsorption. Szleifer [38] used single-chain mean-field theory to show that at molecular weights of 2,200 and higher, there is a threshold density, above which a grafted PEO layer can achieve protein resistance at equilibrium; below this density the presence of grafted PEO brushes can slow the kinetics of adsorption if the molecules are of high molecular weight. Irvine [47] and Sofia [48] have both reported that star PEO layers allow the adsorption of relatively small protein molecules, where grafted linear PEO layers do not. Based on these results it was suggested that increasing the number of branches per molecule, as in a star, increased the segment density, but decreased the degree of overlap of grafted molecules, such that star PEO layers in which the PEO functionality was high allowed the adsorption of small protein molecules.

It may be, therefore, that the grafted PEO layers in such studies are of sufficient density to delay the onset of protein adsorption beyond the time period of the experiment. An additional concern arises from the finding that cell surface receptors are able to remodel their substrates [42], so that on contact with a PEO coating on a surface, they may be able

to reorganize some of that coating, providing access to the surface for endogenous or for serum proteins. Szleifer also described this displacement of the PEO brush as taking place during protein adsorption on PEO surfaces.

None of the substrates investigated was able to completely resist non-specific attachment of the cell type of interest for this thesis: the NR-6 cell line. Examination of attachment and spreading during the early stages of adhesion (that is, after 1 to 2 hours) gives an indication of the effect of grafted PEO. To obtain an indication of the initial spreading rate, the NR-6 spread areas achieved after 2 hours may be compared with those after 24 hours. This ratio, expressed a percentage of the "final" cell area, that is, cell area after 24 hours for each substrate is given in Table 2.6.

Substrate	% final spread area achieved after 2 hours
3k	41
20k	54
Star-460	30
SAM	32
TCPS	61

Table 2.6: Percentage of "maximum" spread area achieved by NR-6 cells 2 hours after seeding.

Again, the data support the suggestion that the presence of grafted PEO serves to retard the spreading of NR-6 cells with respect to tissue culture polystyrene in the early stages of attachment, in accordance with the theoretical results of Szleifer [38]. The star PEO surfaces and the SAMs appear to be most effective in retarding cell spreading in the short

term (within 2 hours after seeding), which can likely be explained in terms of the density of ether units presented at the surface. However, after 24 hours, as previously mentioned, the cells on all substrates achieve roughly the same area, with the exception of cells seeded on the SAMs.

It appears, therefore, that our proposed experiments will present very challenging conditions to the PEO substrates: a high degree of non-specific adhesion must be resisted for a relatively long time, suggesting that a very dense grafted layer of PEO is required . It has been shown that a maximum grafting density is achieved for randomly coiling molecules on a flat surface when the polymer chains begin to overlap [62], [38], [66]. Beyond this density, the addition of more PEO chains becomes energetically unfavourable. The results of these experiments suggest that the substrates used for such experiments must present a PEO density far higher than that typically achieved by covalent grafting, where the maximum PEO density achievable may be limited by steric repulsions.

AFM images allowed a qualitative inspection for uniformity in the grafted PEO layers. No gross defects or non-uniformities in the PEO layer were observed, and the PEO had the expected morphology. PEO surfaces are therefore presumed approximately uniform in thickness and density; accordingly cells are not believed to be attaching to regions of exposed aminosilane or glass substrate. XPS showed that the star architectures provided significantly improved surface coverage over linear molecules, and even provided a higher surface density of ether units than the SAMs. However, star molecules are believed to allow protein adsorption in the interstitial space, and have been shown to provide inferior protein resistance compared with linear molecules.

SAMs were selected for this study, based on the work of Prime and Whitesides [29], who studied the adsorption of proteins on mixed self-assembled monolayers (SAMs), consisting

of oligo(ethylene oxide) (OEO)-terminated alkanethiolates and unmodified alkanethiolates in varying proportions. Based on their results, it has been suggested that if a very high surface density of PEO were achieved, as few as 2 ethylene oxide units would be sufficient to completely repel proteins; a high PEO molecular weight is not necessary. That the alkylsiloxane SAMs, presenting the highest density of ether units at their surface, were unable to prevent non-specific attachment was disappointing, especially since OEO-terminated SAMs formed from alkanethiolates on gold substrates were found to resist attachment of both NR6 and CHO cells for 24 hours in serum-containing media (G. Maheshwari, unpublished results), and since other investigators have found OEO-terminated alkanethiolate SAMs to be completely resistant to attachment of endothelial cells [51].

Two fundamental differences between the OEG surfaces used by Prime [29], and those prepared by Lee [53], were considered as possible reasons for the difference in performance. First, the triethylene glycol segments used by Prime were terminated with hydroxyl groups, while those prepared by Lee were methoxy-terminated. One possibility, therefore, was that the methoxy-capped OEG films presented a very dense, hydrophobic layer at the surface, nullifying the protein resistance of the hydrophilic ethylene glycol units, and promoting the adsorption of proteins. Prime found, however, that there was negligible difference in protein resistance between methoxy- and hydroxy-capped OEG-terminated SAMs. Furthermore, Lee found that the methoxy-capped OEG surfaces definitely showed improved protein resistance over methoxy-terminated alkylsiloxane surfaces, suggesting that the protein resistance of the OEG segment is not completely negated by the methoxy cap. The second difference lay in the functional group used to anchor the alkyl chain to the surface: thiol in the work of Prime, and trichlorosilane in the case of Lee. Methoxy-terminated alkanethiolates showed significantly lower fibrinogen adsorption than did methoxy-terminated alkylsiloxanes. [53]. Self-assembled monolayers

consisting of alkanethiolates on gold have a stronger tendency to form uniform, oriented films than those formed from alkyltrichlorosilanes [54], as monolayer formation of alkanethiolates on gold is directed by the crystalline lattice structure of the gold substrate. On the other hand, substrates used in the formation of alkylsiloxane SAMs are amorphous, causing the packing of the alkyl chains to be determined by the poorly controlled polymerization of the siloxane, rather than by ordering the substrate. Any heterogeneities in the siloxane layer could contribute to non-specific attachment of proteins, and therefore of cells. Finally, the conformations of methoxy-terminated OEG segments have been studied [67], and such surfaces have been found to exhibit different protein adsorption behaviour, depending on whether the OEG layer is amorphous, crystalline, or densely packed in an "all-trans" (restricted) conformation.

2.6 Conclusions

The resistance of PEO-treated surfaces to non-specific attachment of cells and proteins has been extensively discussed. Surfaces having graft densities of PEO comparable to the highest reported in the literature were prepared and tested. However, many investigators have studied model systems in which the adsorption of a single protein to a PEO surface has been measured over periods of two to four hours. Alternatively, investigations of cell adhesion to PEO surfaces have also monitored cell attachment in the short term (that is, 30 minutes to 4 hours). Since the surfaces to be prepared for this research are intended for quantitative studies of receptor-ligand interactions, the requirement that they resist non-specific interactions completely is a crucial one. Furthermore, our studies were designed to be performed over 24-hour periods; it is therefore important to resist the non-specific interactions for at least that period of time. For *in vivo* applications, surfaces should definitely be protein resistant for longer periods of time.

The resistance of PEO-grafted surfaces to non-specific attachment of cells appears to be cell type- and substrate-specific; it is possible that cells which secrete relatively large amounts of matrix proteins or that have high receptor densities can attach and spread faster than cells which are not highly secretory or have lower numbers of receptors. Model protein adsorption experiments, though instructive, cannot easily be used to predict the performance of such surfaces over extended periods, nor can they predict their ability to resist cell adhesion. In addition, the single-protein model cannot indicate the ability of such surfaces to resist adsorption of several proteins from solution. What is of greatest interest to us for this project is the performance of PEO-coated substrates in practice, especially under cell culture conditions. Hence, while theory remains a valuable guide for selecting surfaces which will effectively repel proteins, it is essential that PEO surfaces be tested experimentally under the specific conditions of interest.

CHAPTER 3. PREPARATION OF A "BIOINERT" SUBSTRATE

3.1 Radiation-Crosslinked PEO Hydrogels

The preparation of hydrogels by radiation crosslinking offers distinct advantages over chemical crosslinking techniques. Chemical crosslinking requires the presence of initiators or other crosslinking agents, and these chemical agents may cause undesired interactions with cells. In contrast, radiation crosslinking of aqueous solutions of PEO can be used to create a pure PEO surface, as other reagents are unnecessary. PEO hydrogels prepared in this manner have been shown to display excellent cell resistance [68]. In addition, radiation crosslinking takes place along the polymer backbone, leaving the chain ends free for subsequent functionalization and ligand attachment. However, radiation crosslinked PEO hydrogels are not commonly used because their preparation is much more complicated than that of covalently grafted brushes.

Radiation crosslinking occurs when products of the radiolysis of water attack polymer chains in solution, abstracting hydrogen and creating polymer radicals which deactivate either by crosslinking or by scission, or both (see Scheme 3.1). Studies by various authors [48], [69], [70], [71] of the crosslinking of PEO in solution by gamma- or electron-beam irradiation defined the conditions under which crosslinking greatly dominates chain scission. It is typically assumed that above the chain overlap concentration of the polymer, the chains are entangled, and that radiation crosslinking takes place primarily at these sites of physical entanglement, giving rise to a spatially uniform network.

radiolysis of water:

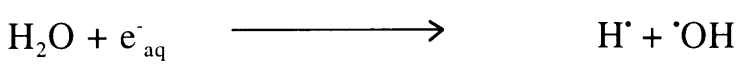

$$H_2O + e^-_{aq} \longrightarrow H^{\bullet} + {}^{\bullet}OH \quad (1)$$

hydrogen abstraction:

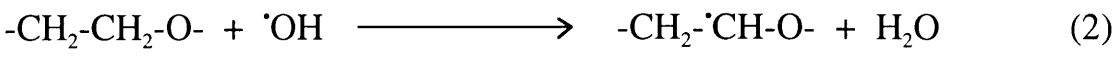

$$-CH_2-CH_2-O- + {}^{\bullet}OH \longrightarrow -CH_2-{}^{\bullet}CH-O- + H_2O \quad (2)$$

crosslinking:

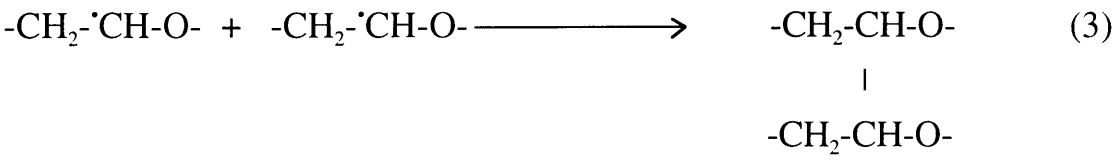

$$-CH_2-{}^{\bullet}CH-O- + -CH_2-{}^{\bullet}CH-O- \longrightarrow \begin{matrix} -CH_2-CH-O- \\ | \\ -CH_2-CH-O- \end{matrix} \quad (3)$$

scission:

$$-CH_2-{}^{\bullet}CH-O-CH_2-CH_2-O- + e^-_{aq} \longrightarrow \begin{matrix} -CH_2=CH_2-O + \\ -CH_2-CH_2-O^- + H_2O \end{matrix} \quad (4)$$

Scheme 3.1 Examples of possible reactions during electron-beam crosslinking of PEO [70]

3.2 Experimental design

In most studies, hydrogels formed are free-standing, or unsupported, as the PEO cross links to itself and not to the vessel containing the solution. For our purposes, however, a PEO hydrogel covalently linked to a support may be expected to provide an excellent substrate for our studies: the hydrogel would present a pure PEO surface to cells, which prevents non specific interactions, yet permits ligand derivatization, and the grafting to a

substrate should ensure its stability and provide mechanical support. Allgor [72] describes a technique by which linear or star PEO molecules may be simultaneously cross-linked and grafted to polymer surfaces such as polyethylene in a two-step process. An intermediate layer of methacrylic acid is cross-linked to the polymer substrate by electron-beam irradiation, then complexes and cross-links with a PEO solution on subsequent irradiation. Methacrylic acid was used in this process as a primer; a means to covalently graft a compound containing a functional group which would complex with the PEO, and thus allow it to crosslink by covalently bonding at the entanglement points. Similarly, to produce graft-coupled layers of PEO on glass, the glass substrate must first be modified with some reactive species. Functional groups which are made reactive under electron beam or gamma irradiation include ether and vinyl [73].

In this chapter, electron beam crosslinking of PEO solutions was investigated as a means of achieving a stable grafted PEO layer of sufficient density. First, a covalently grafted PEO layer was prepared on glass substrates, which provided "anchoring" ether units. These substrates were then coated with a thin layer of a PEO solution and irradiated. This allowed the PEO molecules in solution to crosslink to the grafted PEO chains on the substrate and to each other, creating a covalently grafted PEO surface of significantly higher thickness than those prepared in Chapter 2 using covalent grafting techniques only. The hydrogel consisted of an amine-terminated linear PEO, selected to provide amine functional groups at the surface of the gel, to which ligands could later be tethered using appropriate chemistry. By attaching the hydrogels to glass or silicon supports, we provided not only a "bioinert" background, against which adhesion ligands could be presented, but also a rigid support, believed to be important for adhesion, spreading and cytoskeletal organization [22]. These hydrogel substrates were found to be completely resistant to non-specific attachment of a variety of cell types for 24 hours or more.

3.3 Materials and Methods

3.3.1 Preparation of glass substrates

18 mm glass coverslips (#1 thickness, from VWR Scientific) were cleaned by immersion for 30 minutes, first in a 50 vol. % solution of hydrochloric acid in methanol, then in a 50 vol. % solution of sulfuric acid in water, followed by rinsing several times in water. The coverslips were then immersed in anhydrous methanol, containing 4 mg/ml O-[2-(Trimethoxy silyl)-ethyl]-O'-methyl-polyethylene glycol 5,000 (PEG-silane, Fluka) and 5 vol% water. Surfaces were rinsed three times in methanol, and cured at 50 °C for at least 1 hour.

3.3.2 Electron-beam irradiation of PEO solutions

Amino-functional PEG hydrogels were covalently grafted to aminated coverslips by immersing the coverslips in an aqueous solution of bis (polyoxyethylene bis(amine)) (M.W. = 20,000, hereafter referred to as PEG-NH_2, Sigma Chemical Company), 50 mg/ml in deionized distilled water in a 100 mm glass petri dish (Corning). Immediately prior to irradiation, the excess solution was drained from the dish, leaving only a thin film of PEG-NH_2 solution at the surfaces of the coverslips.

Cross-linking of the PEG-NH_2 solution was achieved by exposure to electron beam irradiation, at a total dosage of 2 Mrad. The source was a 3 MeV Van de Graaf generator, which delivers radiation at a rate of 250,000 rad/second. Because of the large number of steps in the preparation of clustered ligand surfaces, it was not practical to handle all of the gels as sterile after they are prepared. After irradiation, substrates were rinsed briefly in deionised, distilled water, and the petri dishes were sealed with Parafilm™, and stored at 4

°C. Hydrogel-grafted coverslips were used within 30 days after preparation. Prior to use in cell-based assays, surfaces were sterilized by light spraying with a 70% solution of ethanol in water.

Hydrogel preparation is depicted schematically in Figure 3.1

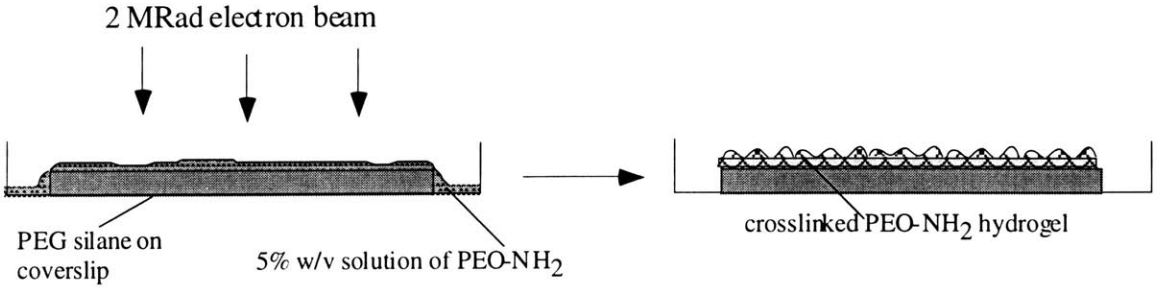

Figure 3.1 Schematic representation of the preparation of PEG-NH_2 hydrogels

3.3.3 Characterization of covalently bound hydrogel layer

A: Topography of hydrogels

The surface topography of dried networks was examined by atomic force microscopy (AFM) in intermittent contact, or "tapping mode" in air using a Digital Instruments Nanoscope III instrument. A standard silicon probe of length 125 µm, tip radius between 5 and 10 nm and a spring constant between 20 and 100 N/m was used for imaging. The resonant frequency of the cantilever was found at 300-350 Hz. 1 µm x 1 µm areas were imaged at a scan rate of 2 Hz.

Hydrated gel topography was obtained by equilibration of substrates for 3 days in deionized distilled water, followed by imaging underwater in tapping mode. A standard silicon nitride cantilever, of length 120 μm, radius 20-40 nm and spring constant 0.12 N/m was used for imaging. Probes were tuned at frequencies between 7 and 10 Hz. 1 μm x 1 μm sections were scanned at a rate of 2 Hz. For this investigation, samples were mounted in the commercially available fluid tapping cell (Digital Instruments). No external temperature control was applied during imaging.

In each case, two samples, and 2-3 fields per sample were examined. Images were processed only by flattening to remove background slope.

B: Thickness of grafted PEO layer

Thicknesses of dried and swollen PEO coatings were measured by ellipsometry using a Gaertner L116a model ellipsometer. PEO layers were prepared on silicon wafers using the same procedure as was used for coverslips. Three samples were dehydrated in a graded series of ethanolic solutions, then dried under vacuum for three days. Three samples were immersed in deionized distilled water at room temperature for three days. The refractive index of the hydrated hydrogel was taken as the weighted average of the refractive indices, n_i, of PEO (= 1.44) and water (= 1.33), according to their volume fractions, v_i in the precursor solution, assuming a density of 1.072 g/cm^3 and a molecular weight of 20,000 for PEG-NH_2:

$$n_{gel} = \sum_i n_i \times v_i \qquad (1)$$

$$= (1.33 \times 0.953) + (1.44 \times 0.047)$$
$$= 1.336$$

A total of six samples, taken from two different batches, were measured. Five points were measured on each sample. Thicknesses are reported as mean +/- standard deviation.

The thickness of the dried gels was also estimated by AFM. Hydrogel substrates were dried under vacuum for 3 days and an initial topographical image was obtained in tapping mode. The probe tip was then used to scan a small region of the sample in contact mode, at a relatively high force, to debrade the hydrogel from the substrate. The AFM was then used as a profilometer, to determine the height difference at the edge of the abraded region and thus the thickness of the dried gel .

3.3.4 Characterization of resistance to non-specific interactions

Hydrogels were tested against a variety of cell types, and their performance compared with that of linear PEO-grafted surfaces. Hydrogel-grafted and linear PEO-grafted (M.W. = 20,000) coverslips were glued into the wells of a 12-well culture plate (Corning) using a small amount of a fast-drying epoxy (Devcon). A variety of cell types were seeded on the hydrogel and brush surfaces in serum-containing conditions. Wild-type NR6 cells, Chinese Hamster Ovary cells (CHO-LA), BAF/3 (murine embryonic) cells and Bovine Aortic Endothelial (BAE) cells were cultured as described in Appendix C. Most cell types were removed from culture dishes by trypsinization, then the action of the trypsin was stopped by the addition of a small amount of the culture medium (containing serum). CHO cells were removed from culture dishes by the action of EDTA. Cells were seeded at densities of approximately 8,000 per cm^2 in serum-containing media, and incubated for 24 hours 37 °C. For comparison purposes, cells were also seeded on tissue culture

polystyrene. Wells were then examined using phase-contrast microscopy, and attached cells photographed.

To further test the resistance to cell adhesion of these hydrogels, a more stringent test was applied. Substrates were immersed in a solution of human fibronectin (Sigma) in phosphate-buffered saline (PBS), of concentration 10 μg/ml, for 24 hours. Substrates were then immersed in a 1% solution of bovine serum albumin (Gibco) for 1 hour, and rinsed gently in PBS. NR6 fibroblasts were seeded on these substrates under serum-containing conditions, and incubated at 37 °C for 24 hours.

3.4 Results and Discussion

3.4.1 Physical properties of dried hydrogel

Figures 3.2 and 3.3 show the AFM images obtained from dried gels on glass coverslips. Figure 3.2 is a topographical image of the dried hydrogel surface. Figure 3.3 shows the cross-section of the abraded region from which the thickness was estimated. The vertical scale has been greatly exaggerated to show detail.

As can be seen from Figure 3.3, the thickness measured using AFM was approximately 14 nm, in excellent agreement with the ellipsometric measurement. XPS examination reveals that a significantly higher amount of PEO is coupled to the slides by electron-beam irradiation than by covalent grafting of a brush layer, revealed by comparison of the ether to hydrocarbon peak ratios.

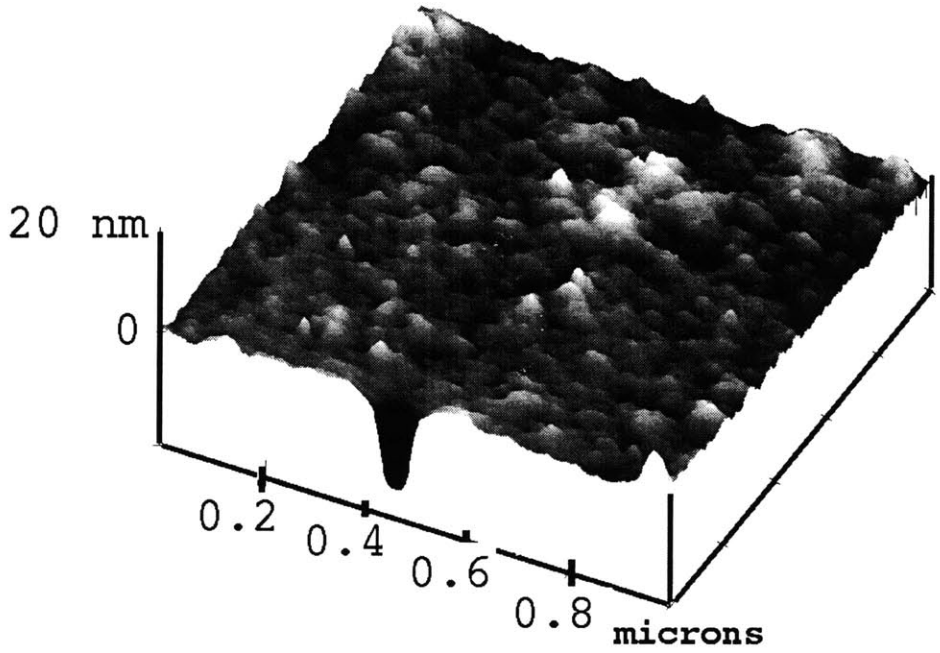

Figure 3.2: Tapping Mode AFM image of dried hydrogel surface

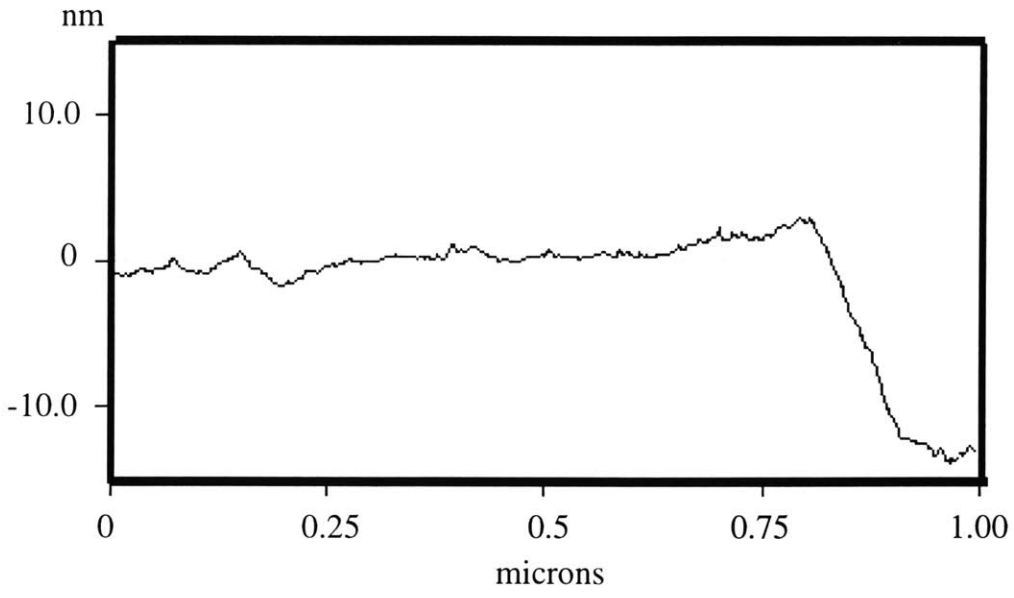

Figure 3.3: Dried hydrogel thickness as measured by AFM

3.4.2 Physical properties of hydrated hydrogel

Figure 3.4 shows a topographical image of the hydrated gel. The image shows an undulating surface, having some raised and some depressed areas. The maximum variation in height between the highest and lowest regions is 15 nm. Typical height variations are reflected in the root-mean-square roughness of the image, determined using instrument software. This is given by the standard deviation of the height of the hydrogel surface about a calculated mean height value, and has a value of ~ 2 nm for the swollen hydrogel. The variations in height of the surface probably reflect local fluctuations in structure, frozen in during the crosslinking process, which creates a random array of crosslinks [74], [75]. A calculation of the surface area of for this image estimates that the area of this surface is greater than the projected area (that is, for a flat substrate) by 1.5%. These estimates, taken together, suggest that the hydrogel, when hydrated, is smooth on the scale of the molecules to be immobilized (estimated diameter of star PEO-RGD conjugates is ~30 nm).

The XPS and ellipsometric measurements are summarized in Table 3.1. As can be seen from the table, the PEG-silane layer, at a molecular weight of 5,000, achieved similar thicknesses to the grafted star PEO layer prepared in Chapter 2, corresponding to a monomer unit density of 0.279 ether units/$Å^2$. In fact, the PEG-silane layer alone showed complete resistance to non-specific attachment of NR6 cells for 24 hours, as is our requirement, however, as the PEG-silane molecule is methoxy-terminated, the derivatization of those chain ends with bioactive molecules was impossible. Therefore, the layer was used only as a means of providing covalently linked ether units on the surface, to which the PEG-NH_2 solution could crosslink.

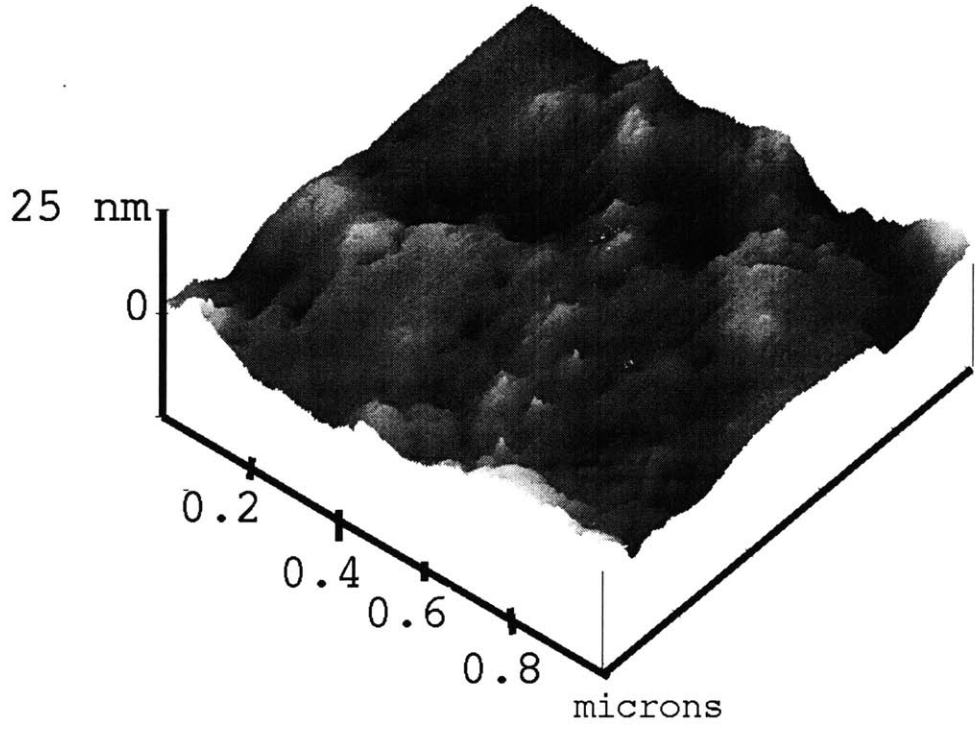

Figure 3.4 Topographical image of swollen PEG-NH_2 hydrogel, obtained from tapping mode AFM, under water.

	Thickness (nm) by ellipsometry	C-O/C-C ratio by XPS
PEG-silane	1.9 ± 0.9	1.72
Crosslinked hydrogel (dried)	13.7 ± 3.8	9.12
Crosslinked hydrogel (relaxed)	302.2 ± 6.7	N/A
Crosslinked hydrogel (swollen)	339.3 ± 3.3	N/A

Table 3.1 Characteristics of PEG-NH_2 hydrogel

3.4.3 Crosslink density and distance between crosslinks

The molecular weight between crosslinks, M_c, and average mesh size of the swollen gel, ξ, are important in predicting how the RGD-star conjugates will interact with the gel. Since these hydrogels are intended as substrates for the immobilization of star PEO-RGD conjugates of average diameter ~ 30 nm, it is important to measure the mesh size of the hydrogel, to determine whether or not the conjugates will be able to bind only at the surface of the gel, rather than diffusing down into the bulk, where they would be unavailable for receptor binding, as shown in Figure 3.5.

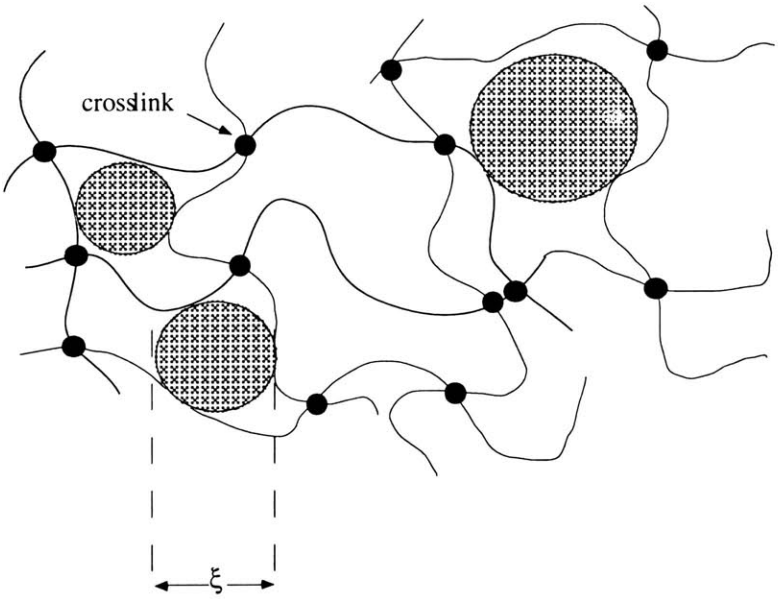

Figure 3.5 Cross-linked structure of hydrogels, showing average mesh size, ξ. Adapted from [76]

The measured thicknesses of the swollen and dry networks were used to estimate the volume and weight fractions of polymer in the dried and swollen states, required for these calculations. The thicknesses of six dried (t_{dry}), six relaxed (t_r) and six swollen (t_s) samples were determined, and from those, the respective weights were calculated, assuming that the dried PEO layer has collapsed down to a bulk density, ρ_{PEO} of 1.072 g/cm^3, and taking the volume of water in the swollen hydrogel as the difference between the dried and swollen volumes. Since the deformation of the hydrogels is expected to be constrained in the plane of the coverslip due to their attachment to the rigid substrate it was assumed, for the purposes of these calculations, that the hydrogels underwent uniaxial deformation, swelling only in the direction perpendicular to the surface of the coverslip when allowed to equilibrate in water. The average weights and volumes of polymer and solvent, as well as their respective weight and volume fractions are calculated shown in Table 3.2.

	Dried gel	**Swollen gel**
Weight PEO (μg)	3.737	3.737
Weight water (μg)	0	82.855
Weight fraction PEO	1	0.044
Weight fraction water	0	0.956
Volume PEO (μl)	3.486	3.486
Volume water (μl)	0	82.855
Volume fraction PEO	1	0.040
Volume fraction water	0	0.960

Table 3.2 Weight, volume, and weight and volume fractions of polymer in dried and swollen hydrogels

The volume fraction of polymer obtained in the swollen gel is roughly four times of that obtained by Dennison [70] at the same radiation dose and initial PEO concentration. This suggests that the hydrogels prepared by Dennison underwent a greater amount of swelling than did those prepared in this study. The difference is probably due to the constrained swelling taking place in the bound hydrogels, as the irradiation effects are probably the same for supported as for unsupported gels, and the crosslink density should be the same in both cases. Since the hydrogels are covalently grafted to rigid substrates, there is probably little or no expansion taking place in the plane of the coverslip, increasing the elastic retractive forces in that plane over those seen in unsupported gels. The most significant swelling in these gels probably takes place perpendicular to the hydrogel surface, hence the simplifying assumption is made that the hydrogel is undergoing uniaxial swelling.

Mesh size was estimated for these hydrogels by two different methods. First, Lopina et al. [69] and Dennison [70] have found that the concentration of radiation-induced crosslinks, μ_r, is relatively insensitive to the molecular weight and concentration of the polymer in crosslinking solution (at radiation doses between 2 and 20 Mrad) and depends only on the administered radiation dose, according to the following relation:

$$\mu_r = 1.22\,D - 1.83 \qquad (2)$$

where μ_r is the crosslink concentration in the relaxed gel, in mM, and D is the radiation dose in Mrad. Using this relation, the density of crosslinks was calculated to be 0.61 mM. The average distance between crosslinks, s, may then be estimated as:

$$s_r = [1 / (\mu_r)]^{1/3} \quad (3)$$

The average distance between crosslinks in the relaxed state was thus approximated at 14 nm. To estimate the average distance between crosslinks in the swollen gel, we use the following:

$$s_s = s_r \left(\frac{V_{2,r}}{V_{2,s}} \right)^{1/3}$$

and obtain a value of ~ 15 nm, smaller than the expected diameter of hydrated PEO-RGD conjugates

The second technique follows the method of Canal [76], and requires the estimation of the molecular weight between crosslinks, M_c, from swelling measurements. Bray has evaluated M_c from swelling measurements for the case of affine deformation [77]. Using the same methods, an expression for the molecular weight between crosslinks can be derived for hydrogels undergoing uniaxial deformation. The derivation starts from the Flory relationship for the free energy change in a crosslinked network on swelling [78]:

$$\Delta F = \Delta F_{mix} + \Delta F_{el} \quad (4)$$

where ΔF_{mix} is the free energy change on mixing with the solvent, and ΔF_{el} is the change in elastic retractive force due to swelling. The criterion for equilibrium is:

$$\mu_1 - \mu_1^0 = \frac{\delta \Delta F}{\delta n_1} = 0 \quad (5)$$

where μ_1 = chemical potential of water in the swollen hydrogel

μ_1^0 = chemical potential of pure water

n_1 = number of moles of water taken up during swelling

Flory obtained the following expression for the mixing component:

$$\Delta F_{mix} = kT\left[n_1 \ln(V_{1,s}) + \chi_1 n_1 (V_{2,s})\right] \tag{6}$$

where: $V_{2,s}$ = volume fraction of PEO in the swollen hydrogel

$V_{1,s}$ = volume fraction of water in the swollen hydrogel

χ_1 = PEO-water interaction parameter = 0.43

Since $V_{2,s}$ and $V_{1,s}$ are functions of n_1, differentiation yields the following:

$$\frac{\delta \Delta F_{mix}}{\delta n_1} = \left[\ln(1 - V_{2,s}) + (V_{2,s}) + \chi_1 (V_{2,s})^2\right] \tag{7}$$

To calculate ΔF_{el}, we assume that $\Delta H_{el} = 0$. Hence,

$$\Delta F_{el} = \Delta S_{el} = S_{swollen} - S_{relaxed}$$

$$= \frac{kT\upsilon_e}{2}\left[\alpha_x^2 + \alpha_y^2 + \alpha_z^2 - 3 - \ln(\alpha_x \alpha_y \alpha_z)\right] \tag{8}$$

where α_x, α_y, α_z are the strains is the x- y-, and z-directions, respectively, and υ_e is the number of effective subchains, given by [78]:

$$\upsilon_e = \upsilon\left(1 - 2\frac{M_c}{M_n}\right) \tag{9}$$

and υ is the total number of subchains. Assuming uniaxial deformation, that is $\alpha_x = \alpha_y = 1$

$$\Delta F_{el} = \frac{kT\upsilon_e}{2}\left[\alpha_z^2 - 1 - \ln(\alpha_z)\right]$$

and

$$\alpha_z = \frac{t_s}{t_r} = \frac{t_{dry} + n_1\dfrac{V_1}{\pi r^2}}{t_r}$$

where V_1 is the molar volume of water, r is the radius of the coverslip.

Differentiation yields:

$$\frac{\delta\Delta F_{el}}{\delta n_1} = \frac{kT\upsilon_e}{2}\left[\frac{V_1}{V_r}\right]\left[2\alpha_z - \frac{1}{\alpha_z}\right] \tag{10}$$

where V_r is the volume of the gel in the relaxed state.

Combining equations (9) and (10), and solving for M_c:

$$\frac{1}{M_c} = \frac{2}{M_n}\frac{v}{V_1}\frac{[\ln(1-V_{2,s}) + V_{2,s} + \chi_1 V^2{}_{2,s}]}{V_{2,r}\left(\frac{t_s}{t_r} - \frac{1}{2}\frac{t_r}{t_s}\right)} \qquad (11)$$

where: M_n = number average molecular weight of PEO = 20,000

v = specific volume of bulk PEO = 0.933 cm^3/g

which gives an average molecular weight between crosslinks of 3,150. Hydrogels are predicted to form at values of M_c between 1500 (below which scission dominates crosslinking [70]) and $2/M_n$ = 10,000 (equivalent to an average of one crosslink per PEO chain). Therefore, bound hydrogels have a relatively tightly crosslinked structure. This is probably due to the low initial volume fraction of PEO in the irradiated solution, since at a given radiation dose, the total number of crosslinks formed is expected to be constant. The result is supported by the relatively low degree of swelling, as evidenced by the small difference between the polymer volume fractions in the relaxed and swollen hydrogels.

The r.m.s. end-to-end distance, r_o, of the unperturbed (dried) chain segment between crosslinks can then be determined using the following:

$$(\bar{r}_0{}^2)^{1/2} = \left(\frac{2M_c}{M_r}\right)^{1/2} C_n{}^{1/2} l \qquad (12)$$

where l is the average bond length (taken as 0.147 nm), M_r is molecular weight of the PEO repeat unit (= 44), and C_n is the characteristic ratio (= 4 for PEO). This gives an r.m.s.

end-to-end distance of 3.5 nm. Then the mesh size for the swollen hydrogel, ξ, is determined from:

$$\xi = V_{2,s}^{-1/3}(\bar{r}_0^{\,2})^{1/2} \tag{13}$$

This method yields a mesh size of 10.3 nm, comparable to the mesh size obtained from the dosage calculation, and significantly smaller than the diameter of the star PEO-RGD conjugates to be immobilized in Chapter 4. Lopina, using a slightly different method for calculating ξ obtained essentially the same result [79].

3.4.4 PEO graft density

Grafting density, σ, was also determined for these substrates, by the method described in Chapter 2. At a dried hydrogel layer thickness of 13 nm, we arrive at a PEO graft density of 4.19×10^{13} molecules/cm^2, or 4.19×10^{-3} molecules/Å^2. This is equivalent to the grafting of 1.90 ether units per Å^2. As expected, the ether unit density of linear chains of molecular weight 20,000 obtained in Chapter 2 is significantly lower: 0.146 ether units/Å^2.

As expected, electron beam irradiation has provided a substantially higher density of PEO on the surface than was attainable by the covalent grafting linear molecules of the same molecular weight. This was accomplished by allowing the PEO molecules to covalently bind to each other as well as to the substrate, allowing a thicker PEO layer to be formed than by surface grafting alone.

3.4.5 Resistance of PEG-NH_2 hydrogels to non-specific cell attachment

Resistance to non-specific cell adhesion is the most critical performance criterion for these hydrogels. As can be seen from Figure 3.6 the hydrogels were able to meet our requirement of complete cell resistance to every cell type examined for 24 hours. It was also observed that cells seeded in wells into which hydrogel-grafted coverslips had been glued failed to attach to the PEG hydrogel, but attached and spread on the surrounding tissue-culture polystyrene within 2 hours. Attachment to polystyrene indicates that the radiation crosslinking process does not create toxic by-products which affect cell behaviour. The cells therefore fail to adhere to the hydrogel surfaces due to the non-adhesiveness of the PEO, and not because of the leaching out of any harmful chemical contaminants into the culture medium.

Further evidence of the superior protein resistance of these hydrogels was seen in a separate experiment, in which hydrogel-coated coverslips were immersed in a solution containing a relatively high concentration (10 μg/ml) of fibronectin (FN) in phosphate-buffered saline (PBS) at room temperature for 24 hours. Since theoretical models predict that grafted PEO can serve merely to delay protein adsorption, and that protein molecules can eventually rearrange the grafted layer to adsorb on the underlying substrate, hydrogel substrates were exposed to FN solution for 24 hours, which is the time scale of a typical adhesion/migration experiment [38]. The FN molecule is rod-shaped, having dimensions of 60 nm x 6 nm [80]. It is therefore unlikely to diffuse into hydrogels of the mesh sizes measured in this chapter. The only possible interaction for these protein molecules with the hydrogel is therefore the adsorption at the surface, which would likely lead to cell adhesion, spreading and reorganization of the FN into fibrils as seen on tissue culture treated dishes with adsorbed FN [42]. Fibronectin is a common matrix protein, secreted by

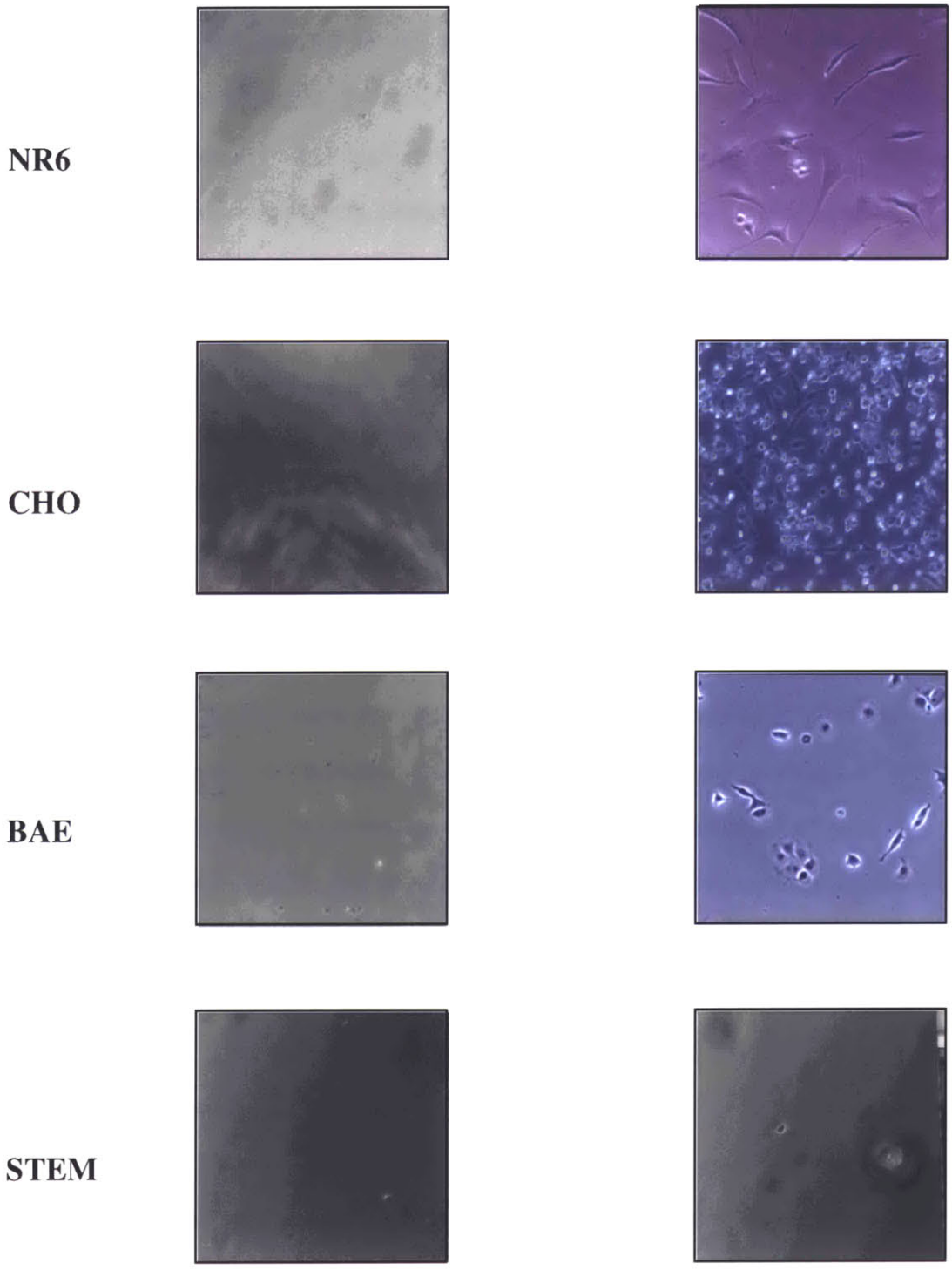

Figure 3.6: Cell responses to PEO hydrogel surfaces after 24 hours

many cell types and involved in cell adhesion and spreading, and its adsorption on the hydrogel substrates would probably obscure specific interactions with immobilized biomolecules. Adsorption of high levels of FN for 24 hours prior to the seeding of cells was therefore considered a very stringent test for the ability of the prepared hydrogels to resist non-specific cell attachment, even under the most severe conditions.

Having allowed 24 hours for FN to adsorb, surfaces were tested for cell adhesion with NR6 cells. As described in Chapter 2, NR6 cells show significant non-specific cell adhesion on a variety of PEG-modified surfaces, hence they were considered a good cell line with which to test the non-adhesiveness of the substrates. After 24 hours' incubation of the substrates with NR6 fibroblasts under serum-free conditions, no cell adhesion was seen, demonstrating the excellent resistance (i) to non-specific adsorption of FN, and (ii) to non-specific cell attachment achieved when PEO is graft coupled to glass substrates in this way. Presumably the increased graft density achieved by the formation of a thin PEO hydrogel is instrumental in preventing the adsorption of serum and endogenous proteins which precede non-specific cell attachment. This thick, dense layer of PEO apparently screens out interactions between proteins and the underlying glass surface, and PEO is itself inert to interactions with proteins.

3.5 Conclusions

A pure, stable and modifiable PEO surface, resistant to non-specific adhesion of a variety of cell types, has been achieved by electron-beam crosslinking of a solution of amine-terminated PEO. PEO hydrogels prepared in this way are covalently grafted to glass coverslips, and present amine functional groups at their surfaces, providing sites for later immobilization of bioactive ligands. Cells plated on these surfaces showed no signs of attachment and spreading for over 24 hours, providing an inert background which can be

used to examine specific receptor-ligand interactions. These gels make it possible to quantitatively study effects of concentration and distribution of ECM fragments over relatively long periods of time, difficult to do in the past because of non-specific adsorption of proteins to other model surfaces.

CHAPTER 4. PRESENTATION OF CLUSTERED ADHESION LIGANDS AGAINST INERT BACKGROUND

4.1 Introduction

Investigating the relationship between chemistry and physics at biomaterial surfaces and the cellular response is currently an area of great activity. Several simplified systems have been developed, which aim to simulate the essential features of the extracellular matrix by immobilizing natural or synthetic ligands on various substrates. In particular, the advances in understanding the interactions between integrin receptors and peptides containing the RGD sequence have stimulated considerable interest in the development of synthetic biomaterials which promote cell attachment and growth [81]. Most studies, however, aim to measure the quantitative response of cells to variations in ligand density *at uniform distribution* [16], [82], [31]. In this study, bioactive surfaces were prepared on which surface density and spatial distribution are simultaneously varied.

4.2 Experimental Design

This objective of the work described in this chapter was to prepare a series of well-defined clustered ligand surfaces, as well as a parallel series of surfaces on which ligands were uniformly distributed (equivalent to 1 ligand per cluster). To the non-adhesive hydrogel substrates previously described, we wished to tether the adhesion ligand RGD in islands, or "clusters", each island consisting of between 1 and 20 RGD molecules, and immobilized at spacings of 0 to 500 nm apart (see Figure 4.1 for a schematic representation). Spatial control on this scale has not previously been reported; various researchers have created

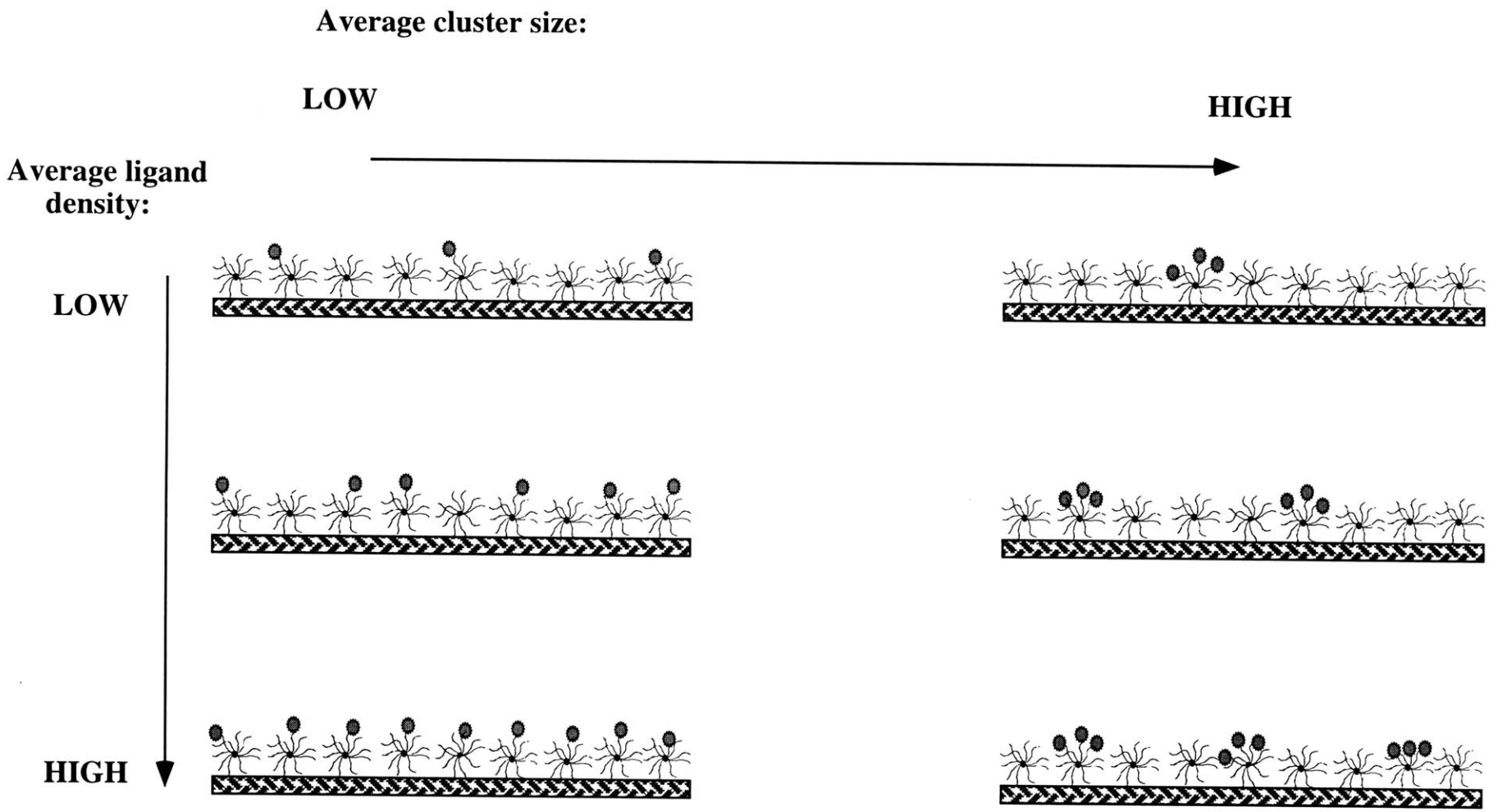

Figure 4.1: **Schematic represeantation of the means of varying RGD cluister size and spacing on PEO surfaces**

RGD islands 3 μm in diameter [83], which may be comparable to or larger than the size of a focal contact. Our objective here, however, is to control ligand presentation at the molecular level, varying the density and distribution of adhesion ligands on substrates with the aim of controlling receptor clustering, and therefore cell behaviour. In addition, we wish to determine whether there exists a minimalistic density and configuration of RGD for controlling cell behaviour.

A modular, or flexible approach was taken to the design of the desired model bioactive substrates which specifically support integrin-mediated cell adhesion. Surfaces were viewed as consisting of three separate components, each of which could be modified or replaced independently. The first component, a completely "bioinert" substrate, which was absolutely non-adhesive to cells for 24 hours or more has been discussed in Chapters 2 and 3. Second, the ligand of interest must be immobilized in the correct orientation and conformation, both of which can strongly affect its recognition specificity [17], [82]. For this reason, the third component, a flexible tether, linking ligand to substrate was considered necessary.

In order to achieve the desired control over the spatial distribution of ligands, RGD peptide molecules have been tethered to bioinert substrates via star PEO molecules. The grafting of ligands to surfaces via star (rather than linear) molecules is expected to offer a high local ligand density, due to the high density of chain ends on the star molecule. Tethering ligands to the surface via the PEO molecule is expected to allow significant diffusive mobility for the RGD molecules, allowing them to assume the correct orientation for binding to the receptors. Furthermore, the use of star PEO as a tether also allows us to create RGD islands at the submicron length scale, below the resolution easily achievable by photolithographic techniques or microcontact printing.

The selection of PEO-RGD coupling chemistry is of extreme importance in the preparation of bioactive surfaces. Coupling agents must be chosen which will provide a highly reactive activated species, and which can form the desired conjugate under relatively mild conditions [64]. Water is often used as the solvent for coupling reactions, as many ligands of interest are biopolymers. At the same time, many conjugations take place by nucleophilic substitution of the amino-terminal of the ligand and the release of some leaving group. Since water is also nucleophilic, the activated sites often become deactivated by hydrolysis. Furthermore, some investigators have observed [41] that secondary and tertiary amines grafted to otherwise poorly adhesive substrates supported adhesion and spreading of fibroblasts, presumably due to electrostatic interactions with cell surface proteoglycans. For this reason, we wish to avoid the introduction of charged spacers between the molecules to be conjugated wherever possible.

The crosslinker selected was 1-ethyl-3-(3-dimethylaminopropyl)carbodiimide hydrochloride, or EDC. EDC reacts with carboxylic acids to form a highly unstable *O*-acyl isourea, which has a lifetime of less than 1 second in aqueous solution, but the active carboxyl may be stabilized by the addition of *N*-hydroxysulfosuccinimide, or sulfo-NHS, which forms a more stable succinimidyl ester [84]. This system was chosen for a variety of reasons. First, EDC is known as a "zero-length" crosslinking agent, that is it facilitates conjugation of two molecules in solution without the introduction of a spacer. The ligand would therefore be coupled directly to the PEO via an amide bond, without the introduction of secondary amides or fluorinated groups. Second, the NHS-active ester, when hydrolyzed, decays to the original carboxyl group, which may be re-activated in aqueous solution by EDC/Sulfo-NHS, if required. This is of extreme importance, since our need to know both RGD cluster size and cluster spacing necessitates the activation and coupling of star PEO twice: once with RGD in aqueous solution and a second time with the amine

groups at the surface of the hydrogel. In other systems with which we are familiar, for example, the tresyl chloride activation of terminal hydroxyl groups, the preparation of tresylate is done under strict anhydrous conditions, and can be very time-consuming. The ability to dissolve and activate PEO-RGD conjugates in aqueous solution simplifies the surface preparation considerably. In addition, the amide linkage thus formed is very stable in water; more stable to hydrolysis than an ester linkage, for example.

4.3 Materials and Methods

4.3.1 Molecular weight determination for star PEO

Star PEO, lot 460 was obtained from Shearwater Polymers (Huntsville, AL) by the "core first" method, starting from divinyl benzene (DVB) cores [85] [86]. Since the PEO arms are grown from the cores by anionic polymerization, it is typically assumed that all of the arms are of the same length, and that any polydispersity arises from distribution of sizes of the DVB cores, expected to lead to variability in the number of arms per molecule. The star PEO used here (designated star PEO 460) had an average of 60 arms per molecule, and an arm molecular weight of 9,100, per the manufacturer.

The molecular size and molecular weight distribution were determined for the star polymer before and after functionalization, (i) to characterize the distribution in sizes and functionalities of the as-received polymer, and (ii) to ensure that the carboxylation chemistry did not have any destructive effects on the polymer molecules. Gel permeation chromatography measurements were taken by Diane Rintzler Yen on a Waters Model 150C instrument, containing two Tosohaas TSK gel columns (G6000PW and G4000PW) in series. The molecular weights present in the eluant sample are determined by passing the sample through a Wyatt Dawn Model F laser photometer, then the concentrations of each

fraction are determined using the Waters Model 150C refractive index detector. 3 mg/ml solutions of star PEO 460, dissolved in an aqueous solution containing 0.02 percent (w/v) sodium azide and filtered using a 0.45 μm filter were analyzed. The differential refractive index increment, *dn/dc* was assumed to equal that of linear PEO, which is 0.135 at a wavelength, λ, of 632.8 nm. The system was controlled and the data analysed using a software package designed for use with the Wyatt light scattering system, run on a 386 PC.

4.3.2 PEO functionalization

As received from the suppliers, star PEO molecules are terminated by hydroxyl groups. The end groups of the PEO tethers were first converted to the carboxyl functional group which could be made to react, both with the ligand to be immobilized, and with the substrate, by a method similar to that described by Royer [59]. Details of the carboxylation procedure are given in Appendix A.

4.3.3 Peptide preparation

The RGD peptide used in this work, YGRGD is shown schematically in Figure 4.2. As can be seen from the structure, there are charged guanidine and carboxyl groups in the side chains of arginine and aspartic acid respectively, which are capable of participating in the chemical reaction desired at the N- and C-termini. These amino acids are therefore supplied with protected arginine and aspartic acid side chains (YGR(Pmc)GD(tBu), American Peptide Company), which can be removed after the synthesis reaction, based on recommendations of Lin et al. [82]. The tyrosine residue was supplied unprotected as a site for radiolabeling; unprotected tyrosine does not participate in any of the activation or coupling reactions.

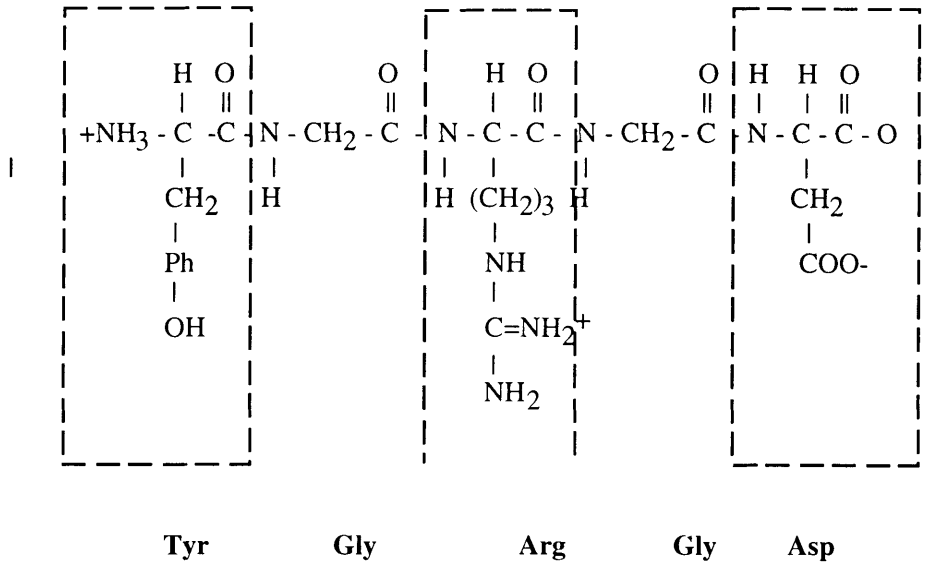

Figure 4.2 Primary structure of adhesion peptide YGRGD

The peptide was labeled for quantitation by iodination of the tyrosine residue, using a variation on the method of Massia et al [14]. Briefly, 20 µl of a 1 mg/ml solution of protected peptide, dissolved in 2-[N-morpholinoethane sulfonic acid] buffer (hereafter referred to as MES buffer, Sigma Chemical Company) was reacted with 2 mCi $Na^{125}I$ using the Iodobead method [87] for 15 minutes at room temperature. Iodination protocol is given in Appendix A. Labeled peptide was separated from free iodine by reverse-phase chromatography, loading the mixture on a C_{18} Sep-Pak cartridge (Waters), which had been equilibrated prior to loading, first with a solution of trifluoroacetic acid (TFA) and water in methanol (1 vol%: 19 vol%: 80 vol%, respectively), and then with PBS. Unincorporated iodine was flushed first from the cartridge using a 1% solution of TFA in water, then the peptide was fractionated using successive solutions of TFA and water in methanol, from to 1:89:10 to 1:79:20, and so on, increasing the methanol concentration by 10 vol% each

time) until a mixture of composition 1:19:80 was reached. The fractions containing peptide were pooled.

The radiolabeled peptide solution was adjusted to a pH of 6 by the addition of 1N sodium hydroxide, and stored at 4 °C until use. Because of the believed instability of iodinated species [88] (radiolysis of water molecules generates free radicals, which in turn may attack the already weak carbon-iodine bond), the RGD samples were typically used within a week of iodination.

4.3.4 PEO-RGD conjugation

Star PEO-carboxylate was dissolved in MES buffer, pH = 6.1 to a concentration of 7e-7 mol of (total) chain ends per ml. Chain ends were activated by adding a 1.5-fold molar excess of 1-ethyl-3-(3-dimethylaminopropyl)carbodiimide hydrochloride (EDC) (Pierce Chemical) and a 2-fold molar excess of N-hydroxysulfosuccinimide (sulfo-NHS) (Pierce Chemical) over (total number of) chain ends, with stirring, for 20 min.

RGD peptide was added to the reaction mixture, in the molar ratios indicated in Table 4.1. The conjugation reaction was allowed to proceed for 12 hours. The PEO-ligand conjugate was separated from unreacted ligand, excess crosslinker and buffer salts by dialysis against distilled water, with 4 to 6 water changes until the radioactivity detected in the water decreased to background (Pierce dialysis cassettes, MWCO = 10,000). Dialysis against water typically causes the sample solution to take on a relatively large volume of water; the volume after dialysis is usually 250 to 300% of the initial volume. The product was frozen at -20 °C, lyophilized and stored at -20 °C until further use. Quantitation of the product was achieved by dissolving a known mass of PEO-RGD conjugate in PBS, and measuring its activity on a Packard gamma counter.

SAMPLE	MOL RATIO RGD:PEO	PEO MASS (mg)	QUANTITY OF PEO (mol)	RGD MASS (mg)	QUANTITY OF RGD (mol)
#1	1.5	30	5.36E-08	0.117	1.34E-07
#2	3	30	5.36E-08	0.234	2.68E-07
#3	6	30	5.36E-08	0.469	5.36E-07
#4	18	30	5.36E-08	1.406	1.61E-06
#5	26	30	5.36E-08	2.109	2.41E-06
#6	35	30	5.36E-08	2.812	3.21E-06

Table 4.1: RGD-PEO ratios during conjugation in aqueous buffer

4.3.5 Surface immobilization

In order to achieve the desired variation in spacing between ligand clusters, PEO-ligand conjugates were immobilized on gel substrates from solutions containing a mixture of unmodified and ligand-modified star PEO. 5 % w/v solutions of the PEO-RGD conjugates were prepared in MES buffer. At the same time, a 5 % w/v solution of unmodified star PEO was prepared. Carboxyl-functional chain ends were activated with EDC and Sulfo-NHS, as before. The two solutions were mixed, in the proportions shown in Table 4.2. Then 125 µl aliquots of activated PEO-RGD were coupled to each substrate (18 mm hydrogel-grafted glass coverslip), and the coupling was allowed to proceed for at least 12 hours in a humid chamber at room temperature. Substrates were rinsed several times in deionized water, then immersed for four hours in a 50 mM solution of Tris-HCl, pH = 6.1, to block any remaining activated chain ends. Finally, coverslips were rinsed again in water.

SAMPLE	[PEO-RGD*], mg/ml	[PEO], mg/ml	% PEO-RGD*	Vol. (PEO-RGD*), ml	Vol. (PEO), ml
# 1	50	0	100	0.750	0.000
# 2	10	40	20	0.150	0.600
# 3	5	45	10	0.075	0.675
# 4	2.5	47.5	5	0.038	0.713
# 5	1	49	2	0.015	0.735

Table 4.2: Modified-unmodified PEO ratios during immobilization

Deprotection of the arginine and aspartic acid side chains was performed by immersion of substrates in a cleavage mixture known as "Reagent K" [89] for one hour. The protocol for deprotection is listed in Appendix A.

In order to verify that the deprotection mixture was not destructive to the PEO chains, a solution of linear PEO (M.W. = 20,000, Fluka) was prepared in "Reagent K", and analyzed by high performance liquid chromatography (HPLC) immediately after dissolution, and again after one hour. HPLC data were collected by Jeffrey Sperinde. No significant differences were observed between chromatograms, indicating that the molecular weight of the PEO sample had not changed significantly. It was therefore deemed safe to immerse the prepared surfaces in the solution for one hour. In a second control, hydrogel-coated coverslips were immersed in the deprotection solution for one hour. The coverslips were rinsed thoroughly in water, and NR-6 fibroblasts were seeded on the surfaces in serum- containing medium. After 24 hours, cells had not attached, suggesting that the integrity of the hydrogels had not been compromised.

To determine the ligand density and cluster spacing, bioactive surfaces were prepared using iodinated RGD peptide. Three coverslips at each cluster size and spacing were crushed and their activity measured on a Packard gamma counter.

4.3.6 Validation of covalent linkages

The following tests for non-covalent association between the star PEO and the RGD peptide, and between PEO-RGD conjugates and the gel substrates were performed. First, RGD peptide and star PEO 460 and were dissolved in MES buffer, at a 35 to 1 molar ratio, stirred for 12 hours *without EDC/Sulfo NHS crosslinker.* The mixture was purified by dialysis, as usual, and lyophilized. Then the specific activity of the recovered product was measured using a gamma counter.

In a second control experiment, star PEO-RGD conjugate, containing 9 moles of PEO per mole of star molecules was dissolved in Tris-HCl (pH of 6.1) at a concentration of 50 mg/ml, and allowed to stir for 20 minutes, to allow the Tris solution to deactivate any active chain ends remaining from the first conjugation step. The solution was then coupled to gel-coated coverslips in the usual fashion, allowed to bind for 12 hours, then rinsed thoroughly in water and counted for radioactivity.

4.4 Results

4.4.1 Characterization of star molecules

The typical yield of carboxylated polymer obtained from this reaction (the amount of polymer recovered after carboxylation and purification) is approximately 98%. The extent of conversion of chain ends was determined to be roughly 50% (see Appendix B). GPC

measurements revealed that the as-received polymer had an extremely broad molecular weight distribution with a polydispersity of approximately 9.2, as determined by the instrument software, based on monodisperse star PEO standards (see Figure 4.3). As can be seen from the data, the carboxylation reaction does not appear to cause a change in the positions of the peaks, although there are some shifts in the relative peak heights, especially at high elution volumes (low molecular weights).

Examination of the light scattering data in Figure 4.3 shows the various molecular weights present in the as-received polymer. Refractive index data indicate the weight fractions of each species. From comparison with monodisperse star PEO standards, a more detailed picture of the molecular weight distribution of star molecules may be obtained. Using the results of Yen [90]:

$$\log (MW) = (-0.55 * \text{elution volume}) + 14.8 \qquad (3)$$

which is Yen's result for a monodisperse star PEO having arm molecular weights of 10,000. This equation was used to estimate the molecular weight distribution of star PEO 460, before and after end-group modification, assuming a constant arm molecular weight of 9100.

Measurement of the peak areas in the refractive index curve yielded the information in Table 4.3. The first peak in the table represents a very high molecular weight entity, present in trace amounts. This is attributed to the presence of unusually large aggregates the divinyl benzene (DVB) monomer which have been observed to form in cases in which the ratio of DVB to initiator is higher than optimal, or when the DVB and initiator are mixed too quickly [86]. As this component is present at such low concentration, it was assumed unlikely to affect the conjugation and immobilization reactions, and was omitted from consideration. The fourth peak represents a very low molecular weight impurity, probably unreacted DVB, initiator or potassium salts. This fraction appears to increase in weight

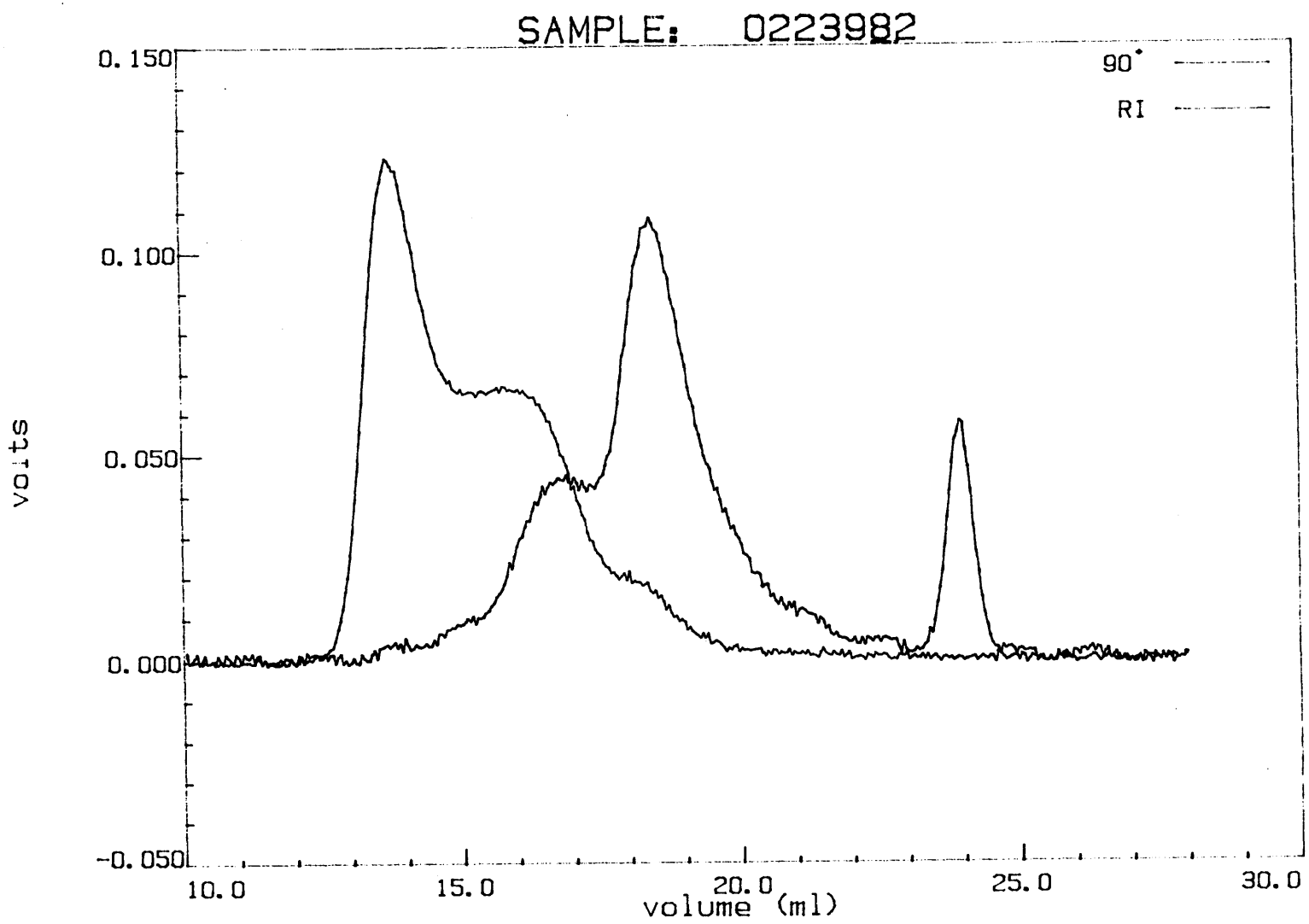

Figure 4.3(a) Gel Permeation Chromatogram of Star PEO 460, as received

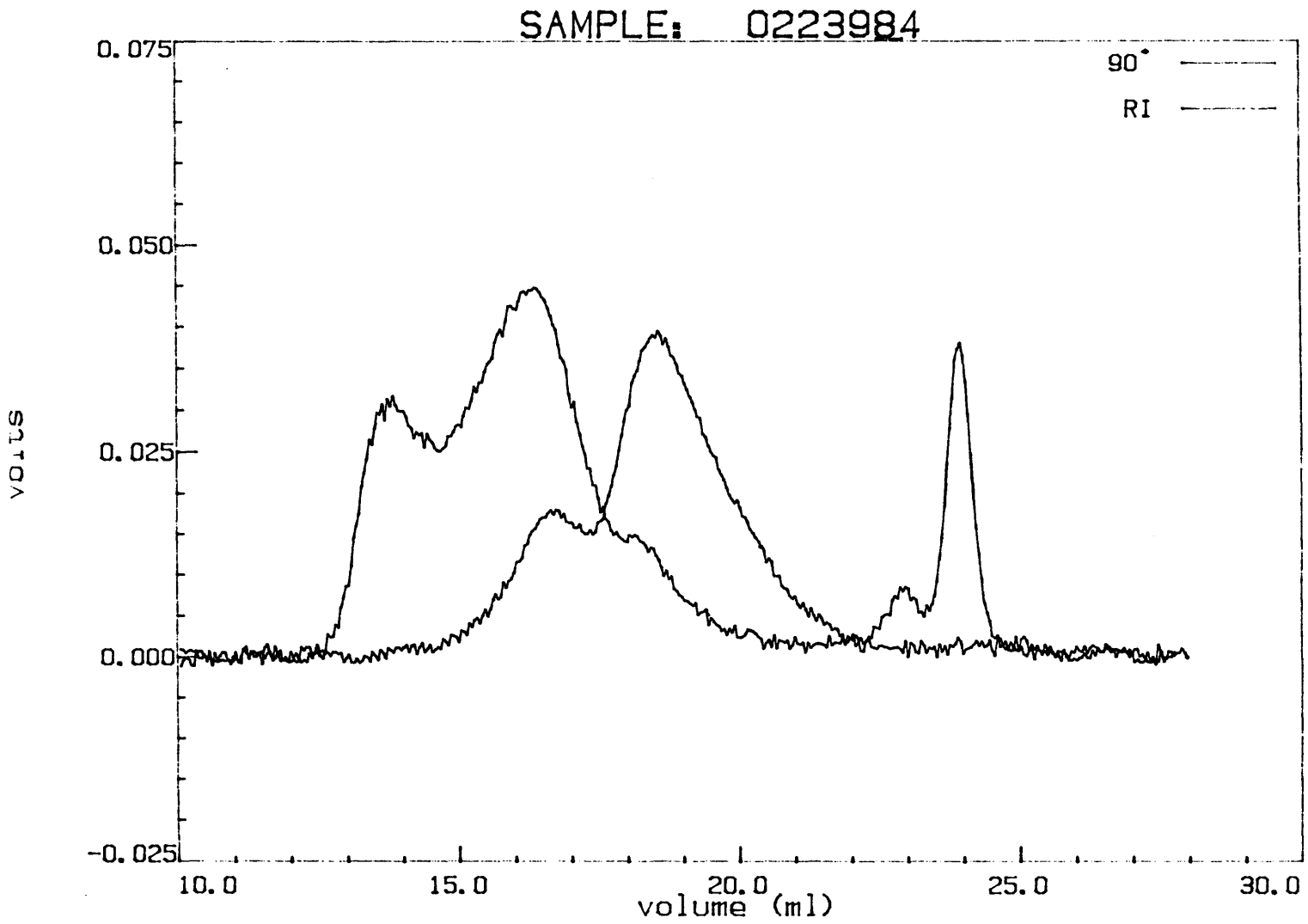

Figure 4.3(b) Gel Permeation Chromatogram of Star PEO 460, post carboxylation

fraction after carboxylation from 11% to 16%, possibly due to the introduction of the bromine- and potassium-containing side products or buffer salts during the carboxylation. As these were not expected to participate in the conjugation and immobilization reactions, they were excluded from the estimation of the effective PEO molecular weight .

Elution volume (ml)	Equivalent star molecular weight	weight %, as received	weight %, post carboxylation
13.7	1.92×10^7	negligible	negligible
16.7	4.30×10^5	32	28
18.3	5.51×10^4	57	55
23.8	53	11	17

Table 4.3 Molecular weights of star PEO fractions obtained from GPC measurements

The majority of the polymer sample (85 to 90%), consists of two molecular species: one of molecular weight 430,000, which would correspond to a star of 48 arms (at M(arm)= 9,100), and a second, present at a significantly higher concentration, of molecular weight 55,000, or a star of 6 arms. Those two peaks were averaged to obtain an effective molecular weight for the useful fraction which can be used in further calculations. Using instrument software to estimate, a weight-average molecular weight of 316,000 was obtained, which would correspond roughly to a 35-arm star molecule (at M(arm) = 9,100), on average.

4.4.2 Cluster size determination

The molar ratio of RGD peptide to star PEO obtained by this technique is shown in Figure 4.4. As can be seen from the figure, there is a steady increase in the number of RGD

molecules coupled to each PEO molecule as the concentration of RGD in the coupling solution increases until a plateau is reached at about 9 - 10 RGD molecules per star. Between 0.2% and 2 wt % of RGD was obtained in the final product from the range of initial molar ratios in solution. Typically, 75 to 80% of the polymer was recovered after conjugation and purification.

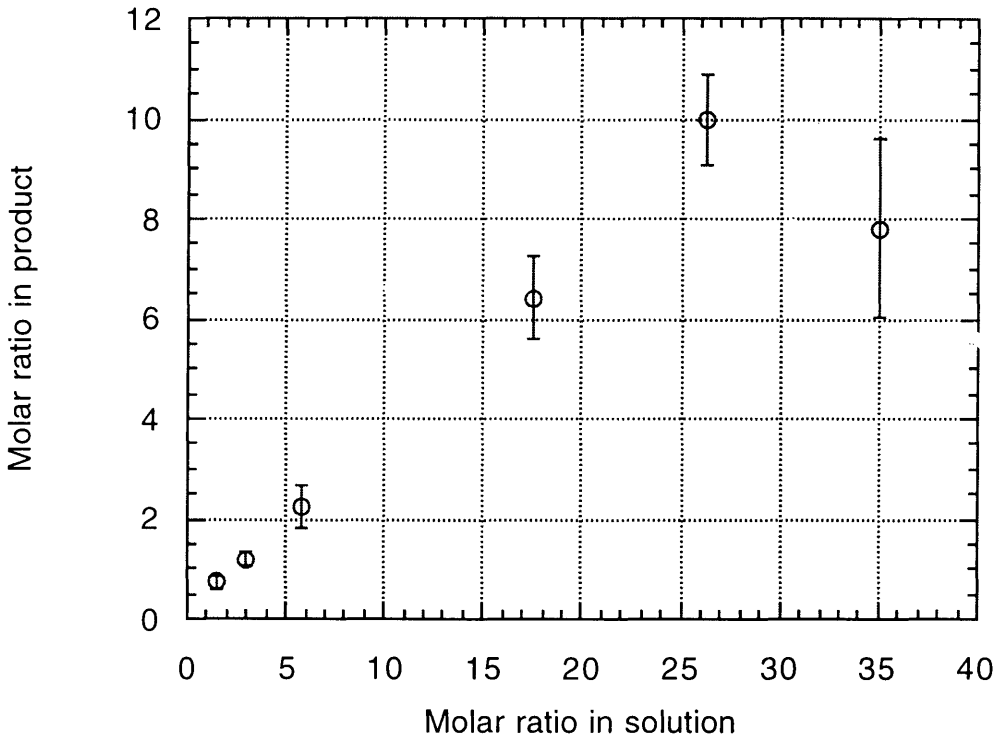

Figure 4.4 Average molar ratio, RGD to star PEO

4.4.3 RGD density determination

The average density of RGD, measured by radiolabeling the peptide, is shown in Figure 4.5. As can be seen from the figure, by varying the average number of RGD peptide

molecules conjugated to each star molecule, and by varying the proportions of modified and unmodified star molecules, we can achieve control over the average ligand density, varying the number of RGD peptide molecules per unit area over two orders of magnitude.

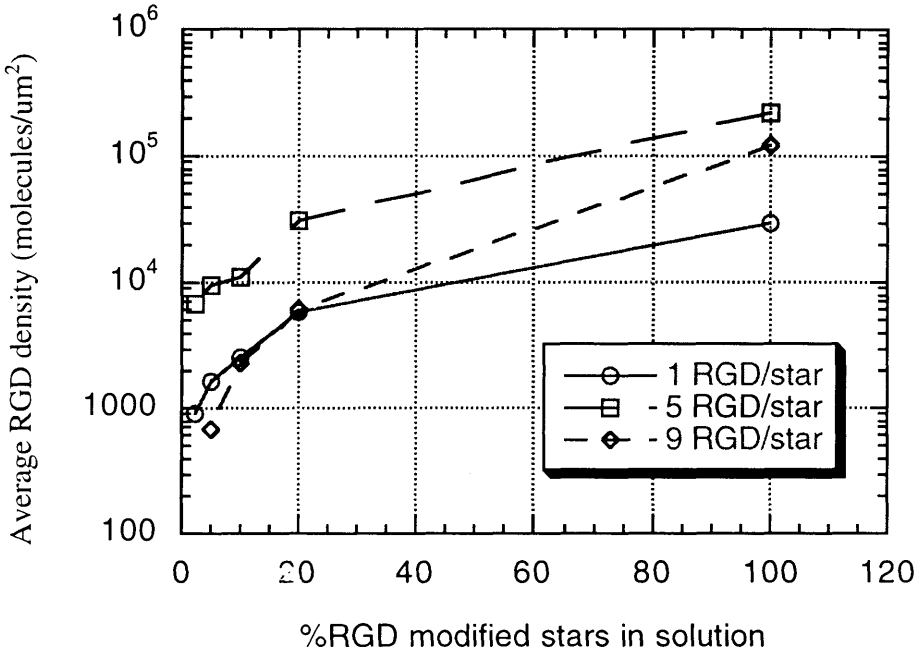

Figure 4.5: Average ligand density on tethered RGD surfaces

4.4.4 Controls for non-specific association

The results of the two control experiments described in section 4.3.5 are shown in Figures 4.6 and 4.7. Figure 4.6 shows the RGD to PEO ratio obtained when RGD peptide is combined in MES solution at a 35 to 1 molar ratio, either in the presence or in the absence of EDC and Sulfo-NHS. The data indicate that there is only very slight non-covalent association between the star molecules and the peptide- about 2% of the PEO-RGD product

contains non-covalently linked RGD. The free RGD may have become entangled in the arms of the star PEO molecules, and though unbound, it may be unable to separate from the star molecules during dialysis.

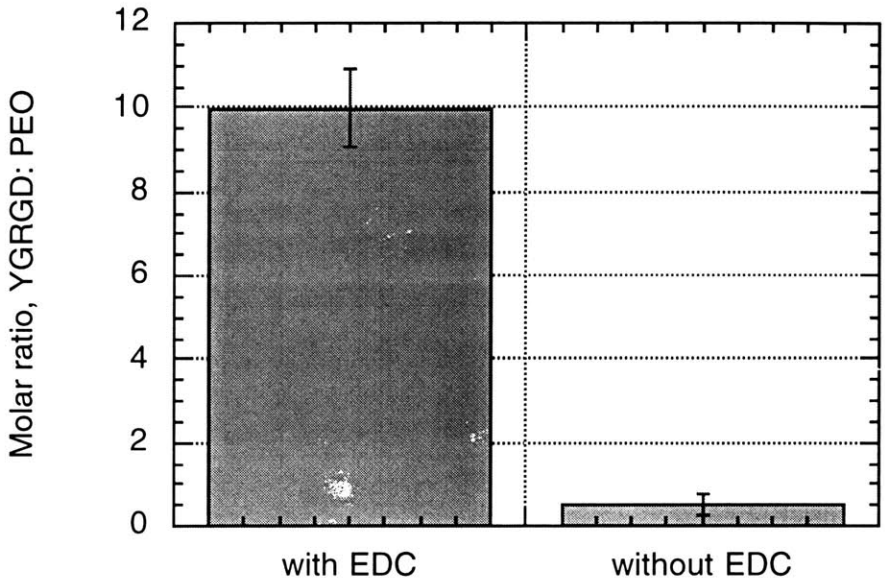

Figure 4.6: Average ratio of star PEO to RGD obtained with EDC/Sulfo-NHS (n = 3) or without EDC/Sulfo-NHS (n=2).

Figure 4.7 shows the surface RGD density obtained when PEO-RGD conjugates (a 9:1 molar ratio) are coupled to PEG hydrogel surfaces in the absence of crosslinker. PEO-RGD solutions in this case were prepared using Tris-HCl (pH = 6) as a solvent, to deactivate any chain ends which may have remained reactive after the conjugation step. Again, only a very small amount of non-covalent association is seen: the amount of RGD which attaches to the surface without crosslinker is only ~ 5% of that bound covalently using EDC/Sulfo NHS. It is not clear, however, the percentage of the star RGD

conjugates in the control samples which were not deactivated by Tris-HCl, and which would therefore have bound covalently to the hydrogel substrate without re-activation.

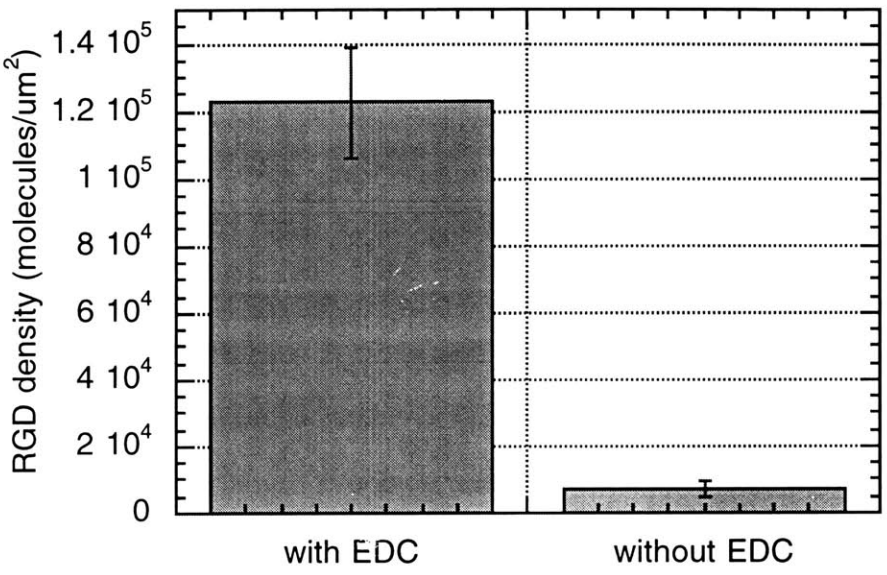

Figure 4.7: Average RGD density obtained with EDC/Sulfo-NHS (n=3) or without EDC/Sulfo-NHS 9 (n=3).

4.5 Discussion

4.5.1 Molecular weight distribution of star molecules

The method by which star PEO molecules are synthesized creates significant polydispersity in the product [86]. Star PEO is currently synthesized by the "core-first" method, preferred because it generates star molecules whose ends can be functionalized. The synthesis

begins with the anionic polymerization of DVB in tetrahydrofuran, using potassium naphthalene as an initiator. This creates crosslinked DVB cores, each having a number of active carbanion sites. The number of active sites per DVB core depends on the amount of time allowed for reaction, and the ratio of DVB to initiator. Ethylene oxide gas in then introduced into the reaction mixture, and its anionic ring-opening polymerization is presumed (as always) to proceed at the same rate from each active site on the DVB core, creating a batch of star molecules in which all the branches are of equal length. Star branches are terminated by the addition of acidified methanol. The total number of arms in the product is assumed equal to the quantity of initiator used, and by determining the amount of ethylene oxide recovered after the synthesis, the amount of ethylene oxide consumed during the reaction is calculated. The ratio of the number of moles of ethylene oxide polymerized to the total number of branches is the polymer yields the number average degree of polymerization of the branches, or the arm length, M_n(arm). To determine the functionality of each star molecule, the weight average molecular weight of the polymer, M_w(star) is determined by light scattering, and the ratio of M_w(star)/ M_n(arm) is taken as f, the average number of arms per star molecule. Comparing the weight average molecular weight of the entire molecule with the number average molecular weight of an individual branch, however, is only meaningful if the stars are monodisperse.

It is widely recognized that the characterization of the star molecules using these techniques is inaccurate. First, the polymerization of DVB is not well controlled, and generates crosslinked DVB cores of broad molecular weight distribution; one would therefore expect these to produce polydisperse star molecules. Hence, the functionality determined by the method described is probably too high [86]. Second, it is not necessarily true that every carbanionic site on the cores generates a star arm. If a significant number of sites fail to initiate PEO branches, the functionality of the star would again be overestimated; in this case the estimate of arm length would also be inaccurate. On the other hand, determination

of the total number of arms by titration of the hydroxyl end groups, performed by Gnanou et al. [86] gave significantly lower values for arm molecular weight than predicted by the DVB/initiator molar ratio. An arm molecular weight for star 460 of 9,100 was reported by the manufacturer, and used in the estimation of the effective molecular weights. Because of the inaccuracy of the determination methods, however, that arm molecular weight may be incorrect.

As mentioned before, the polydispersity of the as-received polymer was 9.2. This denotes a significantly broader distribution of molecular weights than has been encountered in previous work with star PEO (note that star PEO 3510, of f = 72, and M(arm)= 4,500, had a PDI of 3.5 [72]). Yen et al. attempted to narrow the molecular weight of star PEO molecules by fractionation from various salt solutions, and found that the sensitivity of the cloud point to molecular weight essentially disappeared at molecular weights above approximately 250,000 [91]. Gnanou [86] was also unsuccessful at fractionating star PEO. Hence, fractionation was not attempted on the as-received polymer.

The GPC data also indicate that the carboxylation reaction did not change the positions (elution volumes) of the species present; all of the peaks present in the GPC trace of the as-received polymer reappeared in the polymer sample post-carboxylation. No new peaks appeared, indicating that the carboxylation process did not have any deleterious effects on the star molecules.

This distribution may also be used to estimate the range of molecular sizes expected in solution. Using the empirical relation of Bauer et al. [92] for star molecules in good solvents,

$$R_g / R_{g,arm} = 1.37 f^{0.175}, f \geq 3 \quad (4)$$

and calculating the radius of gyration of a linear PEO molecule of molecular weight 9,100 using the Flory equation [78]:

$$(\overline{R}_g^2)^{\frac{1}{2}} = \frac{\alpha l \left(3C_\infty \frac{M}{M_r} \right)^{\frac{1}{2}}}{6^{\frac{1}{2}}} \quad (5)$$

where: α = expansion parameter for PEO in water

l = average bond length = 0.147 nm

C_∞ = universal constant for PEO = 4, [72]

M = PEO arm molecular weight = 9,100

M_0 = repeat unit molecular weight = 44

$$\alpha^5 - \alpha^3 = 2C_M \left(\frac{1}{2} - \chi_1 \right) M \frac{1}{2}, \text{ and} \quad (6)$$

where C_M = 0.175 for PEO in water

χ = 0.43 for PEO in water at 25 °C

Solving Equation (6) for α yields a value of 1.89, and the radius of gyration of the arm is approximately 5.65 nm, and the radius of gyration of the star molecule may be calculated using Bauer's relation in Equation (4). The formula may be used to determine the radius of gyration for each molecular weight fraction found in the polymer sample, as well as for the

average. Values of R_g, are shown in Table 4.4, along with the square of the radius of gyration, R_g^2, a measure of the area of cross-section of the star molecule at each molecular weight.

MW (star PEO)	Number of arms	R_g (nm)	R_g^2 (~ cross section area) (nm^2)
55,100	~ 6	11	121
316,000	~ 35	14	196
430,000	~ 48	15	225

Table 4.4: Range of molecular sizes present in star PEO 460

The packing density of star molecules on a surface is greatly affected by the size differences between stars. As can be seen from the table, the difference in radius between stars at the two extremes of the distribution is approximately 27%. This translates to a difference in the area of cross-section of roughly 70%, and therefore a difference in packing density between the larger and the smaller stars of ~86%. Although the average star size (M.W.= 316,000, R_g= 14) is used in all calculations, it is clear that there will be a distribution of cluster sizes and spacings obtained using this polydisperse polymer. More recently, Yen [90] has synthesized nearly monodisperse star PEO molecules (PDI = 1.15), having between 16 and 256 arms, and arm molecular weights between 2,000 and 20,000. The technique used by Yen, unlike the current practice affords significantly tighter control over the molecular weight distribution, and allows for the selection of desired functionality and arm molecular weight. Should these stars become commercially available, they will yield more precise control over the cluster sizes and spacings.

4.5.2 Average RGD cluster size

In order to vary the molar ratio of RGD to star PEO, the concentration of PEO in the coupling solution was held constant, while that of RGD was varied. Figure 4.4 shows that as the amount of RGD in the reaction mixture increases relative to the amount of PEO, the percentage of star arms derivatized with RGD increases, until a plateau at 9 - 10 RGD molecules per star is reached. The surface area of a (35-arm) star molecule is ~2,500 nm^2, while the area of cross-section (equal to the projected area) of an RGD peptide molecule is estimated at ~7 nm^2. Therefore, over 350 RGD molecules should be able, in theory, to surround a star molecule of that size without crowding. The plateau in Figure 4.4 is therefore not attributed to a limit on RGD coupling due to steric hindrances.

It seems more likely that the plateau in cluster size is caused by the hydrolysis of the NHS-active chain ends in aqueous solution, taking place simultaneously with the conjugation reaction. The half-life of the NHS-active ester at a pH of 6.0 is roughly 40 minutes. If the reaction between star PEO and RGD is diffusion-controlled, then it is possible the NHS-active star chain ends become deactivated before a coupling ratio greater than 10 RGD/star can be reached.

4.5.3 Average RGD density

Figure 4.5 shows the variation in average RGD density obtained as the ratio of modified to unmodified stars in solution was changed. A series of surfaces was prepared using star molecules having only 1 RGD molecule conjugated, as a means of obtaining a series of surfaces on which the RGD peptide was uniformly distributed. Interestingly, at no concentration of PEO-RGD conjugate does the average PEO density on surface with 9-

RGD clusters equal 9 times that on the surfaces with 1 RGD clusters, while those with 5-RGD clusters consistently have about six times the RGD loading as those with 1-RGD clusters. In fact, at lower star-RGD conjugate concentrations, the 9 RGD/star surfaces and the 1-RGD/star

substrates appear to have comparable loadings of ligand. This can most likely be explained in terms of the different reactivities of modified and unmodified conjugate, and the effects of the hydrolysis of the NHS-active ester.

Figure 4.7 shows the three reactions expected to be taking place in the system:

(1) unmodified stars, 50% carboxyl substituted, are covalently attaching to the PEG-NH_2 substrate at a rate R_1.

(2) RGD-modified stars, their modified chain ends unavailable for activation and reaction with the surface must compete with unmodified stars for surface sites on the PEG-NH_2 gel. As the number of carboxyl-terminated arms may be expected to decrease as the number of RGD molecules per star increases from 1 to 5 to 9, their ability of the star molecules to compete effectively for surface sites should similarly decrease. The rate of this reaction is R_2.

(3) hydrolysis of the NHS-active ester at a rate R_3. The half-life of the NHS-active ester at a pH of 6 is approximately 40 minutes [93]. As the degree of modification of the star molecules increases and the number of remaining available arms correspondingly decreases, the rate of hydrolysis is expected to become more significant relative to the rate of binding.

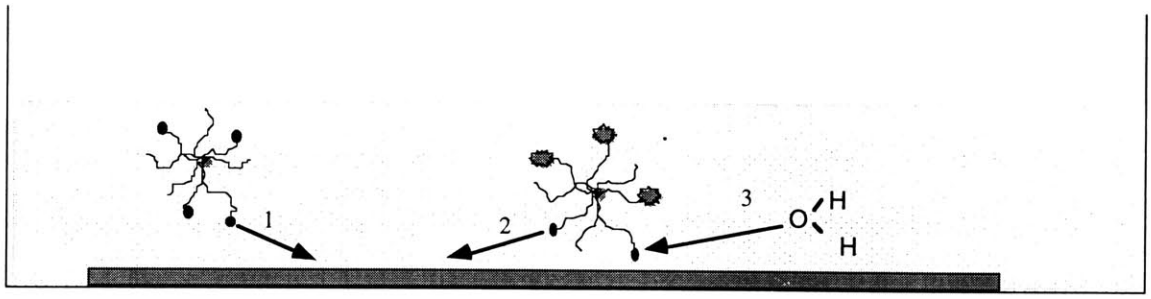

Figure 4.7 Schematic representation of the competing reactions taking place during immobilization of star-RGD conjugates on gel substrates: (1) immobilization of unmodified stars, EDC-activated, (2) immobilization of less-reactive star-RGD conjugates, EDC-activated, (3) hydrolysis of EDC-activated chain ends

It is likely that the relative rates of reaction change with RGD substitution. In the case of unmodified star molecules, approximately 50% of the chain ends have been carboxylated, therefore about half of the arms per molecule can be activated for reaction with the PEG-NH_2 surface. For the 1 RGD/star conjugates, only one arm per molecule has been made unavailable for binding to the substrates. Hence, for the 1 RGD/star conjugates, we assume that $R_1 \sim R_2$, and R_1, $R_2 \gg R_3$. For the 5 RGD/star conjugates, there are fewer arms available after RGD conjugation, hence $R_1 > R_2$, and R_1, $R_2 \gg R_3$. In the case of the 9 RGD/star conjugates, because the number of available carboxyl chain ends is so drastically reduced in comparison with the 1 RGD/star conjugates, it is possible that the sticking probability is significantly reduced, and the binding rate becomes comparable to the hydrolysis rate, that is, $R_1 \gg R_2$, R_3 and $R_2 \sim R_3$.

Therefore, in solutions containing only RGD-modified stars (that is, at 100% RGD-modified stars in solution, $R_1 = 0$), the average RGD density attained on 5-RGD cluster

surfaces is roughly six times that seen on 1-RGD cluster surfaces, because the binding of 5-RGD and 1-RGD clusters can occur faster than hydrolysis can render the conjugates inactive. The average density obtained on 9-RGD/star conjugates is, at most, only approximately four times that on the 1 RGD/star surfaces. Presumably, at the highest degree of substitution, the sticking probability is so reduced that $R_2 \sim R_3$, and the modified stars are not able to attain such high densities before hydrolysis of the NHS-active ester.

A Langmuir model of competitive adsorption [94], with the additional consideration of hydrolysis of the NHS-active esters at the star PEO termini provide a reasonable fit for the data. In cases where there are unmodified stars, the Langmuir model of (non-dissociative) competitive adsorption may be used as a simple way to explain the data. The adsorption isotherm may be written as:

$$\Theta_{star-RGD} = \frac{K_{star-RGD}[star-RGD]}{1 + K_{star-RGD}[star-RGD] + K_{star}[star]} \quad (8)$$

where $K_{star\text{-}RGD}$ = equilibrium constant for binding of star-RGD conjugate

[star-RGD] = concentration of star-RGD conjugate in coupling solution

K_{star} = equilibrium constant for binding of unmodified star PEO

[star] = concentration of unmodified star PEO in coupling solution

If we assume that 1 RGD/star conjugates have the same reactivity as unmodified stars, the ligand-modified stars should bind to the substrate with the same equilibrium constant as their unmodified counterparts, that is, $K_{star\text{-}RGD} = K_{star}$. Therefore, the 1 RGD/star conjugates should be able to bind to the PEG-NH_2 substrate according to their proportion in solution, and equation (8) reduces to

$$\Theta_{star-RGD} = \frac{K_{star}[star - RGD]}{1 + K_{star}([star] + [star - RGD])} \quad (9)$$

This model fits the experimental results quite well, as illustrated in Figure 4.8. If [star-RGD] is expressed in units of "fraction of RGD-modified stars in 5 % (w/v) solution", then the value obtained for K_{star-} is 1.34 x 10^8, which will be taken as $K_{star-RGD}$ for the 1 RGD/star conjugates. In the cases where an average of 5 or 9 RGD molecules have been conjugated to each star molecule, the reactivity of the star-ligand conjugate is probably reduced below that of unmodified stars. Although its carboxyl terminal of the peptide is supplied unprotected, the peptide is particularly hydrophobic because of the presence of the protecting groups. One might expect the peptide-modified chain ends to "bury" themselves in the star molecule, in much the same way as the "stealth" liposome and other biomolecules have their stability *in vivo* enhanced by conjugation to PEO [95].

Since $$K = \frac{k_{ads}}{k_{des}} \quad (10)$$

where k_{ads} = rate of adsorption of molecule on surface

k_{des} = rate of desorption from surface

and we might expect that the rates of the reverse reaction for both modified and unmodified star PEO molecules should be the same, any change in adsorption rate would result in a change in K of similar magnitude. Therefore, for the 5- and 9-RGD conjugates, equation (8) may be solved for $K_{star-RGD}$, using the K_{star} obtained previously.

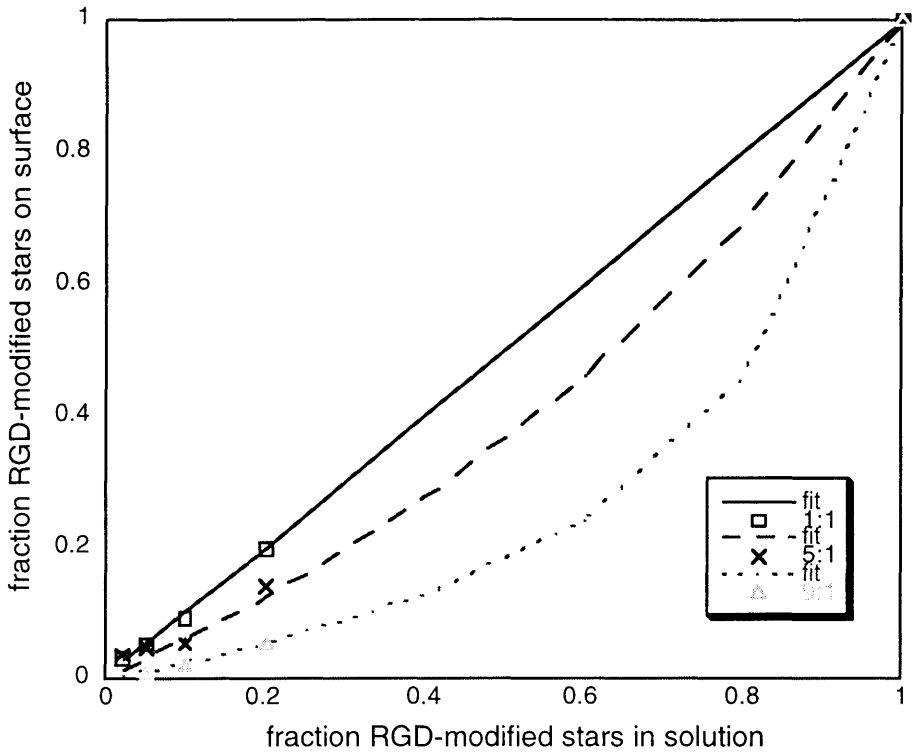

Figure 4.8: Comparison of efficiency of binding of ligand-modified stars

Values of K are tabulated below:

Molar ratio, RGD:PEO	$K_{star\text{-}RGD}$	$K_{star\text{-}RGD}$/ $K_{star\text{-}RGD}$ (1:1)
1:1	1.34×10^{8}	1.00
5:1	7.64×10^{7}	0.57
9:1	2.83×10^{7}	0.21

Table 4.5 $K_{star\text{-}RGD}$ values for 1-, 5- and 9-RGD conjugates, and their magnitudes when normalized to the $K_{star\text{-}RGD}$ for the 1-RGD conjugate

If we assume that out of a total of 35 arms per star molecule (on average) 17 are available for reaction, then we can assume that in the case of 1 RGD/star conjugates, roughly 16 of the 17 arms are available for reaction, so that $K_{star\text{-}} = K_{star\text{-}RGD}$. When an average of 5 RGD

molecules are conjugated to each star, there are 12 arms remaining which can be activated and coupled to the substrate. $K_{star\text{-}RGD}$, would therefore be expected to decrease to 12/17 (~ 70%) of its initial value; the data show a decrease to roughly 60% of the value for the 1-RGD conjugates. When an average of 9 RGD peptide molecules are conjugated per star, there should be 8 remaining arms per molecule (50% of the initial number) to participate in immobilization, however, the $K_{star\text{-}RGD}$ in this case is about 0.21. These $K_{star\text{-}RGD}$ values are lower than might be predicted based strictly on competitive adsorption, possibly because simultaneous hydrolysis of the NHS-active ester reduces the effective reactivity.

Given the average cluster size and RGD density, the average spacing between RGD-modified stars on the surface may be calculated. The results are displayed in Figure 4.9.

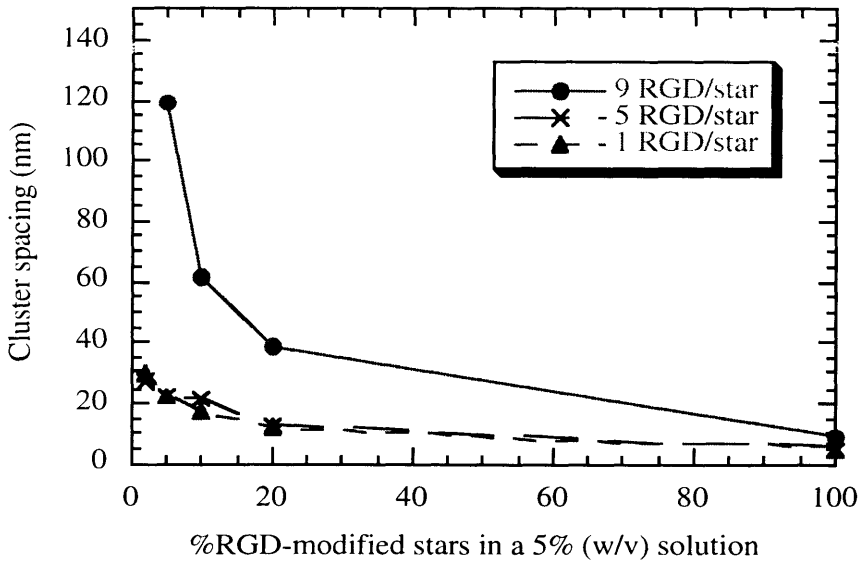

Figure 4.9: Average spacing between RGD-modified stars

The equivalent hard sphere radius for a 35-arm star, $R = [(5/3)^{0.5} R_G] \sim$ 18 nm. Hence, if these stars exhibit hard-sphere behaviour, the diameter in a good solvent is expected to be approximately 36 nm. Figure 4.10 shows the how the average spacing between 1-RGD

clusters varies as the RGD-modified stars are "diluted" with unmodified PEO. As can be seen from the figure, the RGD clusters tend to be more closely spaced on average than would be predicted based on a model of packing of hard spheres of radius 18 nm. Various possible reasons for this behaviour were explored. They included:

(i) Roughness of the gel substrate: one possible explanation was that if the surface of the hydrogel substrates was relatively rough, the surface area of the substrate, calculated based on a round coverslip of diameter 18 mm, might be an underestimation of the actual surface to which the stars are binding. AFM observation of the hydrated gel surfaces (see Chapter 3) suggests that this is not the case. The validity of the suggestion was further investigated by immobilizing star-ligand conjugates on aminosilane-treated glass coverslips, observed to be relatively smooth by AFM. Immobilization of star-ligand (1:1 ratio) conjugates from a 5% (w/v) solution yielded an RGD density of 20,400 molecules/μm^2. This translates to a spacing between clusters of 7 nm, compared with the apparent spacing of 5.7 nm between molecules on hydrogel surfaces; this was therefore dismissed from consideration.

(ii) Broad size distribution of star PEO molecules: as mentioned above, this is likely to have a significant effect on the molecules' ability to pack into a regular, two-dimensional lattice structure. This bimodal distribution of star molecules clearly cannot be expected to pack in a regular 2-dimensional lattice, and may explain why the curve in Figure 4.10, of the average spacing between RGD-modified star molecules (1:1 ratio, where competitive adsorption effects are absent) seems to take the expected shape, but is offset towards lower spacings than would be predicted based on a model of hard spheres of uniform size.

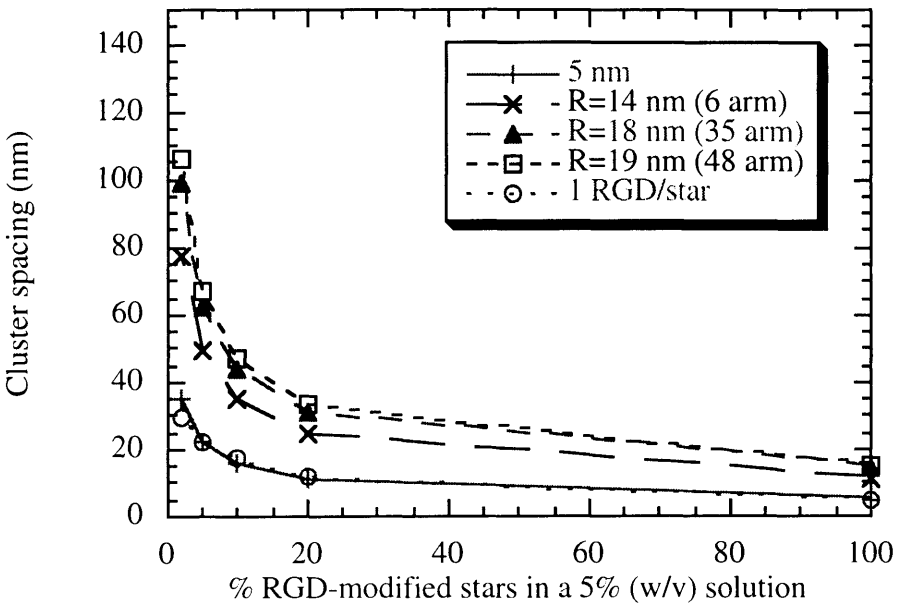

Figure 4.10: Average spacing between 1-RGD clusters compared with theoretical, based on two-dimensional packing of hard spheres of radius 5, 14, 18 and 19 nm

(iii) Significant overlap of star molecules on surface: It is often assumed that star molecules exhibit "hard-sphere" behaviour in solution, that is, they are approximated as non-draining, impenetrable spheres [96]. The determination may be made by comparing statically and dynamically determined radii; this tells us whether the star molecule indeed behaves as a hard sphere (ratio = 1), or if there is a surface layer of the molecule through which solvent can flow and into which other chains can penetrate (ratio > 1). Bauer [92] found that the ratio of thermodynamic to viscometric radius of polyisoprene stars exceeds unity at high functionality (f > 18) and suggested that at large values of f, the molecules may behave as "fuzzy" spheres in good solvent. This seems also to have been found by Yen [90] for star PEO; for a star molecule of M(arm) = 10,000, the ratio of thermodynamic

radius, R_T , to viscometric radius, R_V, was found to be 1.33 for f= 30 and 1.14 for f = 57. Furthermore, given the molecular dimensions of star molecules in aqueous solution, the critical overlap concentration, c* may be estimated. Using the formula:

$$c^* = \frac{3M.W.}{4N_A \pi R_g^3} \tag{7}$$

where N_A is Avogadro's number, the concentration at which (35-arm) star molecules (M.W. = 316,000) begin to overlap in solution is 0.046 g/cm^3, or ~ 5 % (w/v). If the star molecules are allowed to overlap significantly, both in solution and when immobilized on the surface, then the spacings between star molecules appear more reasonable.

4.5.4 Expected effect of polydispersity on ability to assess biological response

GPC data indicated that there are 2 dominant populations of star molecules, each with M(arm) = 9,100, one with an average f = 6 (M.W. = 55,100), and one with average f = 48 (or M.W. = 430,000). Thus, two populations of RGD cluster sizes are expected. It is likely that integrin clustering, like many biological phenomena, exhibits a threshold response at some critical minimal value, ***n***, of ligand number. Complete analysis of the biological response, then, requires knowledge of the density of ligand clusters which are above the critical size. The value of ***n*** is unknown for integrins, so the approach we take is to interpret the biological responses (cell adhesion strength and migration) in light of the estimated densities of clusters above some selected threshold size.

Two key assumptions are required to estimate these cluster densities. First, we assume that the fraction of star arms modified with RGD is a constant fraction of the total number of arms on any given star based on the calculated coupling efficiencies presented earlier (9/35

~ 25% for the maximum degree of RGD modification; 5/35 ~ 14% for the intermediate degree, and 1/35 ~ 3% for the smallest). Thus, at maximum modification, $n = 2$ corresponds to an 8-arm star, $n = 3$ to a 12- arm star, and so on. The second assumption is that the polydispersity of the stars on the surface is the same as that in the original coupling solution. Since it is not possible to separately label the each population of stars, we are unable to determine the proportions when stars are covalently linked to the surface, but the good fit between the kinetic model and the data for the 3 different average ligand functionalities supports this assumption. We will defer assumptions about the accessibility of the RGD to cells -- that is, assumptions regarding the extent to which RGD might be "buried" in the surface brush of PEO -- for this analysis as it is more relevant to the discussion of data on biological response. Steric issues will almost surely reduce the value of n we calculate for a free star (by perhaps 25 - 50%), and we will acknowledge this effect throughout the following discussion by designating the values we calculate as n_0 to suggest these estimated values represent maximum achievable values.

The relatively low resolution characteristic of GPC analysis precludes precise determination of the weight or mole fraction of stars corresponding to each threshold ligand value, but the GPC data (Fig. 4.3) do allow reasonable bounds to be derived. Resolution of the center two peaks, which are presumed to contain the relevant material, reveals that 64% (by weight) of the polymer falls in the peak with $\overline{M_w} = 55{,}100$ ($\overline{f_{arm}} = 6$) with the remaining 36% within the peak with $\overline{M_w} = 430{,}000$ ($\overline{f_{arm}} = 48$). The valley between the two peaks corresponds to Mw ~ 145,000 (elution volume ~ 17.5 ml), and further analysis of the chromatogram indicates that 31% (by weight) of the material has Mw > 145,600 (16 arms). Maximum modification (25%) would yield a product in which 31 wt.% had 4 or more conjugated RGD molecules (n = 4). Distinctions between n = 2, 3 and 4 (f = 8, 12, 16) are thus not readily discernible; likewise, distinctions between n = 4, 5, and 6 (f = 16, 20,

24) are difficult to resolve. We thus take n = 4 as a natural breakpoint for parsing the effects of polydispersity on cluster spacing.

Precise conversion of this weight fraction to a mole fraction would require more detailed information from the chromatogram than the GPC provided, however, an estimate was obtained by considering the distributions of stars larger and smaller than the threshold functionality of 16 as roughly centered around the two dominant peaks. The weight fractions were converted to mole fractions using average molecular weight values for those two peaks [$\overline{M_w}$ = 55,100 ($\overline{f_{arm}}$ = 6), and $\overline{M_w}$ = 430,000 ($\overline{f_{arm}}$ = 48)]. Thus, ~ 8.3 mol % of stars have sufficiently high functionality to tether at least four ligands to the surface, while the remainder are of functionality, f ≤ 16, and would tether less than 4 ligands. The estimated spacings between RGD clusters above the threshold, n_0 ~ 4, are given in Table 4.6. The table suggests that if a minimum of ~4 ligands per cluster is required for receptor clustering, then the actual spacing between RGD clusters which support receptor clustering varies from ~ 30 nm at the minimum to > 400 nm at the maximum, in contrast to the spacings between stars bearing RGD clusters of any size (~ 10 to 120 nm, as shown in Figure 4.9).

% RGD modified stars in solution	Density of RGD modified stars (cm^{-2})	Mol% stars with required functionality	Spacing between clusters ≥ n_0
100	1.36×10^{12}	8.33	30
20	6.90×10^{10}	8.33	132
10	2.65×10^{10}	8.33	213
5	7.07×10^{9}	8.33	412

Table 4.6 Spacings between RGD clusters at n_0 = 4 (f ≥ 16).

At the intermediate degree of modification (14 % of arms modified with RGD), a threshold cluster size of n_0 ~ 4 requires a larger molecule, f = 28 on average. The resolution achieved in the GPC data did not permit us to clearly distinguish between stars of this size (Mw = 254,000, elution volume = 17.1 ml) and those of 16 arms (elution volume = 17.5 ml), hence their mole fraction on the surface, and therefore their spacings could not be estimated. However, it is understood that the percentage of stars having ≥ 28 arms is somewhat lower than the percentage having ≥ 16 arms, such that at lower degrees of modification, the mol% of stars on the surface above a given threshold cluster size is decreased. We therefore infer that if n_0 ~ 4 is the threshold size for receptor clustering, there may be a discernible difference in the cell response to surfaces having intermediate versus high average cluster sizes.

The preceding analysis, though limited by the information which can be derived from the GPC data, points to a significant limitation in the system: because of the broad distribution of molecular weights in the star PEO, there is probably a corresponding distribution in ligand cluster sizes, which prohibits the precise determination of the threshold cluster size, n_0, from cell-based assays.

4.6 Conclusions

The data suggest that a bioactive substrate on which average RGD density may be controlled, has been achieved. All of the surface linked RGD is tethered via star PEO; linking the star-RGD conjugates to substrates from solutions containing a mixture of modified and unmodified star PEO, "islands" of RGD, approximately 30 nm in diameter, are expected to be formed. Since the RGD is tethered to the surface of a PEG-NH_2 gel, these surfaces are expected to support only specific cell interactions. Very low degrees of non-specific association of star molecules with RGD, and of star-RGD conjugates with the

PEG-NH_2 substrates were observed. The reaction behaviour of star-RGD conjugates is reasonably explained by the model of competitive adsorption put forward by Langmuir. The star molecules appear to overlap considerably on the substrates, achieving significantly higher densities than would be predicted by a "hard-sphere" packing model.

Because of the significant polydispersity in the batch of star PEO, RGD-modified stars did not pack into regular arrays as would hard spheres. However, the packing behaviour followed the expected trends with respect to the spacing between clusters, in cases where competitive adsorption was absent.

CHAPTER 5. NANOSCALE VISUALIZATION OF LIGAND DISTRIBUTION

5.1 Nanoscale characterization of two dimensional arrays of ligand

The increasing interest in controlling the nanoscale architecture of solids and thin films for catalysis, information storage, optical and biomedical applications has led to a concomitant increase in attention to nanostructure characterization. A great deal of effort has been put into extending current techniques and developing new techniques to yield previously unavailable nanostructural information, due to the recognition that the desired properties and performance of many materials depend largely on obtaining well-defined spatial relationships between atomic and molecular moeities in two or in three dimensions.

One approach to achieving well-characterized surfaces is to prepare surfaces which have such well-defined surface chemistry and morphology that they are amenable to the surface characterization techniques currently available. For this reason, self-assembled monolayers (SAMs) have become popular tools for the study of a variety of surface phenomena [54]. There are cases, however, in which a desired surface property or performance cannot be reproduced using SAMs, or in which the surface of the material of interest (especially in polymers) cannot be readily modified by a SAM. For such surfaces, characterization is more complex. In the PEO-RGD model system developed in the previous chapter, for instance, the acquisition of chemical information in 2-dimensions and on the nanometer scale is arguably the most challenging aspect of their preparation. Many spectroscopic techniques commonly used for surface chemical analysis, for example X-Ray Photoelectron Spectroscopy or Attenuated Total Reflection-Fourier Transform Infrared Spectroscopy provide globally averaged data over micron length scales -spot sizes of diameter ~ 1 μm- while features we wish to image are on the order of ~ 50 nm. These

techniques are therefore of limited use when trying to determine chemical composition in two dimensions and at nanometer length scales.

5.2 Experimental design

5.2.1 Required resolution

Resolution requirements are determined by both the feature size, ~ 50 nm, and separation distance between individual features, 0-200 nm in this case. The most well-developed technique for illuminating structure on these length scales is Transmission Electron Microscopy (TEM). In the TEM, a thin specimen (~50 - 100 nm thick) is examined, and the incident electrons which are able to penetrate the specimen and emerge as transmitted electrons are detected by the emission of light from a phosphor screen. Contrast in a TEM image arises because the incident beam can (i) be deflected by elastic collisions with nuclei of atoms in the specimen, (ii) lose energy because of inelastic collisions within the specimen, or (iii) pass straight through unaltered [97]. In both elastic and inelastic collisions, the number of electrons scattered depends on the atomic numbers of the elements in the sample. Since most polymers contain primarily carbon and hydrogen, which have low atomic numbers and low densities, they typically have to be stained or otherwise labeled with an element of high atomic number, which has a high enough electron density to give reasonable contrast in the image. TEM samples must satisfy very restrictive requirements with respect to electron attenuation, and the thinness of the sample required for transmission of the electron beam usually dictates that surfaces to be visualized be prepared in complicated and often atypical ways. The resolution and field of view, however, are usually superior to those obtained by other techniques; nanometer scale features can easily be imaged in the TEM.

Scanning Electron Microscopy (SEM) techniques have the advantage of ease of sample preparation, as representative samples can be mounted and imaged. Topographical images are typically obtained in the scanning electron microscope by collection of inelastically scattered secondary electrons [97]. Contrast can arise from a number of different sources, including surface texture and composition. Compositional contrast arises from variations in the emission of secondary electrons as a function of atomic number, however such variations are not predictable.

The development of high-resolution, low-voltage scanning electron microscopy (HRLVSEM) has dramatically improved our ability to obtain topographical images of polymer specimens at a scale of ~ 10 nm, approaching resolutions achievable with the TEM. The improved resolution is typically accomplished using a field emission electron gun, which produces a beam of high brightness, small spot size and low energy spread [98], compared with conventional electron sources, which generate secondary electrons at greater distances from the point of incidence of the beam. For non-conducting surfaces, the greatest success is achieved when performed at very low voltages (~5 kV) or with a field emission source. The problem of charging of the nonconducting sample surface makes the application of a thin (~60 A) coating of carbon necessary, however, carbon's low efficiency as a secondary electron emitter can lead to low contrast in the image.

Other techniques, such as Chemical Force Microscopy and autoradiography are less well developed for the types of samples and the resolution required in this work. Chemical Force Microscopy (CFM) [99] or Chemical Imaging (CI) [100] is a technique which has extended the utility of the AFM to enable the mapping of the spatial distribution of specific functional groups, and the determination of the corresponding surface energetics, by the use of chemically functionalized tips [101], [102], [103]. Contrast in the AFM is derived from a variety of tip-sample interactions, including chemistry, topology, morphology and

mechanics. It is therefore difficult, when two or more of these interactions are expected to be present at roughly the same order of magnitude, to distinguish between them in an image. Thus, this technique is most successful when the substrates under investigation have very well defined surfaces, for example, patterned SAMs on atomically smooth substrates, such as silicon [101]. For the surfaces prepared in this work, there are considerable limitations associated with AFM in general, and with CFM in particular. First, the commercially available probes found to be the most reliable consist of polystyrene latex beads, ~5 μm in diameter, which are covalently modified with the chemical entity of interest. On sharper tips, such as the standard Si_3N_4 pyramidal tip, the functional groups appear to be far more labile, allowing the collection of only very small amounts of data at a time (unpublished data). The use of the larger probes, however, would not provide the nanometer scale resolution required for this project. Second, because of the relative roughness of the star PEO-modified gels, contrast observed in the image would probably contain both topographical and chemical information; separation of the two would be difficult. In addition, the AFM imaging technique is subject to certain limitations: distortions in the image may be introduced when the feature size to be imaged is on the order of the size of the probe tip or smaller [104], or when the tip shape does not permit the accurate tracing of all of the contours of the surface under investigation [105]. For these reasons, lateral distances often cannot be measured accurately, and the use an of accelerated electron method in conjunction with a scanning probe technique such as AFM has been recommended by several authors [106] [107] [108].

Autoradiography is a technique commonly used for the detection of radioactive proteins bound to cell surface receptors, or radioactive antibodies used to probe cell structure. Labeled cells can either be exposed to a photographic film, or to a thin layer of a photographic emulsion cast on the surface of the cell sample. Emissions from the radioactive molecules develop the film or emulsion, allowing the protein distribution to be

determined. The resolution achievable using this method is clearly limited by the grain size in the film or silver-containing emulsion used; the smallest grain size currently available is 130 nm. In addition, emulsion film is typically several layers thick; the exposure of may grains in several different layers due to the spreading of the emitted radiation further limits the achievable resolution to several hundreds of microns. The technique was therefore not expected to provide sufficient resolution for the purposes of this thesis, and was not explored farther.

5.2.2 Methods for Contrast Enhancement in Electron Microscopy: Immunogold Labeling

Gold has a high electron density, and is relatively easy to image against a polymer background in an electron microscope. Immunogold labeling and related bioaffinity/colloidal gold labeling methods have therefore become very important techniques for the visualization of ultrastructure in biological systems. Immunogold labeling, which derives its name from the combination of "immunoglobin" (antibody) and "colloidal gold," typically involves the following steps: an antibody specific to the molecule under investigation ("antigen") is identified; thousands of antibodies are available commercially. Colloidal gold particles, 3-50 nm in size, are prepared from a solution of tetrachloroauric acid ($HAuCl_4$). At the correct pH, the negatively charged gold particles can adsorb proteins such as antibodies on their surfaces virtually irreversibly, and it is this adsorption process which forms the basis of the immunogold labeling technique. Specific antibodies, complexed with colloidal gold, and in contact with a surface to which proteins are bound, will bind to the relevant antigens.

The labeling technique is illustrated in Figure 5.1. Colloidal gold techniques have been used in TEM for thin sections, in SEM for the determination of two-dimensional surface distribution of proteins [109] [110], and in AFM for the labeling of cell-surface proteins

[108], [111]. The resolution and efficiency of labeling obtained from colloidal gold-labeled surfaces depend mainly on the concentration, the size of the gold particle used and the affinity of the antibody for the antigen. Larger gold markers (≥ 10 nm) are usually used in HRLVSEM studies because the resolution which can be achieved using this technique is somewhat inferior to that possible using the TEM.

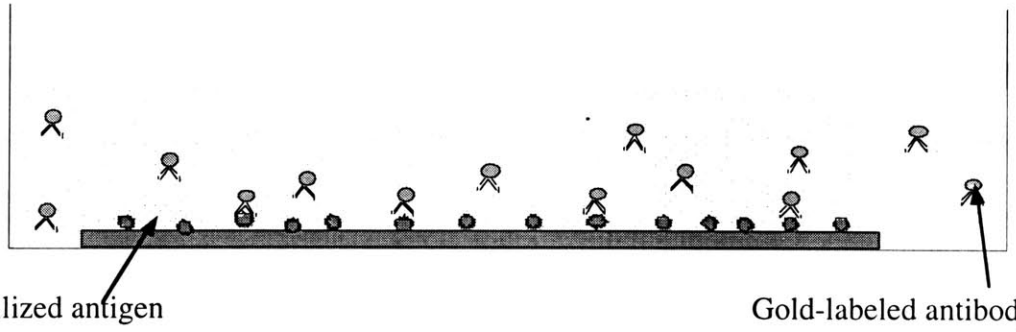

Figure 5.1 Schematic representation of the immunogold labeling process

The interaction between two entities which display specific recognition is typically described in terms of a simple reversible reaction:

$$A + B \underset{k_r}{\overset{k_f}{\rightleftharpoons}} A - B \qquad (1)$$

where A and B are the two interacting molecules, and A-B is the antigen-antibody complex formed.

The chemical equilibrium conditions are usually described in terms of a dissociation constant, K_D, given by:

$$K_D = \frac{k_f}{k_r} = \frac{[A][B]}{[A-B]} \qquad (2)$$

Therefore, a low dissociation constant in equation (2) indicates a high affinity of the antibody for the antigen, or that the equilibrium in equation (1) lies to the right.

For the purposes of this project, a molecular recognition system was desired, consisting of a probe which would interact specifically with immobilized moeities, enabling the location of ligand on the surface. Since there was no commercially available antibody specific to the RGD peptide sequence, a model ligand, biotin was used for visualization experiments. Biotin is widely used in bioanalytical studies, because of its very strong and very specific interactions with the proteins avidin ($K_D = 10^{-15}$ M, [112]) and streptavidin ($K_D = 10^{-14}$ M, [113]), interactions with affinities several orders of magnitude higher than in other receptor-ligand systems (for example, K_D for the integrin-fibronectin interaction $\approx 10^{-6}$ M [114]). Biotin was therefore an attractive option, since its use as ligand would afford us at least two choices of recognition molecule. Furthermore, biotin is available with a wide variety of substituent groups. It can therefore be conjugated to other molecules via a number of coupling chemistries (including the carbodiimide chemistry used for the PEO-RGD conjugation) which leave its bicyclic ring system available for recognition by avidin or streptavidin, either in its native state, or labeled with a marker for detection [115].

It has been shown, however, that the interaction between avidin/streptavidin and a *biotinylated protein* is significantly weaker than that between *free biotin* and (strept)avidin [116], probably due to steric hindrances encountered in the binding of a biotinylated molecule with (strept)avidin (depicted schematically in Figure 5.2). It has also been found that the biotin-binding site on streptavidin, located 1.5 nm below the surface of the

molecule, may be inaccessible to biotin immobilized on a surface, unless (i) the biotin is present at a relatively low density, and (ii) the biotin is linked to the surface via a spacer [117].

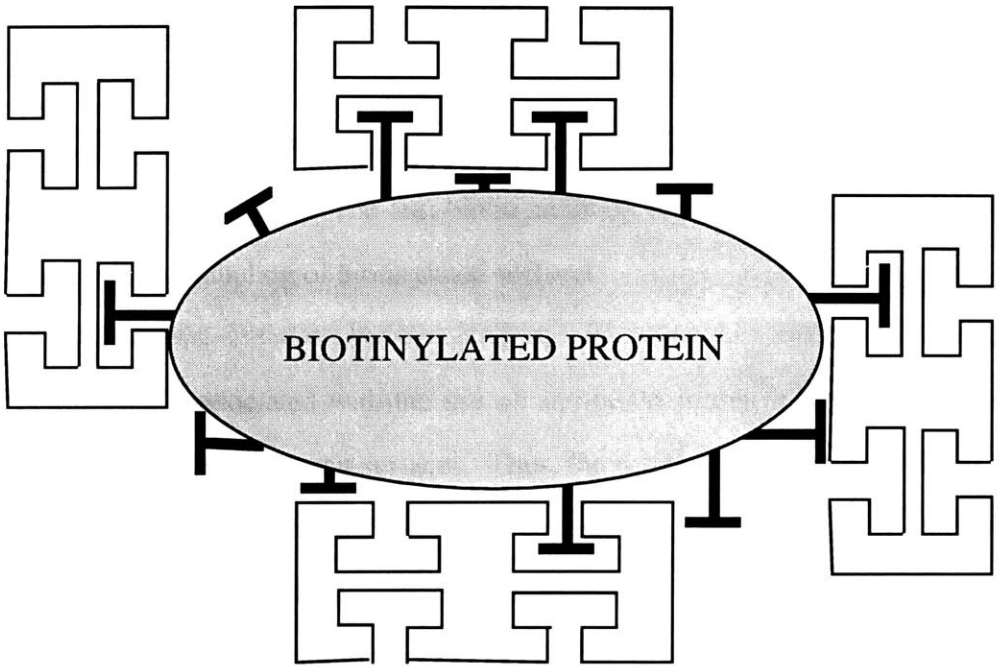

Figure 5.2: Steric hindrances limiting the binding of streptavidin to biotinylated macromolecules (Adapted from [118]**).**

We anticipated that presenting biotin on the end of a long PEO tether would allow sufficient access of biotin to the streptavidin, however, experiments showed that gold-labeled streptavidin bound to linear PEG-biotin surfaces in an unpredictable fashion (unpublished data). One explanation for this observation may be that the streptavidin adsorbs on the surface of the gold particle in a conformation which makes its binding pocket relatively inaccessible to biotin, whether linked to the surface via a flexible PEO tether or not.

On the other hand, an anti-biotin antibody binds to biotinylated macromolecules with similar affinity as streptavidin and is insensitive to the insertion of a spacer [116] and to the density of surface-bound biotin (private communication, British Biocell International). Goat anti-biotin antibody has been found to be up to five times more sensitive than streptavidin in labeling biotinylated surfaces (private communication, British Biocell International, and Gillian Brown, unpublished data). The binding site for biotin on the anti-biotin antibody is relatively close to the surface of the molecule; it is possible that, when adsorbed on the surface of a gold particle, the biotin binding site is more accessible than that of streptavidin. The anti-biotin antibody is therefore usually recommended over streptavidin for labeling of biotinylated surfaces.

One drawback associated with the use of anti-biotin is that it displays considerable non-specific adsorption on many surfaces. Thus, for surfaces on which significant non-specific adsorption was unlikely (that is hydrogel-coated substrates), goat anti-biotin was preferred as a marker. In cases where non-specific adsorption was observed, streptavidin was used as a label, to minimize its effects.

The approach taken for colloidal gold/bioaffinity labeling is as follows: biotin was tethered to the substrate via star or linear PEO. Two parallel sets of surfaces were created. On one set, star molecules were used to create biotin clusters. As the biotin was not radiolabeled, quantitation of the biotin:PEO ratio in the conjugate was not possible. However, the high biotin:PEO ratio in the initial reaction solution was expected to yield a relatively high biotin:star PEO molar ratio in the product. On the second set, a "standard" set of surfaces, having a known (uniform) distribution of biotin was desired. Gold labeling, visualization and analysis of the distribution of the gold markers on a surface having a uniform ligand distribution allowed comparison of the experimentally obtained marker distribution with that predicted for a uniformly distributed ligand in two dimensions. To achieve such a

distribution using star molecules as tethers, however, requires conjugation of only one biotin molecule to each star; higher degrees of modification of the stars would be expected to produce a non-uniform, aggregated distribution of biotin on the surface. A second consequence of the inability to radiolabel the biotin was that it was impossible to determine that biotin:PEO ratio which would produce star molecules modified with a single biotin molecule. On the second set of surfaces, therefore, linear PEO was used to tether single biotin molecules at various densities.

The immunogold labeling technique was used to decorate PEO-biotin surfaces, and the surfaces were examined either by TEM or by HRLVSEM. For TEM studies, thin films of PEO-biotin were obtained by immobilizing PEO-biotin conjugates on an aminosilane-modified, SiO_x-coated TEM grids. Because of the fragility of the TEM grids, it was not possible to coat them with a layer of the protein resistant hydrogel. Biotin was therefore labeled with 5 nm gold-streptavidin (Au-STP) to minimize non-specific adsorption of the label. Comparison of the Au-STP distribution on linear and star surfaces should therefore help to determine the extent of clustering. Although the sample preparation for TEM studies is difficult, and the specimens showed evidence of damage sustained during preparation, the technique allowed the labeling of the ligand and the visualization of its distribution.

For HRLVSEM, PEO-biotin conjugates were immobilized on hydrogels which had been prepared on silicon wafers. The most important criteria for the selection of the marker were, again, the apparent efficiency of labeling and the degree of non-specific adsorption of the marker. Given the proven non-adhesiveness of the PEO hydrogel substrates demonstrated in Chapter 3, non-specific binding of the marker was not expected to be an issue. Therefore, anti-biotin was used as the probe for HRLVSEM studies, because of its

superior sensitivity. Surface-bound biotin was labeled with 10 nm colloidal gold-goat anti-biotin conjugates (Au-GAB) and the biotin distribution visualized using HRLVSEM.

A commercially available linear PEG-biotin conjugate was used as a "calibration standard" to determine whether Au-GAB surface density scales with the biotin density in a predictable manner and to estimate the efficiency of binding. Then star PEO-biotin conjugates were covalently linked to PEG-NH_2 hydrogels, labeled with the marker, and examined for evidence of clustering of the markers.

5.3 Materials and methods

5.3.1 PEO-biotin conjugation

Star PEO 460 was conjugated with 5-biotinamido pentylamine (hereafter referred to as "biotin", Pierce Chemical Company), using the reaction and purification techniques described in Chapter 4. Carboxylated star PEO was activated in MES buffer using EDC and Sulfo-NHS, and reacted with biotin in a 100:1 molar ratio. The reaction product was purified by dialysis against deionized distilled water for 36 hours, with several water changes, then frozen and lyophilized.

5.3.2 Linear PEG-biotin conjugate

A commercially available biotin product, conjugated to a linear PEO molecule of molecular weight 3,400 was also used (biotin-PEG-NHS, Shearwater Polymers). Manufacturer's information indicates a 100 % monosubstituted PEO-biotin product. The free end was pre-activated with EDC/NHS. This conjugate was expected to produce biotin layers of a

known (uniform) distribution, which could later be compared with the ligand distribution on the star PEO-biotin surfaces.

5.3.3 Substrate preparation for, and characterization by TEM

The substrates used for TEM studies were nickel grids, 300 mesh, coated first with a layer of Formvar™ plastic (~ 60 nm), then with a silicon monoxide layer (~ 50 nm) (Ted Pella, Inc.). Grids were first rinsed gently in methanol, then an aminosilane coating was applied to the silicon monoxide surface by immersing in a methanolic solution containing 1% (vol.) trimethoxysilylpropyl diethylene triamine (Huls America, Inc.), 5% (vol.) water for 15 minutes. The grids were then carefully rinsed in methanol several times and then cured at 60 °C for 1 hour.

Star PEO-biotin conjugates were coupled to the functionalized grid surfaces from 5% (w/v) aqueous solution in MES, as described in Chapter 4, varying the surface density of biotin by varying the ratio of biotin modified PEO to unmodified PEO as before. For comparison purposes, surfaces were prepared by coupling linear NHS-active PEO-biotin conjugate to the TEM grids from a 15 % (w/v) solution in MES buffer. The surface density of biotin was varied by varying the relative amounts of PEG-biotin to unmodified linear PEG (PEG-propionic acid, M.W. = 2,000, Shearwater Polymers), activated using EDC and Sulfo NHS, as previously described. The coupling reaction was allowed to proceed for 12 hours, after which the surfaces were immersed in a 50 mM solution of Tris-HCl, to deactivate any excess NHS-active chain ends.

Gold-streptavidin (Au-STP) conjugate was used as a label, as it exhibited lower non-specific adsorption on aminated TEM grids than goat anti-biotin in control experiments (unpublished data). The label consisted of 5 nm gold particles, with an adsorbed

streptavidin layer of thickness 0.5 nm, resulting in a conjugate of diameter 6 nm (manufacturer's information). Gold-streptavidin conjugates (British Biocell International) were first diluted in PBS buffer (pH = 7.4) to 50 times their as-supplied volume, and the suspensions were allowed to equilibrate at 4 C for 20 min. TEM grids, bearing immobilized PEO-biotin were inverted on a 300 µl aliquot of the suspension in a 24 well plate and incubated in a humid chamber for 24 hours at 37 C. Surfaces were rinsed several times in PBS, to remove any Au-streptavidin which may have adsorbed loosely on the substrate surface. Samples were then fixed, using 2% glutaraldehyde in PBS for 20 minutes at room temperature. Surfaces were again rinsed, then dehydrated in a graded series of ethanolic solutions, followed by hexamethyldisilazane. Surfaces were examined using a JEOL Model 1200 EX Transmission Electron Microscope in the Department of Biology at MIT.

5.3.4 Substrate preparation for, and characterization by HRLVSEM

The substrates used in HRLVSEM studies were PEG-NH_2 hydrogels on silicon wafers. Two PEG-biotin conjugates were used in these studies: star PEO-biotin, prepared as described above, and a commercially available linear PEO-biotin conjugate, used as a "calibration" standard. Substrates were prepared for calibration of the labeling technique by coupling linear NHS-active PEO-biotin conjugate (Biotin-PEG-NHS, M.W. = 3,400, Shearwater Polymers) to the hydrogel substrates from a 5 % (w/v) solution in MES buffer. To vary the surface density of biotin, PEO-biotin conjugates were covalently linked to these substrates from solutions containing a mixture of PEO-biotin and unmodified linear PEG (PEG-propionic acid, NHS ester, M.W. = 2,000, Shearwater Polymers), at a total PEO concentration of 5 % (w/v), in the proportions shown in Table 5.1.

Gold-goat anti-biotin (Au-GAB) conjugate of mean diameter 11 nm was obtained from British Biocell International. The gold colloid, as supplied contains > 90% single particles, with no particles larger than triplets (manufacturer's data). The Au-GAB was diluted to 50 times its as-received volume in PBS (pH = 7.4), mixed gently and equilibrated at 4 °C for 20 minutes. Because the PEO substrates used in this study were known to minimize non-specific protein adsorption, the standard step of adding surfactant or albumin to the suspension to minimize non-specific adsorption of the antibody was omitted; control substrates were included to evaluate the effects of nonspecific adsorption, and it was always negligible.

% biotin-modified PEO in 5% (w/v) solution	Conc. PEO-biotin, % (w/v)	Conc. PEO, % (w/v)
0	0	5
20	1	4
40	2	3
60	3	2
80	4	1
100	5	0

Table 5.1: Modified-unmodified PEO ratios during immobilization

Substrates were immersed in the Au-GAB suspension for 12 hours at room temperature, then rinsed several times in water. In lieu of critical point drying, commonly used in the preparation of polymer surfaces for examination under in air or vacuum, substrates were immersed in water in the wells of a 12-well culture plate (Corning), and frozen at - 70°C. Surfaces were then freeze-dried under vacuum, enabling them to be dried without being exposed to an air-water interface. Freeze drying is a commonly accepted procedure for the drying of hydrated hydrogel samples [71], and other solvent swollen polymers [97]. The

distribution of gold was viewed using a LEO Model 982 Scanning Electron Microscope at Harvard University.

5.3.5 Analysis of TEM and HRSEM images

Two samples were examined for each condition. For each set of surfaces (star or linear PEO tethers), three 1 μm x 1 μm areas were selected, and the density of gold particles was determined by direct counting and averaged. Further image analysis of selected areas was done by importing the digital images into Scion Image 1.5 software (NIH), which enabled the co-ordinates of each particle to be determined. Particles were selected manually, and their x- and y-co-ordinates were determined by the software. A Microsoft Excel macro was used to determine the distance between each gold particle in the selected area and every other particle in the image. Then the minimum of the set of distances from a given particle to all other particles in the image was taken as the nearest neighbour distance (NND).

For comparison purposes, two-dimensional arrays of uniformly distributed particles were simulated. A random number generator in Microsoft Excel was used to create x- and y-co-ordinates for arrays of points and the NNDs for these arrays were determined using the macro described above. Since the spacings between points in a 2-dimensional array will necessarily depend on their density, the densities of the points in the simulated arrays had to be equal to those in the experimental arrays with which they were to be compared. Therefore, for each condition of biotin density, a 1 μm^2 array of the same number of particles was generated three times, and the NNDs averaged. These simulations were used to assess the deviation of the experimentally obtained arrays of gold particles on linear PEO-biotin and star PEO-biotin surfaces from a normal distribution.

5.4 Results and Discussion

In the analysis which follows, there are two sets of physical dimensions for the star molecules which must be considered. First, immunogold labeling of the tethered biotin is carried out on PEO in a water-swollen brush; star molecules are therefore hydrated during labeling. Thus, as is commonly done [47], [48], the dimensions of the covalently linked star are assumed the same as those for a star free in solution, calculated using the formula proposed by Bauer [92] and used previously in Chapter 4. These dimensions are used for considerations of possible steric hindrances in effect during labeling. Electron microscopic examination of the gold-decorated surface is done under vacuum, hence the star molecules are assumed to be collapsed to their dried dimensions (hydrated diameters divided by solvent expansion parameter, $\alpha = 1.89$) in all TEM and SEM images, though they should maintain the same centre-to-centre spacings as in the hydrated state. Therefore, all analysis of TEM and SEM images was done using dried star PEO diameters. The dimensions of the star molecules used in the analyses in this section are summarized in Figure 5.3. The low and high values given in the figure represent the ranges for 6-arm and 48-arm molecules respectively, the average diameter is that of a 35-arm star molecule

For TEM and SEM analysis the spatial distribution of the gold markers was taken as representative of the distribution of the biotin ligand. It was assumed that in the absence of steric hindrances to impede binding, the Au markers would distribute themselves in a manner that is indicative of the underlying biotin surface distribution, as the markers should have no preference for one immobilized ligand versus another. Therefore, although the measured densities of the gold markers (see Table 5.2, Figure 5.9) suggest that the amount of biotin labeled with gold was only a fraction of the total amount of biotin on the surface, we assumed that the gold markers, spread randomly on the surface, adopt a spatial arrangement characteristic of the configuration of the underlying ligand.

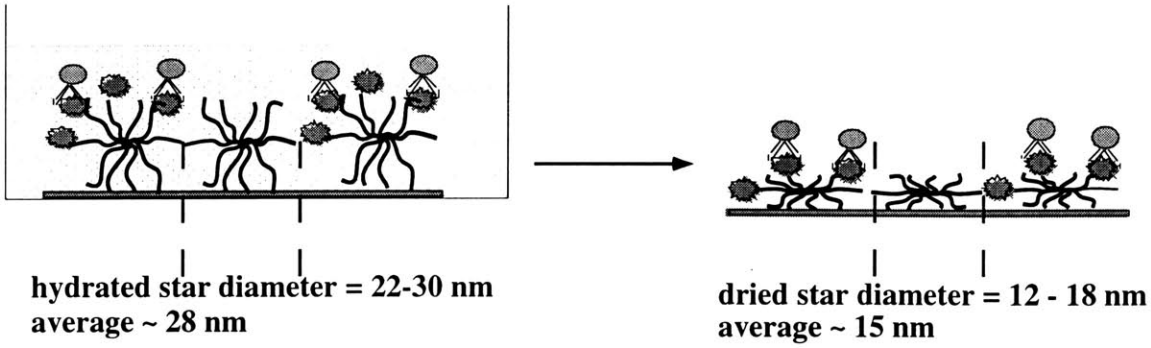

Figure 5.3 Dried and hydrated dimensions of star PEO 460 used in analysis

5.4.1 Transmission Electron Microscopy of PEO-biotin surfaces

The distribution of Au-STP on a linear PEO-biotin surface is shown in Figure 5.4. The star PEO-biotin surface, labeled with Au-STP is displayed in Figure 5.5. Because of the electron density of gold, the Au-STP particles appear in the electron micrographs as black, circular dots, which are very well-defined and easily identified. As can be seen from visual inspection of Figure 5.4, gold particles bound to star PEO-biotin surfaces (upper image) appear more clustered than those on the linear PEG-biotin surfaces shown in Figure 5.5 (upper image). Unmodified star PEO control surfaces were free of non-specific adsorption, as shown in the lower image in Figure 5.5, while linear PEG control surfaces showed some non-specific adsorption, probably due to the low molecular weight of the PEO used (Figure 5.5, lower image).

The average densities of gold markers in each set of specimens was obtained by direct counting, and are given in Table 5.2.

Surface	Conc. of coupling solution	Average gold density (μm^{-2}), n=3
Linear PEG-biotin	10%	410 ± 65
Star PEO-biotin	20%	81 ± 22

Table 5.2 Average density of Au-STP markers on PEO-biotin surfaces

A: Linear PEO-biotin surfaces

Linear PEG-biotin molecules, of molecular weight 3,400 were coupled from a 15% (w/v) solution, well above their critical overlap concentration of 8%. In a pure PEG-biotin coating, that is in a coating prepared from a solution containing only biotin-modified PEO, they would be expected to pack at a minimum spacing of 3.7 nm (equal to the radius of gyration of the hydrated molecule), which corresponds to a biotin density of 73,000 molecules per square micron. It is clear, then, that complete labeling of the immobilized biotin on such surfaces is impossible as the diameter of the Au-STP conjugate is approximately 6 nm; the colloidal particles have an area of cross-section of ~ 28 nm^2, 2-3

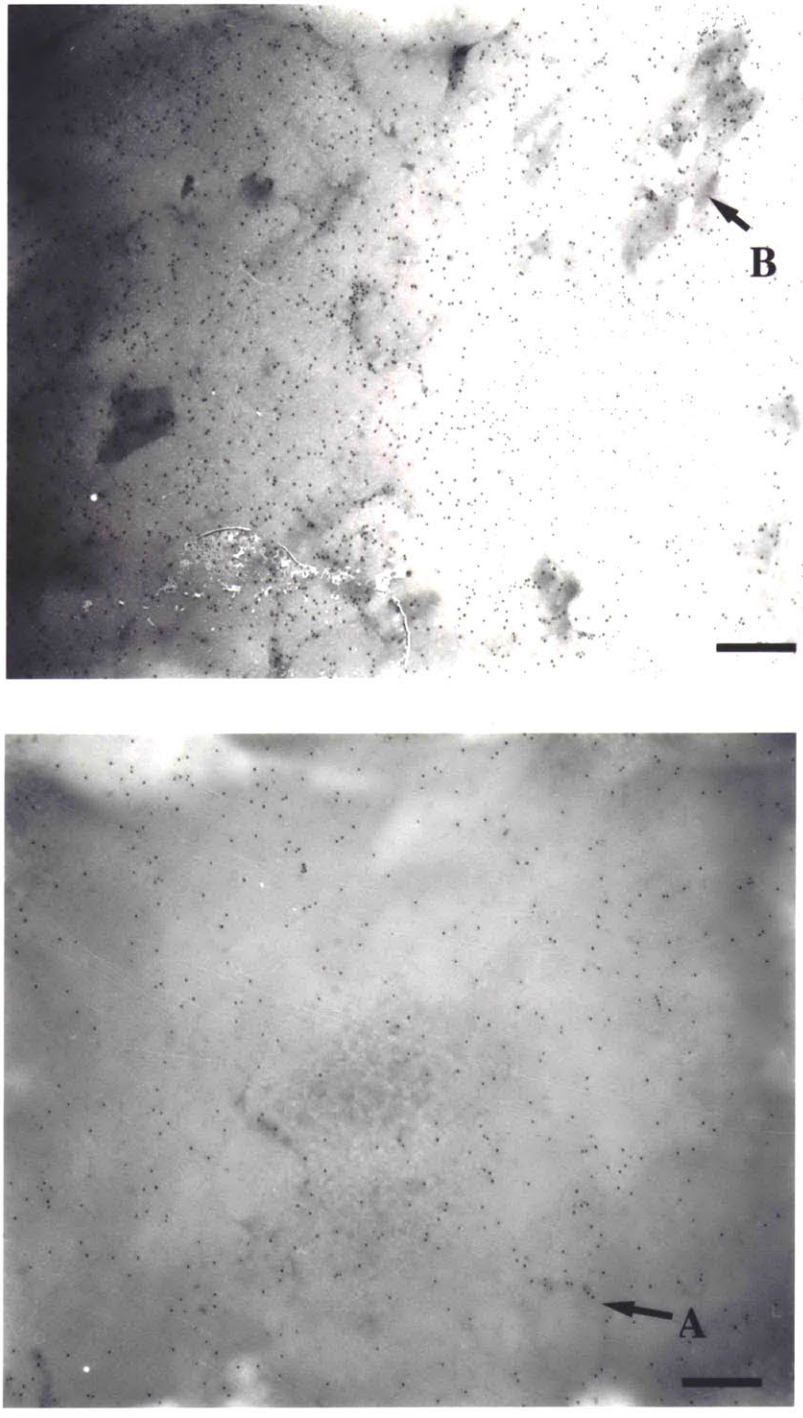

Figure 5.4: TEM images of Au-STP-labeled surfaces

Top: Linear PEO-biotin conjugates, from 10% solution
Bottom: Control surface, linear PEO, no biotin
Scale bar = 200 nm

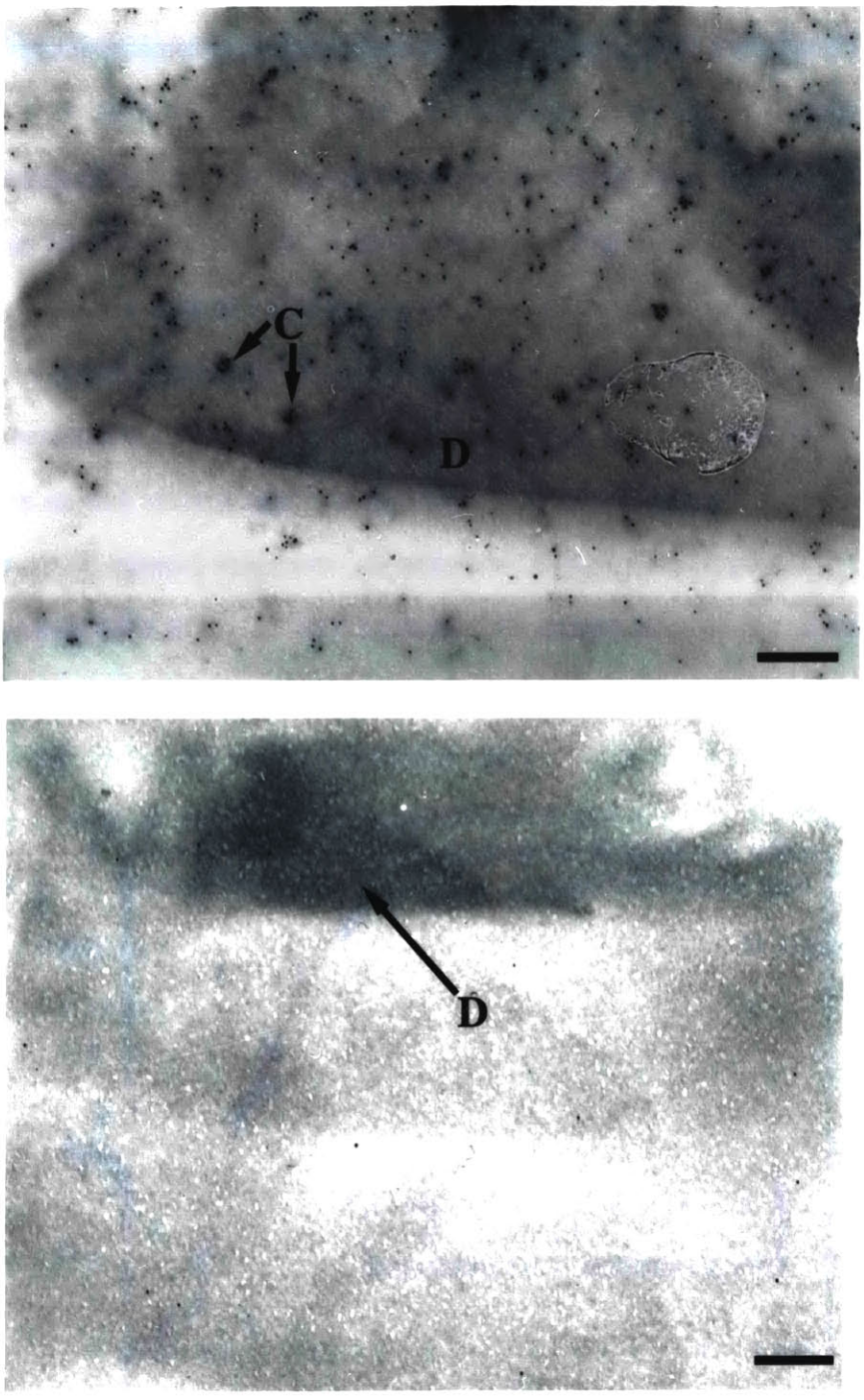

Figure 5.5: TEM images of Au-STP labeled surfaces

Top: Star PEO-biotin, approximately 5% of star PEO molecules on surface modified with biotin
Bottom: Control surface, star PEO, no biotin
Scale bar = 200 nm

times the area occupied by the PEO-biotin conjugate (~ 13 nm), and could either bind to multiple biotin molecules on the surface or hinder the access of other Au-STP conjugates.

When surfaces are prepared using solutions in which only 10% of the (linear) PEO molecules are modified with biotin (as are shown in Figure 5.4), the biotin density should decrease to a maximum of 7,300 molecules per square micron (or lower, if the competitive adsorption model previously described also holds for the case of linear molecules). The spacing between biotin molecules should therefore increase to at least 11 nm, and all biotin molecules should be accessible for labeling by Au-STP. When the cumulative frequency distribution of nearest neighbour distances is plotted (see Figure 5.6), we find that approximately 12 % of the Au-STP particles have nearest neighbour distances of 11 nm or less, suggesting that roughly 12 % of the labeled biotin molecules are "adjacent".

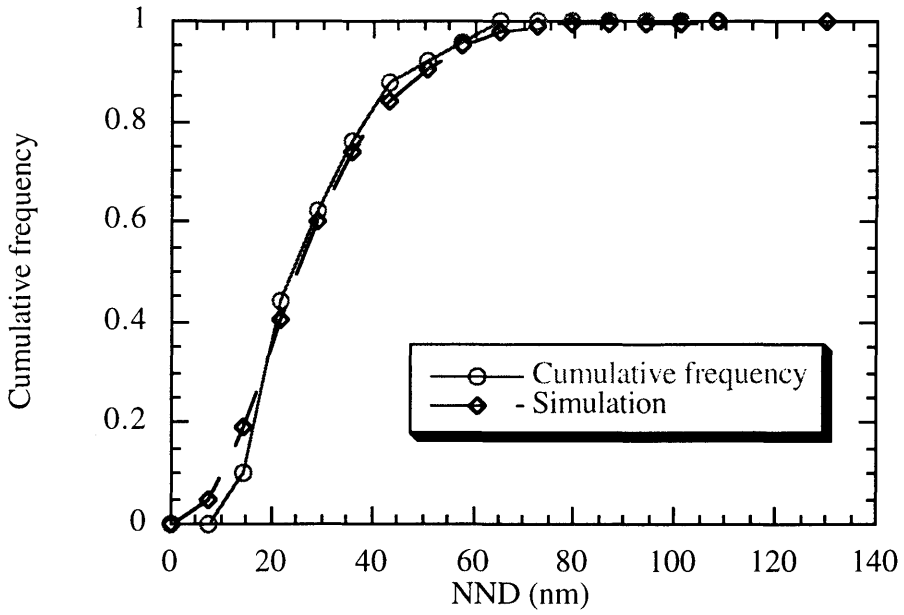

Figure 5.6 Cumulative distribution of nearest neighbour distances on linear PEO-biotin surfaces (from 10% solution, Au-STP labeled, as determined from TEM images) and a computer simulation of a uniform array of particles of the same density

The figure also shows that a computer simulation of an array of particles of the same density produces a cumulative frequency distribution that tracks the experimental curve very closely. We therefore infer that biotin, covalently linked to surfaces via linear PEO tethers, produces the expected uniform distribution of particles

B: Star-PEO biotin surfaces

The molar ratio of biotin to star PEO in the initial coupling solution was selected as 100. Since the biotin was not radiolabeled, an average biotin:star PEO ratio of 10 is assumed, equal to the maximum number of RGD molecules conjugated per star previously obtained. Given the polydispersity of the star PEO used in this work, the expected diameters of the star PEO 460 molecules, in air or vacuum, are expected to fall between 12 and 18 nm. With the addition of Au-STP conjugates of diameter 6 nm, the maximum diameter of a biotin-STP-Au cluster immobilized on a substrate might increase to approximately 18 to 30 nm. We assume, as in the previous case, that the randomly distributed gold markers assume a distribution representative of the ligand distribution. Thus, if biotin molecules tethered via star PEO are indeed clustered, aggregates of gold particles of roughly the diameter of a gold-biotin-PEO complex should be observed in the TEM images. Direct measurement of the diameters of the apparent clusters in the images of star PEO-biotin immobilized from 20% star PEO-biotin solutions reveals diameters of 25 to 30 nm, suggesting that the aggregated colloidal particles may indeed represent clusters of immobilized biotin.

Inspection of the images of star PEO-biotin surfaces also reveals a shaded area, or "haze", ~ 30 - 40 nm in diameter, around many of the Au-STP clusters (labeled "C" in Figure 5.4). This may be due to a rearrangement of the surface layer on drying. The surface tension of

PEO in air at room temperature is roughly 44 mN/m [33], while that of gold is significantly higher (~1400 mN/m). It is therefore possible that when the gold-labeled surface is dried, the nanometer-scale gold particles become buried in the star PEO molecules on the surface, as star PEO would present a lower energy surface in air. Hence, the slightly darker region around the aggregated Au particles may be due to the interaction between the star PEO molecules, which are enveloping the gold, and the electron beam. This phenomenon is not observed on linear PEO-biotin surface, possibly because of the shorter tether lengths (R_g(linear PEO) = 3.7 nm) in the linear case, which would not be sufficiently long to completely cover the high energy gold particles.

The cross-sectional area of a gold-labeled, dried star molecule, assuming an average diameter of ~ 24 nm is on the order of 500 nm. On drying, the star PEO-biotin conjugate should collapse to the substrate, and each biotin in a cluster would therefore occupy an average area of 50 nm^2. The distance between biotin molecules within a cluster should consequently be on the order of 7 nm. If *every* biotin molecule in a cluster is labeled, therefore, the average spacing between the gold particles in the TEM images should be roughly 7 nm. At lower labeling efficiencies, the nearest neighbour separations should generally increase, but if the biotin molecules are clustered, the upper limit on the nearest neighbour separation should be ~ 30 nm, the estimated maximum diameter of the gold-labeled star molecule. When the cumulative frequency distribution curve of star PEO-biotin conjugates immobilized from a solution containing 20% biotin-modified stars in solution is constructed, (Figure 5.7), it shows that approximately 17% of the Au-STP conjugates are within 7 nm of their nearest neighbours, and 50% are within one molecular diameter (30 nm) of each other.

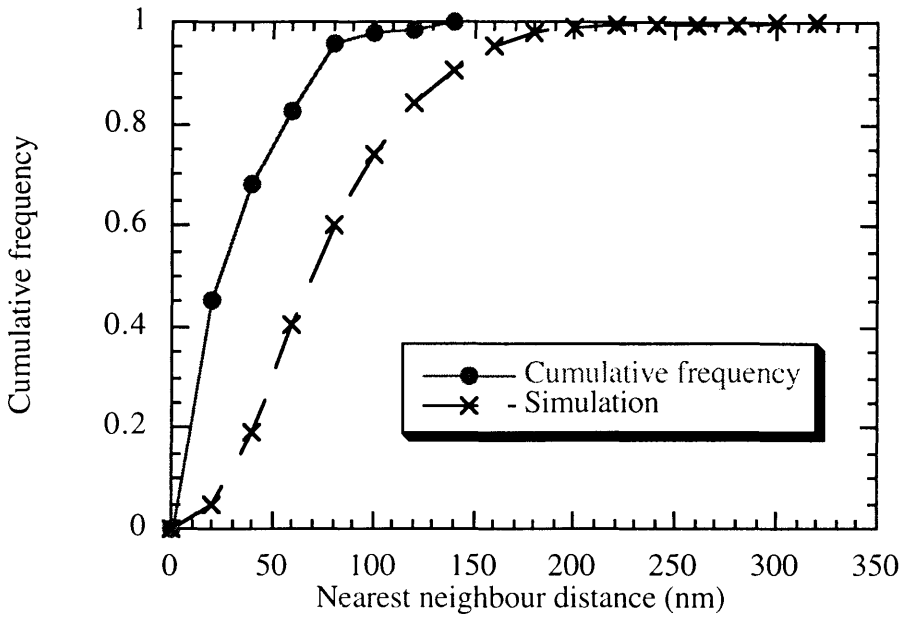

Figure 5.7 Cumulative distribution of nearest neighbour distances on star PEO-biotin surfaces from 20% solution, Au-STP labeled, as determined from TEM images

These results give the first suggestion that the distribution of ligand on the star-biotin surfaces is non-uniform, or clustered. Linear PEG-biotin surfaces, expected to produce a surface of uniform ligand distribution showed a relatively low percentage of biotin molecules occurring within one molecular diameter of each other; on the other hand, when the biotin is tethered by star molecules, the distribution of gold markers shifts, such that roughly half of the Au-STP particles occur within what could reasonably be considered a "cluster".

Finally, a statistical analysis of the gold spatial distribution was performed. Biotin, tethered to the substrate via linear PEO molecules, should be uniformly distributed; the

distribution of nearest neighbour distances between biotin molecules should therefore be normal (Gaussian) [119]. A standard test used to assess the departure of data from a specified distribution is the Kolmogorov test [120], [121]. The Kolmogorov test is often used in studies of biological systems, for assessment of spatial distribution. For example, Van der Smissen [122] used the test to verify the clustering of epidermal growth factor receptors on cell surfaces. The test computes a parameter, known as the Kolmogorov-Smirnov statistic, D_n, which is the maximum vertical difference between the cumulative distribution function for the sample, and that of the model distribution [120]. The value of D_n is dependent on the sample size, n, since larger sample sizes can be expected to more closely approach the ideal distribution. The test is applied as follows: a critical value, K, is selected, and if $D_n < K$, then the experimental distribution is considered similar to the model distribution at some significance level, α, which may be considered the probability that an array will erroneously be found different from the model distribution. Tabulated values of K for different values of n and α are used to determine the significance of the difference from the model distribution.

The nearest neighbour distances (NNDs) were therefore computed for the star PEO-biotin surfaces and linear- PEO-biotin surfaces, using the co-ordinates of the Au-STP particles taken from the 1 μm^2 images. These were compared with the distribution of NNDs obtained from the computer simulations of 2-dimensional arrays of uniformly distributed particles, of area 1 μm^2 and at the same particle density. The values of D_n, the measure of the deviation of from a Gaussian distribution, are shown in Table 5.3. As can be seen from the table, the value of D_n for the linear PEO-biotin surface is all lower than K for the 0.01 significance level, while that for star PEO-biotin surfaces is higher. We can therefore

conclude that the immunogold labeling technique quantitatively showed the expected distribution of markers on biotinylated surfaces.

SPECIMEN	Au-STP density, n (particles/μm^2)	D_n	K	normal distribution?
linear PEO-biotin	410	0.49	0.18	yes
star PEO-biotin	81	0.08	0.09	no

Table 5.3 Results of Kolmogorov test for uniformity of distribution of biotin on TEM specimens

Because of the fragility of the TEM grids, it was very difficult to prepare a series of PEO-biotin surfaces over a range of biotin densities, without significantly damaging many of the specimens. Further studies were therefore performed using HRLVSEM, for which the substrates are far more robust, such that a large number of surfaces can be successfully prepared for examination.

5.4.2 Other features in TEM images

The images also show several features which are artifacts of sample preparation. The fragility of the SiO_x layer on the Formvar-coated grid led to the formation of hair-like cracks into which the Au-STP particles seemed to preferentially deposit (labeled "A" in Figure 5.3). In addition, some unevenness in the substrate itself is apparent, there are light and shaded regions in the images, possibly due to unevenness in the thickness of the aminosilane coating (see for example, the region labeled "B" in Figure 5.3) , or to some

scratching, tearing or kinking of the underlying Formvar coating (see the region marked "D" in Figure 5.4). In addition, close inspection of some TEM images reveals very tiny bright spots, (~ 1 nm in diameter, see region marked "E" in Figure 5.4), which are believed due to damage of the substrate by the electron beam. Nevertheless, regions which were relatively artifact free, and large enough for quantitative analysis could be identified.

5.4.3 High Resolution Low Voltage SEM

In the first experiment, intended for validation of the technique, linear PEG-biotin conjugates were immobilized at different surface densities from solutions containing varying amounts of PEO-biotin in a 5% solution, and then labeled with Au-GAB. Typical Low Voltage SEM images are shown in Figure 5.8 (a) through (e). Control surfaces of unmodified linear PEO on PEG-NH_2 hydrogels showed no non-specific binding of Au-GAB particles (see Figure 5.8(f)). The attachment of Au-GAB particles in Figures 5.8(a) to (e) is therefore assumed due to the specific interaction between the immobilized biotin and Au-GAB.

5.4.4 Quantitative analysis of binding

The objectives of this quantitative analysis were: (i) to determine whether the density of bound gold particles varied predictably with the density of biotin on the surface, (ii) to estimate the efficiency of labeling, or the fraction of biotin on the surface which has been labeled by Au-GAB, and (iii) to verify that biotin molecules tethered to a surface via linear PEO assumes a uniform (normal) distribution.

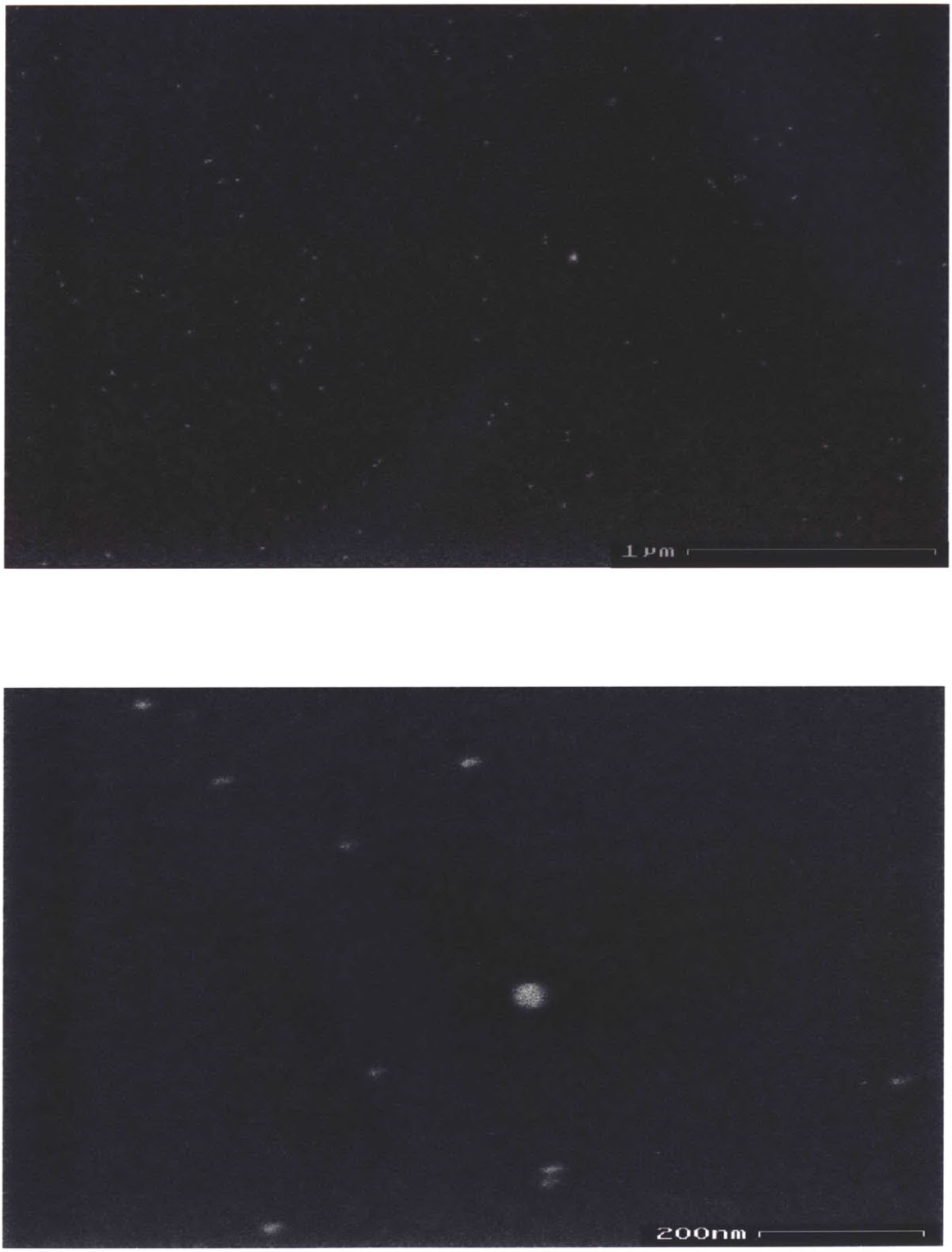

Figure 5.8 (a) Linear PEO-biotin, coupled from 20% PEG-biotin solution
top: low magnification, bottom: high magnification

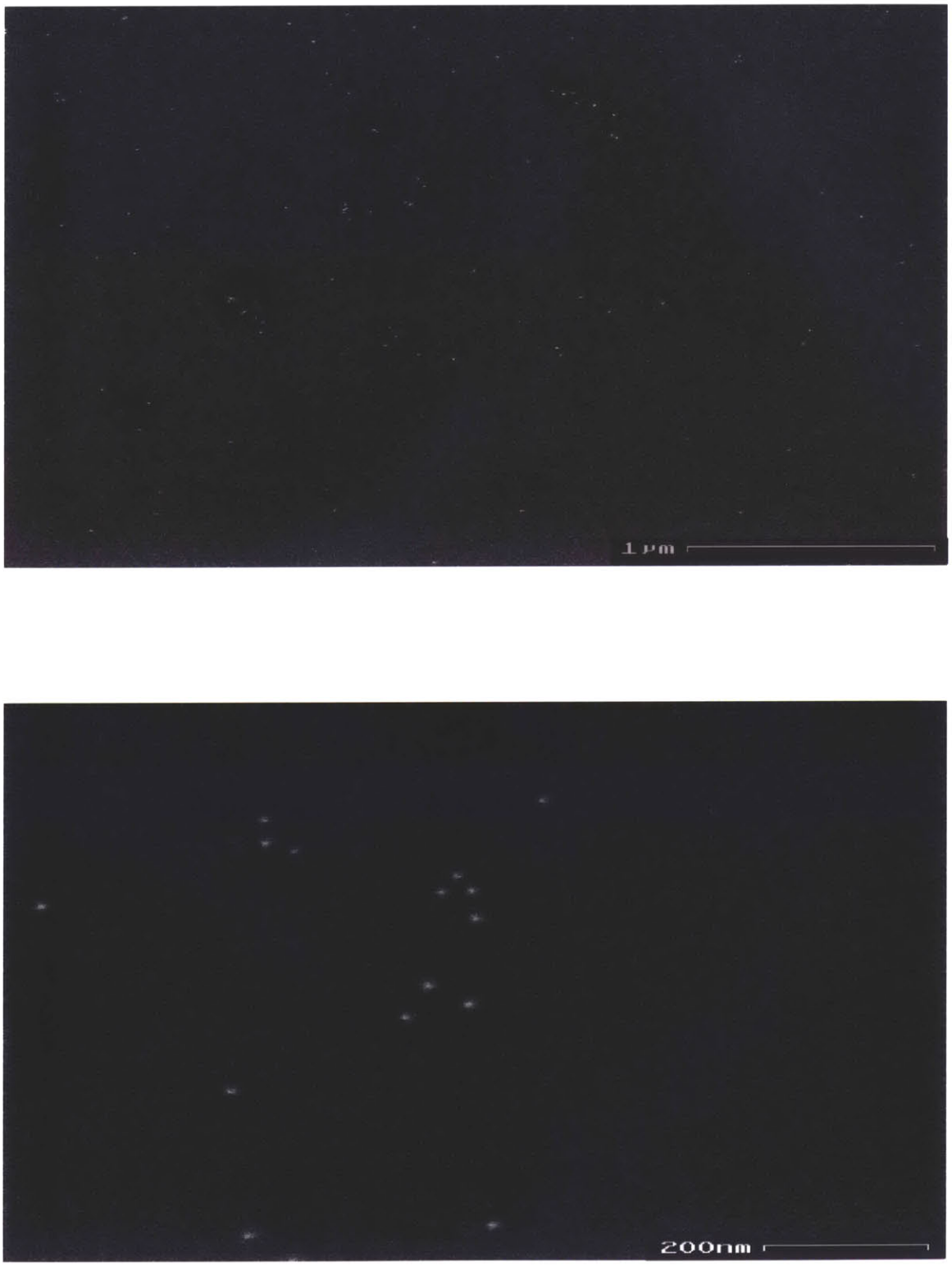

Figure 5.8 (b) Linear PEO-biotin, coupled from 40% PEG-biotin solution
top: low magnification, bottom: high magnification

Figure 5.8 (c) Linear PEO-biotin, coupled from 60% PEG-biotin solution
top: low magnification, bottom: high magnification

Figure 5.8 (d) Linear PEO-biotin, coupled from 80% PEG-biotin solution
top: low magnification, bottom: high magnification

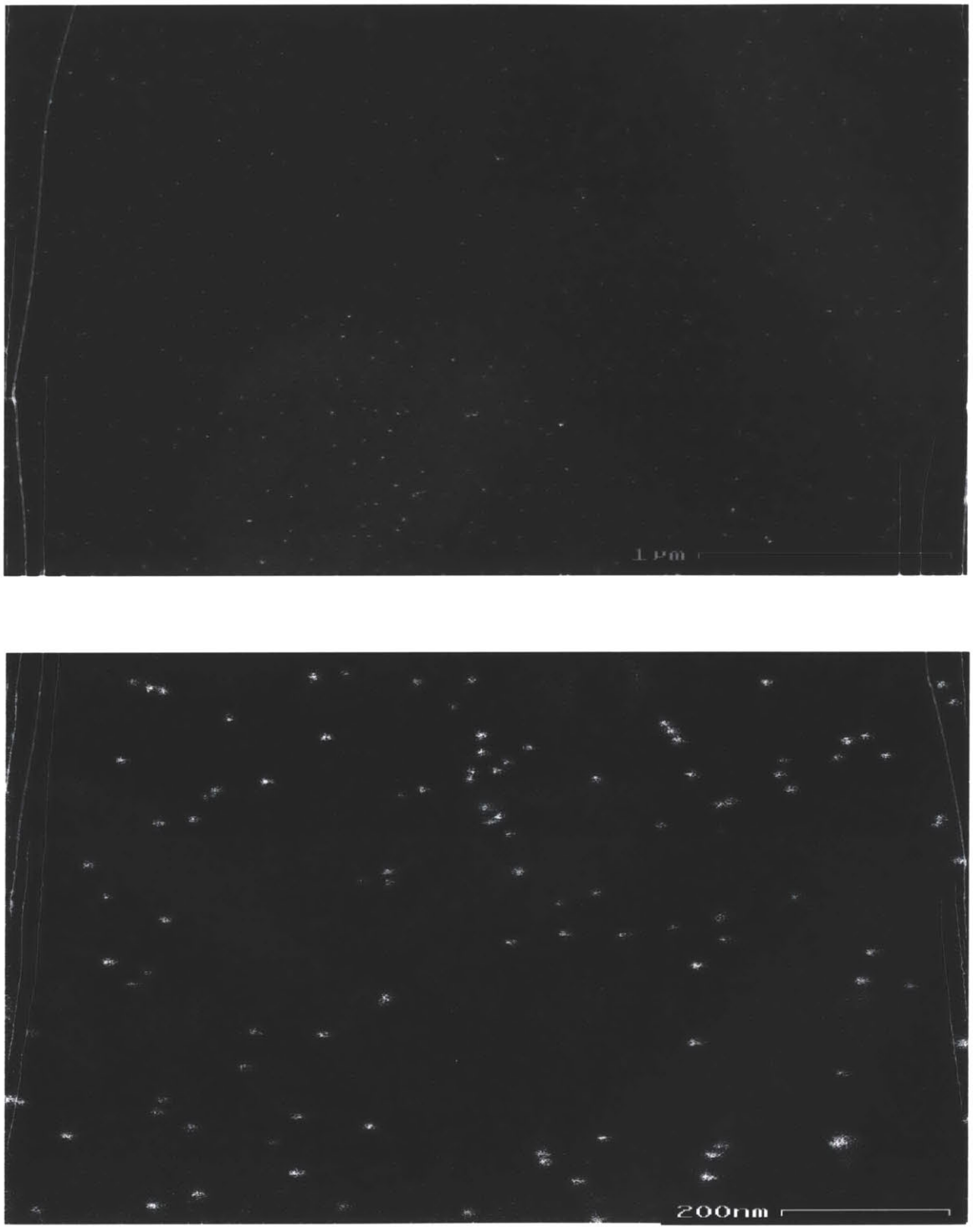

Figure 5.8 (e) Linear PEO-biotin, coupled from 100% PEG-biotin solution
top: low magnification, bottom: high magnification

Figure 5.8 (f) Linear PEO-biotin, control surface, unmodified PEG
top: low magnification, bottom: high magnification

A: Density of bound Au-GAB

The expected surface biotin density can be estimated from consideration of the dimensions of the linear PEO-biotin molecule. Since the total concentration of PEO in solution is less than its critical overlap concentration of 8%, we assume that the molecules are not overlapping, either in solution or on the surface. Hence a good estimate of the minimum spacing between linear PEG molecules is $2Rg \approx 7$ nm, based on the results of previous studies [48]. This suggests a maximum biotin density on the surface of ~ 20,000 molecules/μm^2, when 100% of the molecules in solution are biotin-modified (that is, at the highest biotin density) and molecules are linked at a close-packed density. Direct counting of Au particles in Figure 5.8(a) reveals an average Au-GAB density of 81/μm^2, or a labeling efficiency of ~ 0.4 %. Au-GAB densities were obtained by counting the Au-GAB particles in three 1 μm^2 images and calculating the average, and are shown in Figure 5.9.

The density of the Au-GAB label in general increases with increasing concentration of biotin in the initial coupling solution (Fig. 5.10). In light of the multiple physicochemical interactions which must occur to result in observing the labeled gold it is not surprising that a simple monotonic correlation does not exist. The dotted line represents a quadratic curve fit, and is included only to show the trend; it is not intended to imply prediction of a theoretical or mechanistic model.

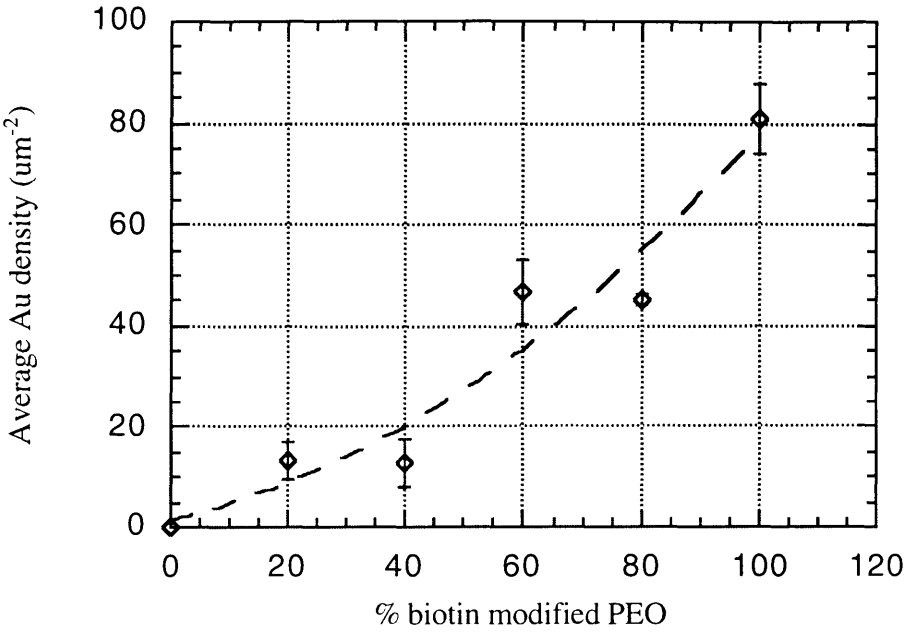

Figure 5.9 Measured Au-GAB densities on linear PEG-biotin surfaces. Values are mean ± s.d., n = 3.

B: Efficiency of labeling

The efficiency of labeling (fraction of immobilized linear PEG-biotin labeled with Au-GAB) was estimated, based on expected surface biotin densities in the linear PEO-biotin system. A range of expected surface densities was calculated for each case using assumptions to bound the high and low extremes. The low value was obtained using the model of competitive adsorption described in Chapter 4. Since biotin-modified linear PEG has half as many available chain ends per mole as the unmodified linear PEG, the equilibrium constants for these molecules were assumed to be the same as those used in

Chapter 4 for unmodified stars (K_{star} = 1.34 x 10^8) and stars which had 50% of their arms modified with RGD (K_{star} = 7.64 x 10^7), respectively. This gives biotin densities of ~ 2,000/μm^2 when 20% of the PEG molecules in solution are biotin-modified to 20,000/ μm^2 at 100% biotin-modified PEG. The high value was obtained by assuming that competitive adsorption was *not* taking place in the linear system, and that the percentage of PEG-biotin on the surface was the same as that in solution (4,000/μm^2 to 20,000/μm^2) . The estimated range in efficiency of labeling was expressed as a percentage of those high and low values.

Using this approach, the fraction of immobilized biotin labeled with Au-GAB is estimated to be consistently less than 1%, and typically lies between 0.3% and 0.6% (Fig. 5.10). Several plausible explanations for this observation exist. It is likely the Au-GAB particles at the surface experience steric hindrance at high surface coverage. The cross-sectional area of the Au-GAB particle (~ 95 nm^2) is roughly twice that of the linear PEG-biotin conjugate (~ 38 nm^2). When bound to the surface, the Au-GAB particle occupies the area of 2 biotin molecules, as a result, the use of 11 nm Au-GAB particles obstructing roughly half of the biotin on the surface from being individually labeled, when the biotin is densely packed.

If a 5 nm particle had been used, as in the TEM studies, the number of particles which would have been able, in theory, to pack into a 2-dimensional array at the surface would have increased by a factor of four. Increasing the size of the gold marker used therefore reduces the attainable labeling efficiency [123]. The visualization of the gold particles in the SEM becomes progressively more difficult as the particle size decreases, however. Further improvements in resolution in the images can be obtained only by increasing the beam voltage in the SEM, which increases the risks of charging and beam damage. This points to one of the considerable advantages of TEM over SEM techniques; the resolving

power of the TEM is unquestionably better, and a higher degree of labeling is possible using a smaller marker.

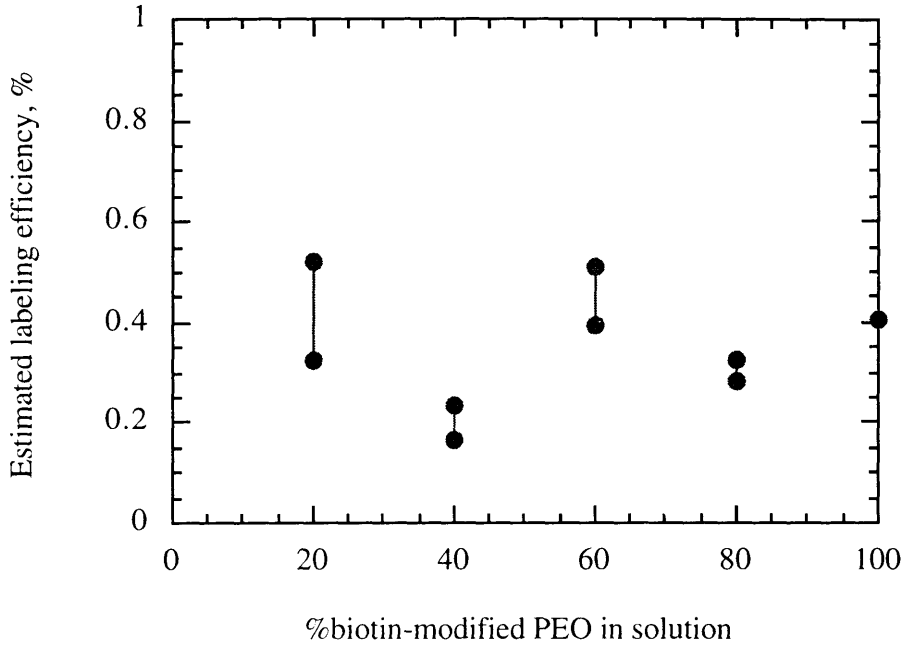

Figure 5.10 Estimated range of efficiencies of gold labeling on linear PEG-biotin surfaces

The binding capacity of Au-GAB may be further assessed by considering the density of bound particles relative to the total number of Au-GAB particles which come into contact with the surface during labeling. This may be done following the method of Park et al. [123], which models the labeling of surface antigens by immunogold particles using Einstein's Law of Brownian motion. The model assumes that the Au-GAB particles arrive at the surface by diffusion; their rate of arrival would clearly depend on their concentration, size and the staining time. An equation is derived for the number of colloidal particles arriving at a unit area of the surface in a time, t as:

$$q = n\left[\frac{kTt}{12\pi\eta r}\right]^{\frac{1}{2}} \qquad (1)$$

where q = number of Au-STP or Au-GAB particles per unit area arriving at the surface in time, t (sec)

n = concentration of colloidal particles (particles/ml)

η = viscosity of the solution (Poise)

r = radius of the gold-protein conjugate (cm)

As supplied, concentration of gold particles in the colloidal suspension is 1.7×10^{13}/ml, each gold particle having ~12 antibodies adsorbed on its surface (private communication, British Biocell International). Because of compression of the antibody layer, however, the reported diameter of the Au-GAB conjugate is 11 nm. When diluted to 50 times its original volume, the concentration of Au-GAB, n, is 3.4×10^{11} particles/ml. The viscosity, η, is taken as 0.0007 P [123]. Substituting these estimated values into equation (1), we obtain a value of approximately 1200 Au-GAB particles/μm^2 reaching the surface in 12 hours. This is clearly significantly lower than expected the density of biotin on most surfaces (up to 20,000/ μm^2), and therefore imposes an upper limit on the labeling efficiency which can be obtained. In addition, it indicates that there is a substantial number of particles which collide with the surface, but which do not stick. This observation may be expressed in terms of a *sticking probability,* p, given by [123]:

Q = number of bound gold particles per unit area

= $p * q$

The sticking probability is therefore equal to the number of particles bound divided by 1,200, and increases from ~ 0.01 to 0.06 as the biotin concentration in solution increases from 20% to 100% . Such values are significantly lower than those reported by other investigators, who obtained sticking probabilities of 0.5 and higher in other colloidal gold systems [124], [123].

A possible reason for the low sticking probabilities obtained may be a possible slowing of the binding kinetics because of the presence of a substantial poly(ethylene oxide). Steric repulsions due to the grafted PEG background may affect the approach and binding of binding the gold-STP markers to the surface, such that, even at relatively long times (24 hours) and high temperatures (37 °C), the probability that a colloidal particle will contact and bind to the surface may be significantly lower than would be seen in systems where such steric repulsions are absent.

C: Spatial distribution of linear PEG-biotin

Finally, the spatial distribution of the gold particles was analyzed. Biotin, tethered to the substrate via linear PEO molecules, should be uniformly distributed; the distribution of nearest neighbour distances between biotin molecules should therefore be normal [119]. A standard test used to assess the departure of data from a specified distribution is the Kolmogorov test [120], [121]. The Kolmogorov test is often used in studies of biological systems, for assessment of spatial distribution. For example, Van der Smissen [122] used the test to verify the clustering of epidermal growth factor receptors on cell surfaces. The test computes a parameter, known as the Kolmogorov-Smirnov statistic, D_n, which is the maximum vertical difference between the cumulative distribution function for the sample, and that of the model distribution. The value of D_n is dependent on the sample size, n,

since larger sample sizes can be expected to more closely approach the ideal distribution. The test is applied as follows: a critical value, K, is selected, and if $D_n < K$, then the experimental distribution is considered similar to the model distribution at some significance level, α, which may be considered the probability that an array will erroneously be found different from the model distribution. Tabulated values of K for different values of n and α are used to determine the significance of the difference from the model distribution.

The nearest neighbour distances (NNDs) were therefore computed for the biotin surfaces at different densities, using the co-ordinates of the Au-GAB particles taken from the 1 μm^2 images. For comparison purposes, 2-dimensional arrays of uniformly distributed particles, of area 1 μm^2 were simulated, and the distribution of NNDs obtained.

The simulated and experimental cumulative distribution functions for the linear PEO-biotin system are plotted in Figure 5.11. As can be seen from the figure, at the lower biotin densities (20% and 40% PEG-biotin in solution), the deviations of the experimental curves from the model appear large, and both curves are not smooth, due to the small sample sizes involved. At higher biotin densities, however (60 - 100% PEG-biotin in solution), the experimental curves follow the simulated curves very closely, suggesting that the experimentally obtained distribution of gold particles on linear PEG-biotin surfaces is uniform. The values of D_n, the measure of the deviation of from a normal distribution, are all lower than K for the and K for the 0.01 significance level are shown in Table 5.4.

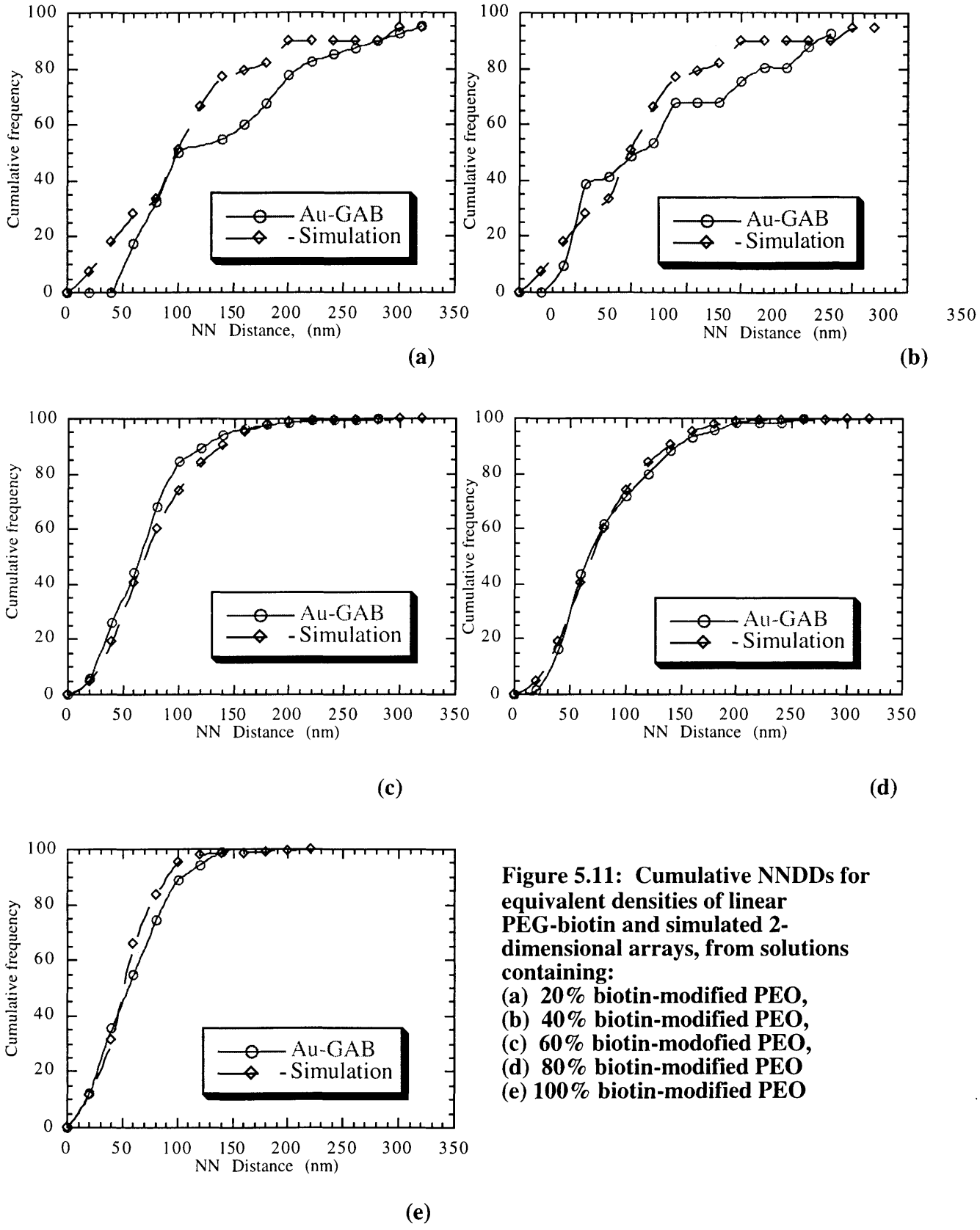

Figure 5.11: Cumulative NNDDs for equivalent densities of linear PEG-biotin and simulated 2-dimensional arrays, from solutions containing:
(a) 20% biotin-modified PEO,
(b) 40% biotin-modified PEO,
(c) 60% biotin-modofied PEO,
(d) 80% biotin-modified PEO
(e) 100% biotin-modified PEO

%biotin-modified PEG in solution	Au-GAB density, n (particles/μm^2)	D_n	K	normal distribution?
20	13	0.22	0.43	yes
40	13	0.14	0.43	yes
60	47	0.10	0.24	yes
80	45	0.04	0.23	yes
100	81	0.11	0.17	yes

Table 5.4 Results of Kolmogorov test for uniformity of distribution of biotin on linear PEO-biotin surfaces.

As can be seen from the table, all of the linear PEO-biotin surfaces examined showed a uniform distribution of Au-GAB, as expected. This further supports the conclusion that that, although it yields very low binding efficiencies, the immunogold labeling method may be used to indicate the ligand distribution on surfaces when at least 45-50 particles are examined, although measurements of spacings between ligands cannot be taken.

5.4.5 LVSEM examination of star PEO-biotin surfaces:

The surfaces for SEM studies were prepared with the intent of studying ligand spatial distribution over a wide range of ligand densities. However, if star molecules are considered to pack at the surface into a hexagonal lattice, for simplicity, then the appearance of isolated "islands" or clusters will only occur when one PEG molecule in six, or ~ 16% of the star PEO molecules at the surface, is biotin-modified, allowing a biotin-modified star

molecules to be completely surrounded by unmodified star PEO molecules. Therefore, surfaces having more than 16% of their area occupied by biotin-modified stars are not the clustered ligand surfaces in which we are interested for studies of cell behaviour, however, the presence of unmodified stars, even at low percentages, should ensure that the biotin distibution on the surface is not uniform; surfaces having less than 100% biotin-modified stars should therefore have significantly different biotin distributions from a simulated uniform surface, per the Kolmogorov test.

The expected fractions of biotin-modified PEG present on the surface were estimated from the Langmuir model developed in Chapter 4 for a cluster size of 9 ligands, and are shown in Table 5.5.

% RGD-modified stars in solution	% RGD-modified stars on surface
20	5
40	12
60	24
80	46
100	100

Table 5.5 Estimates of actual percentages of biotin-modified stars on linked to PEO-biotin surfaces.

Immunogold labeling of star PEO-biotin surfaces was carried out using the same technique as was used as was used for linear PEO-biotin surfaces. SEM images are shown in Figure 5.12 (a) to (f).

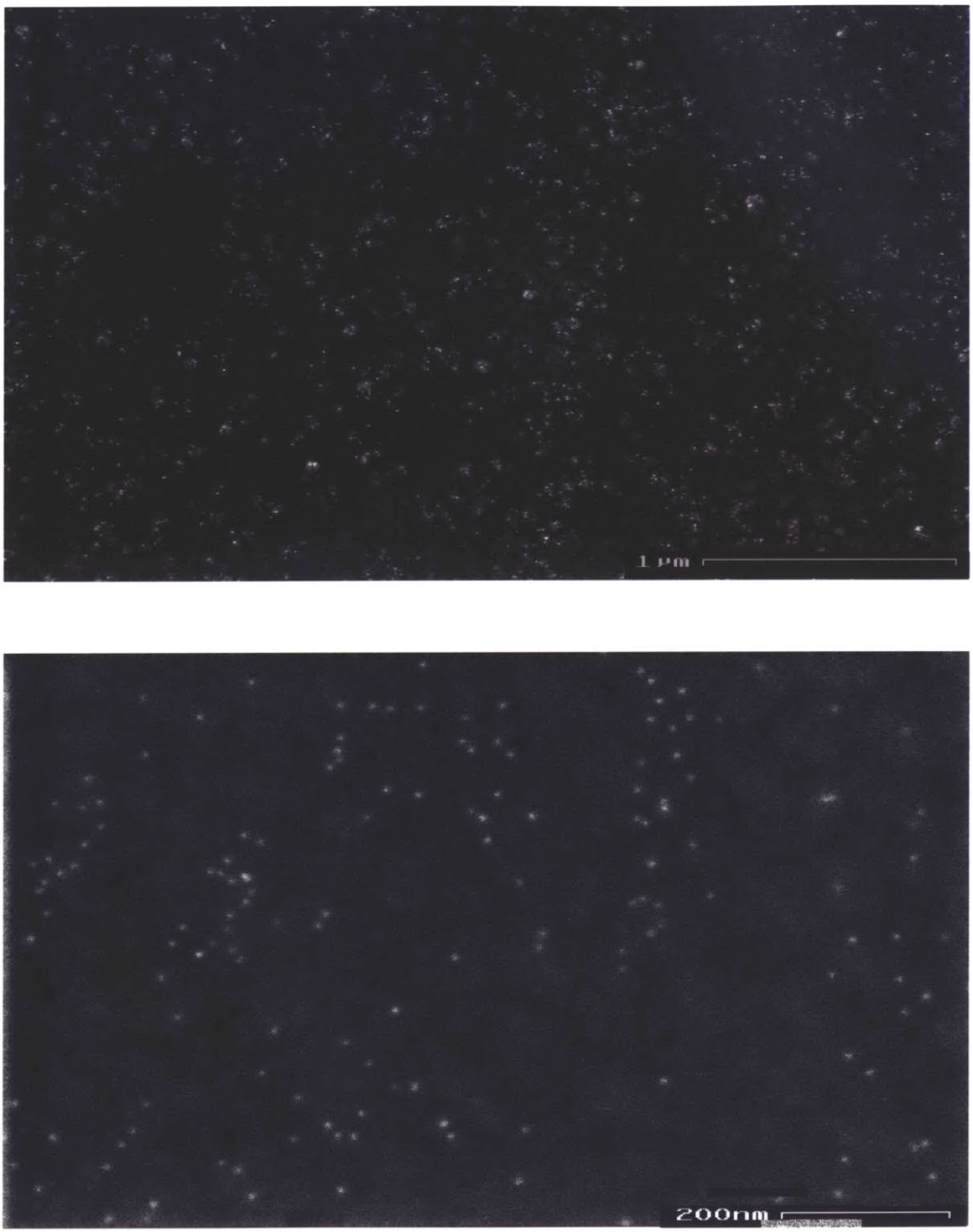

Figure 5.12 (a) Star PEO-biotin, coupled from 20% PEG-biotin solution (approximately 5% biotin-modified PEG on the surface)
top: low magnifiaction, bottom: high magnification

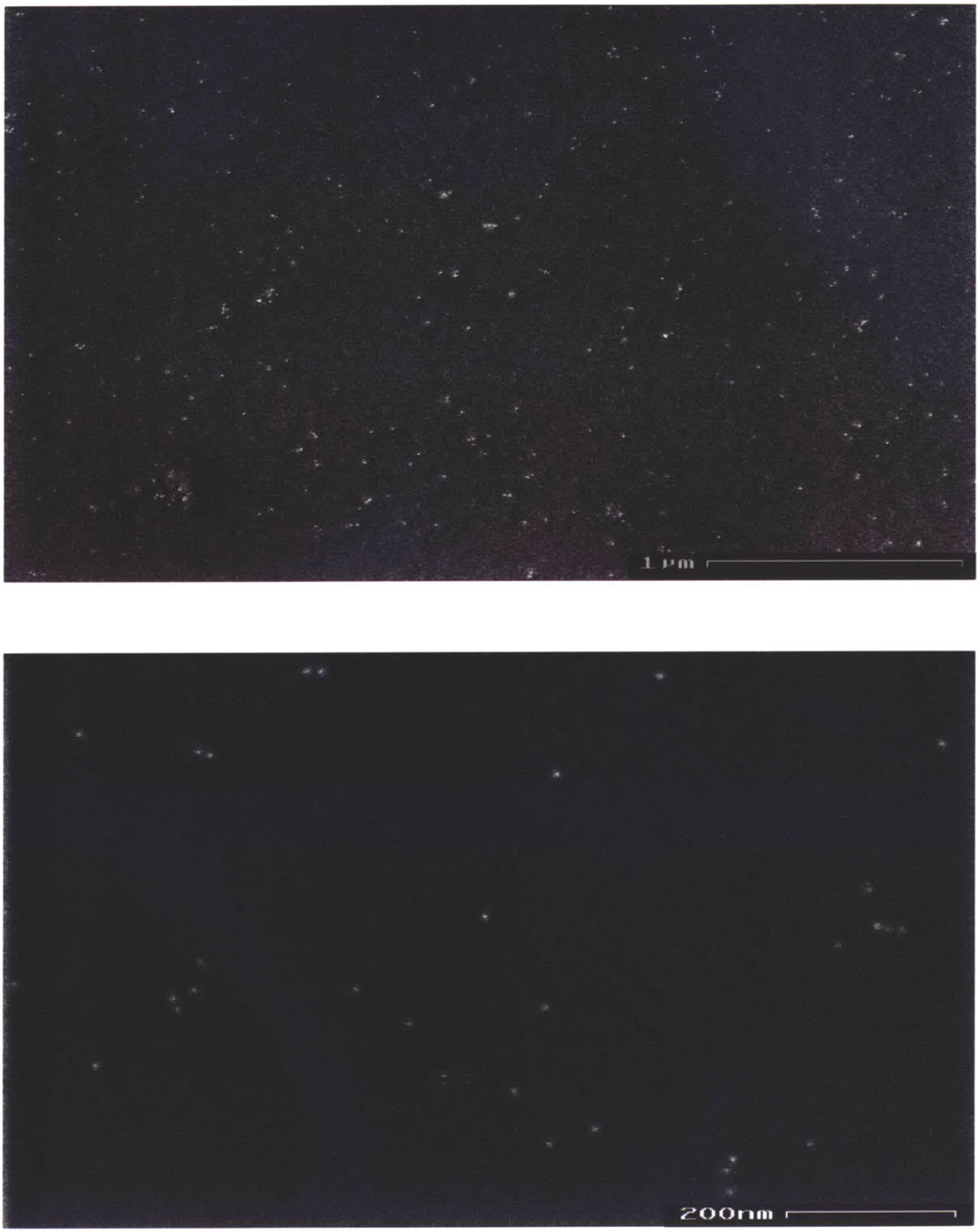

Figure 5.12 (b) Star PEO-biotin, coupled from 40% PEG-biotin solution (approximately 12 % biotin-modified PEO on the surface)
top: low magnification, bottom: high magnification

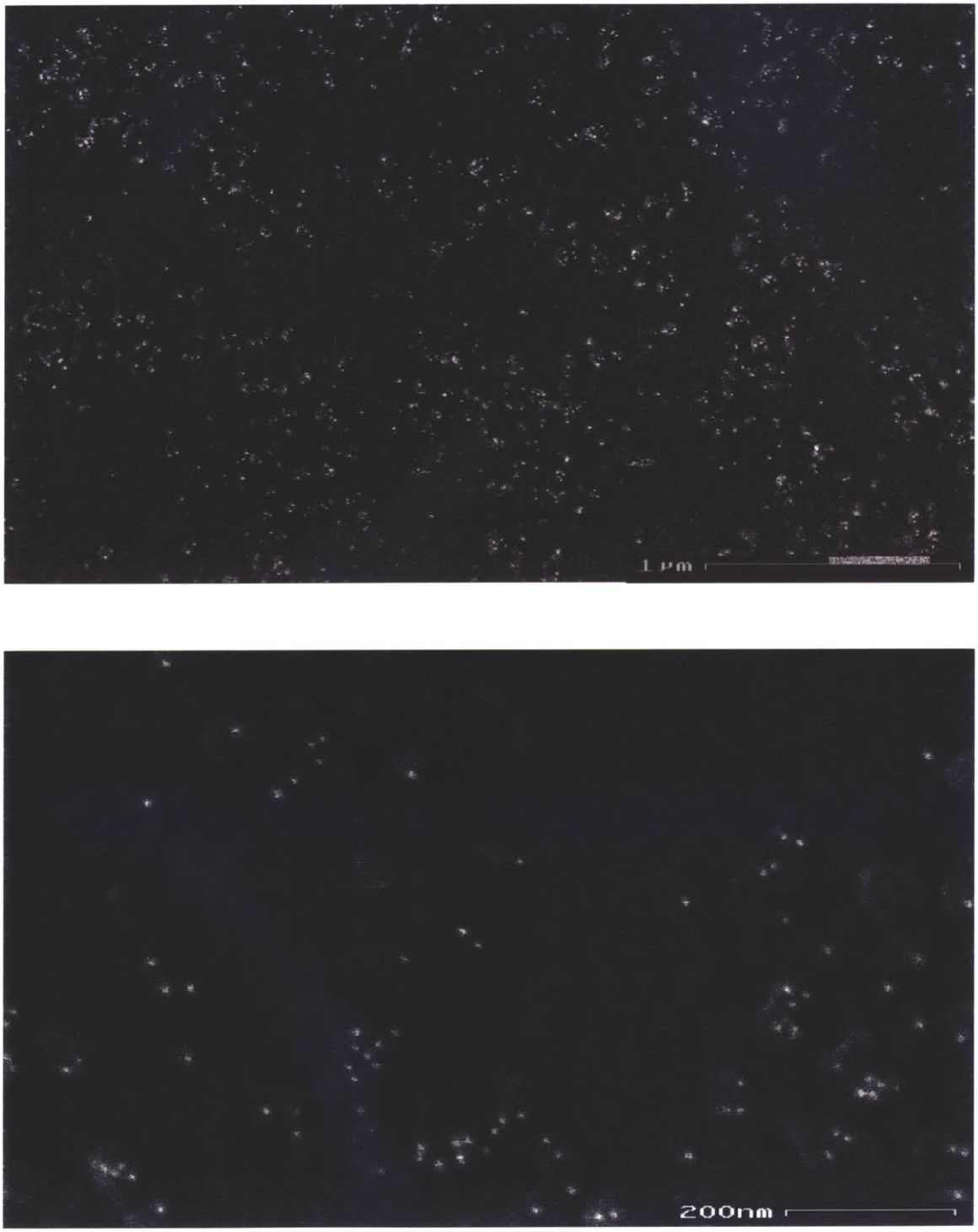

Figure 5.12 (c) Star PEO-biotin, coupled from 60% PEG-biotin solution (approxiamtely 24 % biotin-modified PEO on the surface)
top: low magnification, bottom: high magnification

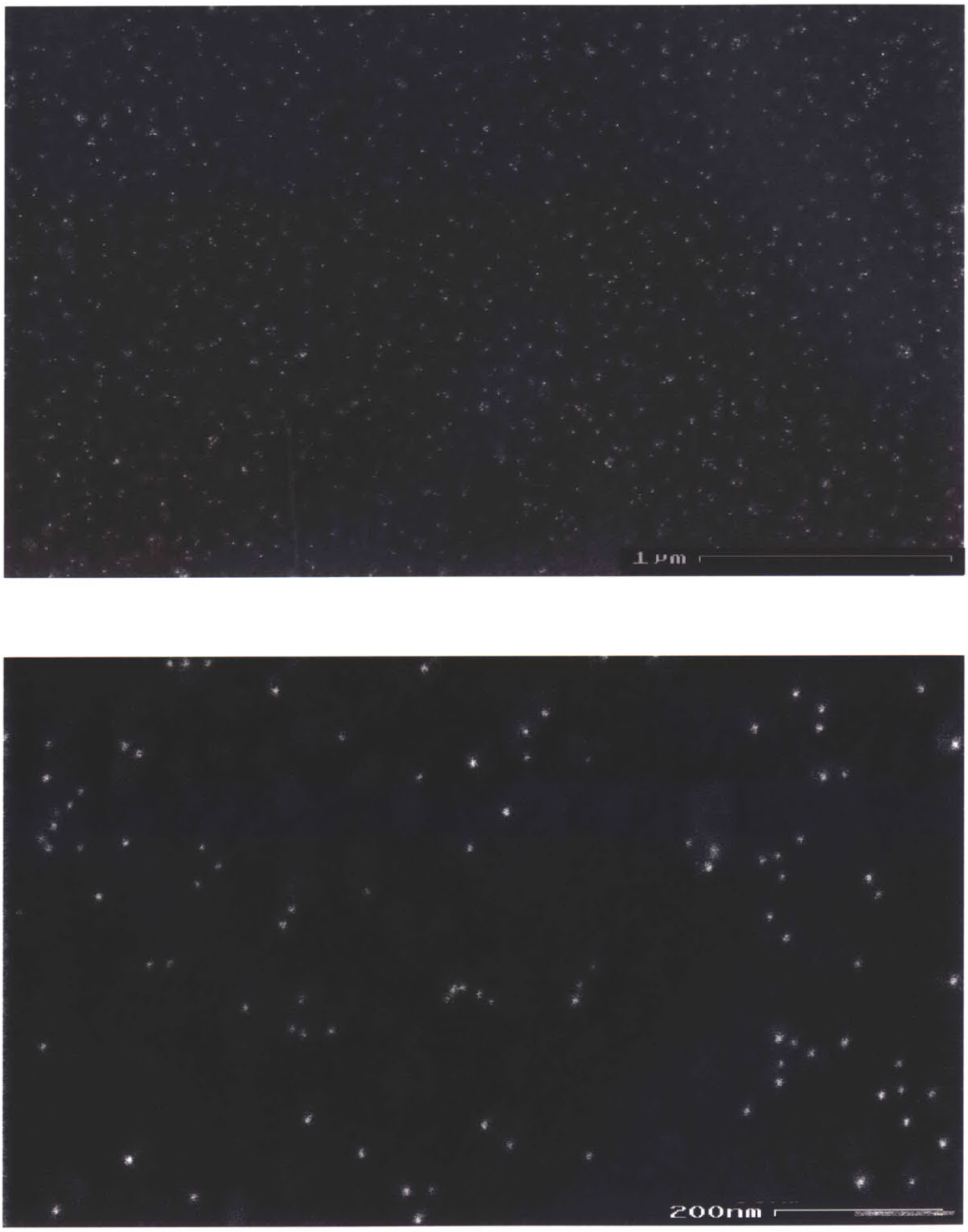

Figure 5.12 (d) Star PEO-biotin, coupled from 80% PEG-biotin solution (approximately 45% biotin-modified PEO on the surface)
top: low magnification, bottom: high magnification

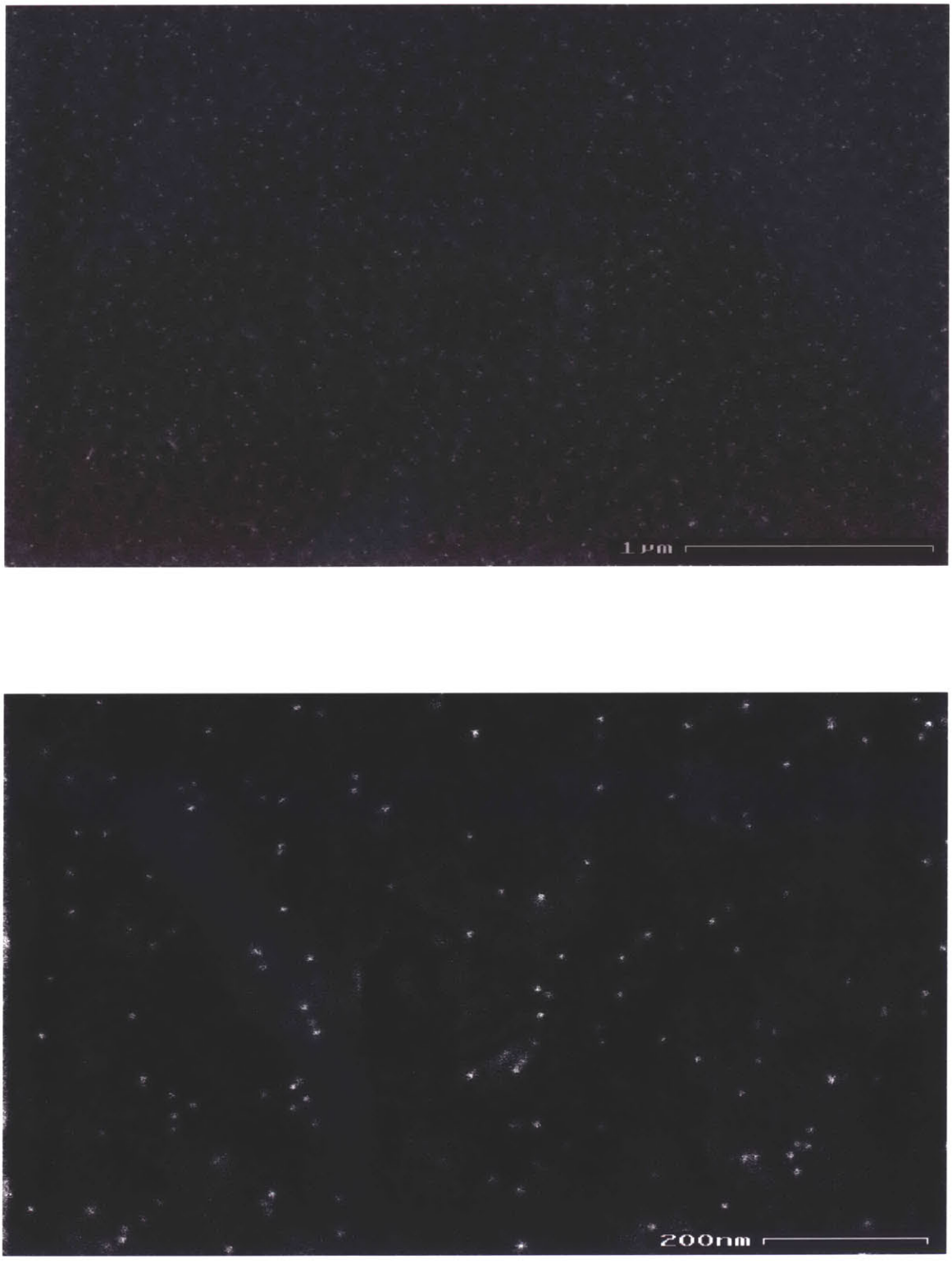

Figure 5.12 (e) Star PEO-biotin, coupled from 100% PEG-biotin solution
top: low magnification, bottom: high magnification

Figure 5.12 (f) Star PEO-biotin, control surface, unmodified star PEO
top: low magnification, bottom: high magnification

Gold particles bound to star PEO-biotin surfaces appear more clustered than those on the linear PEG-biotin surfaces shown in Figure 5.12, consistent with the observations from TEM studies. Again, the apparent gold clusters seem to be surrounded by a "haze", a brighter region which, again, is possibly due to the enveloping of the high-energy gold particles by the lower-energy star molecules. Unmodified star PEO control surfaces showed very low non-specific adsorption compared with biotin-modified surfaces, see Figure 5.12(f).

A: Assessment of steric hindrances during labeling

The surface area of a hydrated star (average diameter = 28 nm) is estimated at roughly 2,500 nm^2, while the area projected by an 11 nm Au-GAB particle on the surface of that star is ~95 nm^2. Even in the most extreme case, if we assume that Au-GAB can bind only to a hemispherical cap at the surface of the star molecule, then it should be possible for ~ 13 Au-GAB particles to pack at the surface of each star. Therefore, when the star PEO-biotin conjugates are hydrated, as would be expected during labeling, the binding of Au-GAB is *not* expected to be limited by steric hindrances due to the size of the gold marker.

While it is unlikely that there will be 13 biotin molecules available at the star surface, it is evident that the binding of Au-GAB to star-biotin conjugates should not be limited by crowding of the gold particles. It is therefore likely that the binding efficiency of the gold markers is significantly higher for these surfaces than for the linear PEO-biotin surfaces.

Several antibody molecules (up to ~ 10) are believed to adsorb on each gold particle (private communication, British Biocell International) during the preparation of the colloidal gold conjugate. Hence, it is also possible that each Au-GAB binds more than one biotin-

conjugated star molecule on the surface, provided that the star PEO-biotin is dense enough to be able to access the binding sites on one central Au-GAB particle (see Figure 5.13).

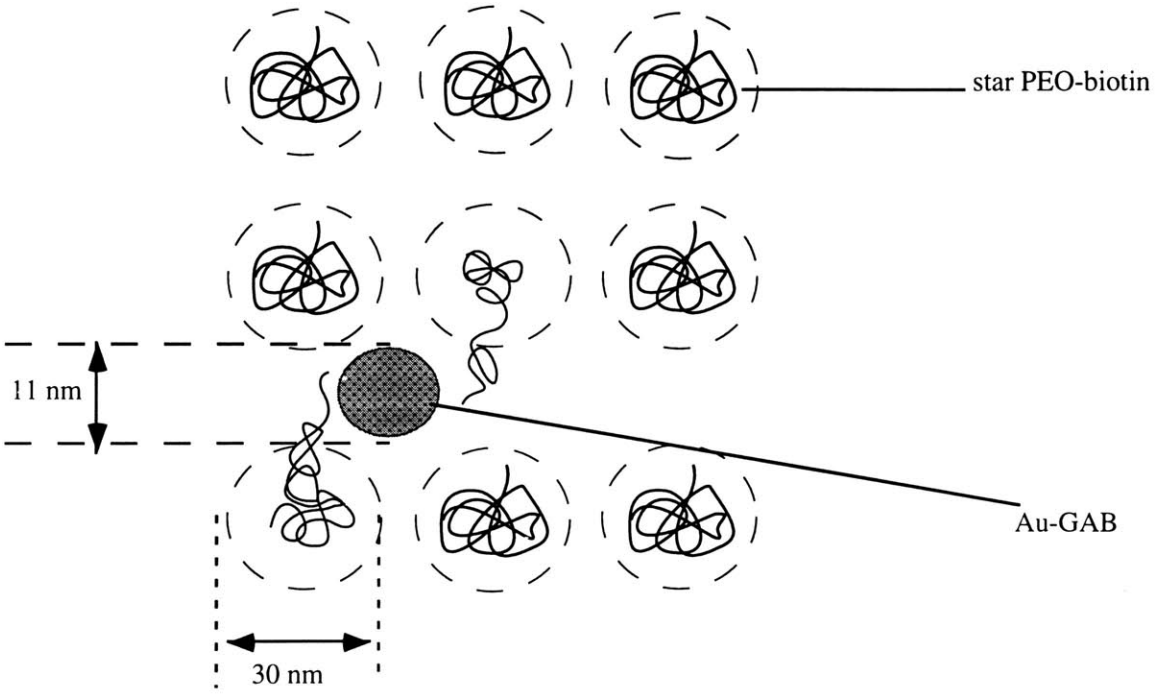

Figure 5.13 Diagram showing ability of Au-GAB to bind multiple tethered biotin molecules

To estimate the extent of this effect, we assume that as the spacing between biotin clusters is increased, that is, as star PEO-biotin molecules are progressively diluted by unmodified stars, the likelihood of more than one star molecule binding to a Au-GAB particle is reduced. The maximum spacing at which this could be observed is dependent on the length of the star arms and their ability to stretch out from their coiled conformations to interact with a Au-GAB particle. Wong and coworkers [125] have suggested that when there is a strong interaction between a receptor and a tethered ligand (for example, in the avidin-biotin system), a flexible tether (for example, PEO) is able to assume a variety of conformations, including near-full extension. Although the likelihood of a PEO molecule completely

unraveling itself to reach its fully extended chain length is extremely small, this condition was set to obtain a limit on the required intercluster spacing; above a spacing of (2 x fully extended arm length), each Au-GAB particle can influence only one star-biotin conjugate.

The fully extended chain length of an arm of star PEO 460 (M_{arm} = 9,100) is approximately 62 nm. Therefore, we can say with absolute certainty that two star PEO-biotin conjugates, spaced at a distance of greater than ~ 120 nm will be unable to interact with the same Au-GAB conjugate. If the spacings between biotin-modified stars are assumed to be the same as the distances between RGD-modified stars calculated in Chapter 4, for n(cluster) = 9 (see Figure 4.9), then the cluster spacing at which one Au-GAB becomes unable to influence more than one star-biotin cluster occurs when the percentage of biotin-modified stars in the initial coupling solution is ~ 5 - 10%. This implies that, in all of the surfaces examined by SEM (prepared for 20% to 100% biotin-modified star PEO solutions), there is the possibility that a Au-GAB particle cold be linked to biotin molecules on more than one star. Even at the lower densities produced from 5 - 10% coupling solutions, however, there is a strong possibility that more on Au-GAB particle can bind more than one biotin molecule on a *single star* , reducing the apparent cluster sizes in the image.

B: Analysis of the spatial distribution of gold markers

Cumulative nearest neighbour distance distributions (NNDDs) for the star PEO-biotin surfaces were calculated, and are displayed in Figure 5.14. Comparison of these cumulative NNDDs with those obtained from simulations of uniform distributions will give an indication of whether or not clustering has occurred. If clustering is occurring in the star PEO-biotin system, then the NNDs of a significant fraction of the gold particles are constrained to be less than or equal to the diameter of one Au-GAB-biotin-star PEO complex. For the star system, the characteristic diameter is taken as the diameter of the

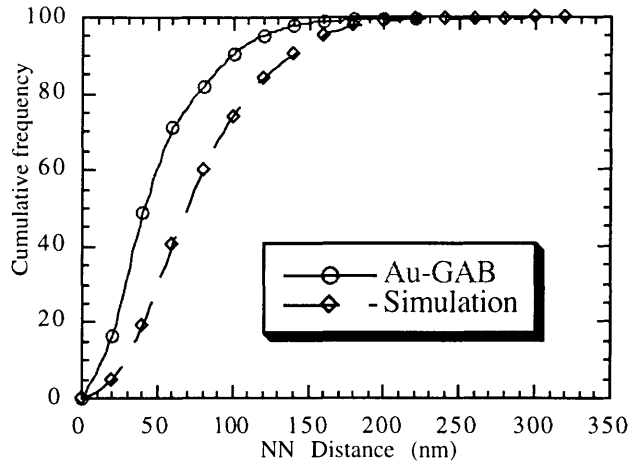

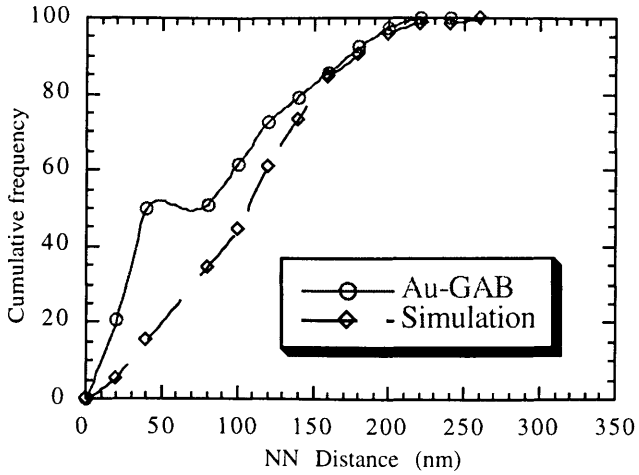

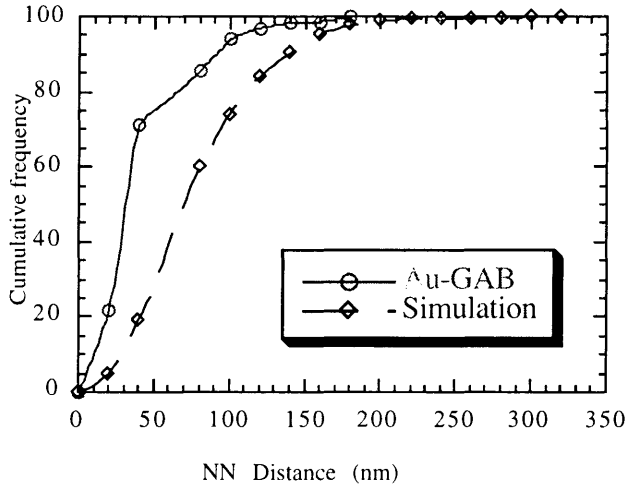

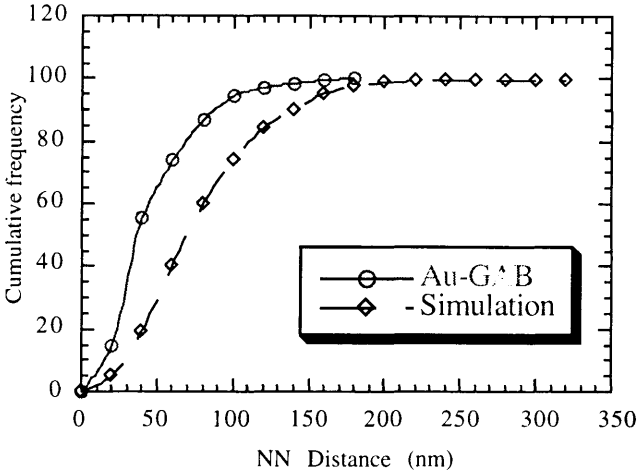

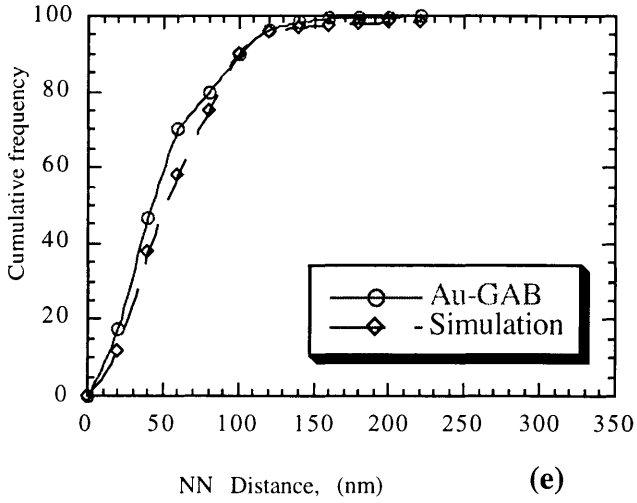

Figure 5.14: Cumulative NNDDs for equivalent densities of star PEO-biotin and simulated 2-dimensional arrays
(a) 5% biotin-modified PEO,
(b) 12% biotin-modified PEO,
(c) 24% biotin-modofied PEO,
(d) 46% biotin-modified PEO
(e) 100% biotin-modified PEO estimated on surface

dried star molecule (12-18 nm) plus the twice the diameter of a Au-GAB particle (11 nm), or approximately 34-40 nm. The plot in Figure 5.15 shows that the percentage of gold markers having NNDs less than or equal to 35 nm (that is the percentage of gold markers possibly labeling an individual cluster) is consistently between 35 and 40 percent, except at the highest biotin density, where it rises to approximately 50%. For the linear system, the characteristic conjugate diameter is taken as 11 nm; any particles occurring at NNDs less than or equal to 11 nm would be considered aggregated.

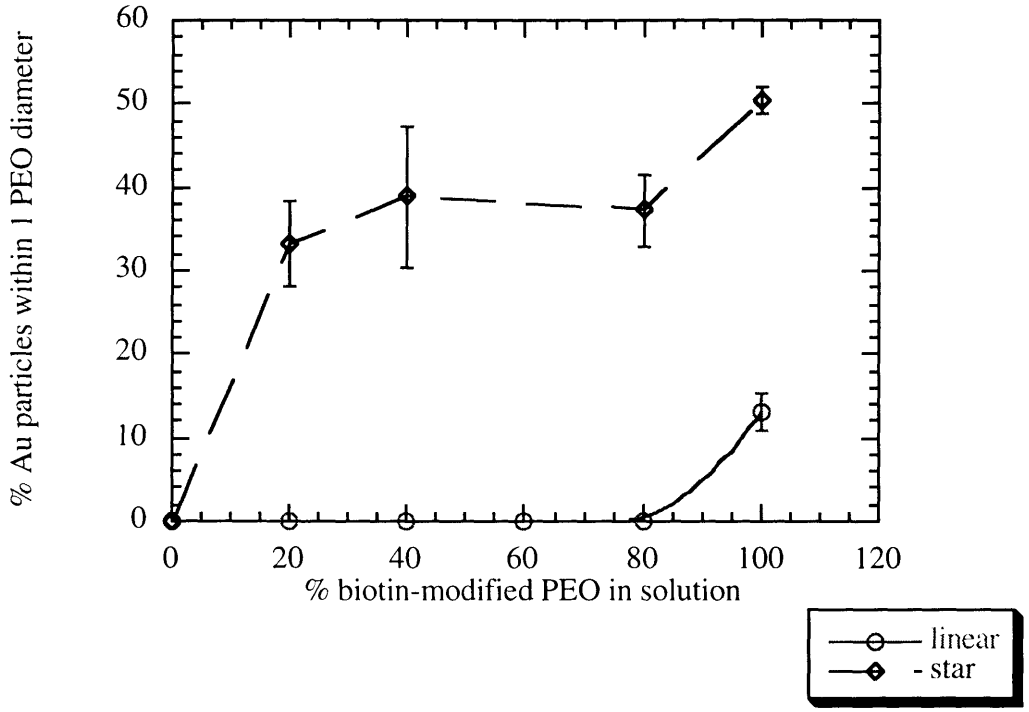

Figure 5.15:Probability of gold marker occurring within one molecular diameter of its nearest neighbour

As can be seen from Figure 5.15, it is only at the highest biotin density (estimated at ~ 120,000 molecules/μm^2, based on RGD data) that such low NNDs are observed in the

linear system. Even at this relatively high biotin density, only ~15% of the markers have NNDs less than or equal to the characteristic spacing. For these surfaces, the observation of some markers at this spacing is not attributed to aggregation of the markers or clustering of the ligand, as the distribution was shown to be normal by the Kolmogorov test. Rather, it is expected that the average spacings between ligands is lessened at higher biotin densities; the probability that two gold markers will label "adjacent" biotin molecules should therefore increase. In addition, the gold density increases at higher biotin densities (see Figure 5.9); an increased density of gold particles should result in reduced NNDs.

Finally, the Kolmogorov test was again performed on NNDDs obtained from star PEO-biotin surfaces, and the results are displayed in Table 5.6.

% biotin-modified PEG on surface	Au-GAB density, n (particles/μm^2)	D_n	K	normal distribution?
5	94	0.31	0.16	no
12	26	0.34	0.31	no
24	50	0.51	0.23	no
46	108	0.36	0.15	no
100	95	0.16	0.17	yes

Table 5.6 Results of Kolmogorov test for uniformity of distribution of biotin on star PEO-biotin surfaces.

The analysis shows that the gold markers take on a non-random distribution on surfaces prepared with a mixture of biotin-modified and unmodified stars for all biotin surfaces prepared from solutions with biotin-PEG concentrations of 20% to 80%. As discussed

previously, the test reveals a significant deviation from the test (Gaussian) distribution. Such a deviation is not necessarily proof of formation of isolated clusters, however, the non-uniformity in the biotin distribution is presumably caused by the mixing of unmodified stars with modified stars on the surface, creating domains in which there is a zero probability of locating biotin. If these domains occupy a large enough percentage of the total area, they may be expected to become continuous, creating isolated domains, or "clusters" of biotin on the surface. As mentioned previously, such isolated domains are expected to form when the biotin-modified stars occupy ~ 16% of the surface, which happens when the percentage of biotin-modified stars in soluition is ~ 50% (from Table 5.5). As anticipated, labeling appeared random on substrates prepared using solution containing 100% biotin-modified PEO, indicating all regions of the surface are equally likely to present biotin.

Since the labeling efficiency of the Au-GAB was so low in the linear PEG-biotin system, an attempt was not made to measure cluster sizes and spacings directly from SEM images. In addition, since the cluster size, and therefore the average biotin surface density could not be determined, the labeling efficiency was not estimated. The density of gold on the surfaces having the highest biotin density was the same as that on the lowest density surfaces, again suggesting that the relative values of marker density cannot be used to precisely indicate ligand densities or labeling efficiencies

5.5 Conclusions

The ability to present ligands on bioactive surfaces in spatially separated domains, or clusters, has been demonstrated. Immunogold techniques were developed for the labeling of bioactive ligands on representative surfaces, which could then be easily imaged by High Resolution SEM and TEM. There were several limitations associated with the technique,

including the prevention of full labeling due to steric hindrances, low labeling efficiency, non-specific adsorption and the appearance of defects in the TEM images. However, two objective tests showed that the gold markers assumed a non-random, or aggregated distribution on star PEO-biotin surfaces in both TEM and HRSEM images. While the limitations of the biotin-anti-biotin system prevent strict quantitation of ligand density, the technique is well suited for the objective determination of ligand distribution.

CHAPTER 6. CELL INTERACTIONS WITH RGD SUBSTRATES

6.1 Introduction

The central hypothesis in this thesis is that the presentation of ligands to cells in a spatially controlled fashion would fundamentally alter cell responses to adhesion peptides, that is, that we would be able to control the clustering of integrin receptors by presenting the RGD peptide to cells in domains of high concentration, or "clusters" against an inert background. In most quantitative studies of cell interactions with RGD surfaces, the peptide is immobilized on its substrate at a uniform distribution [16], [30]. We expected that clustered ligand surfaces would allow focal contact formation at lower overall RGD ligand densities than surfaces on which ligand is uniformly distributed, and perhaps enable the observation of certain physiological behaviours (for example, adhesion and migration) at lower overall ligand densities.

To test this hypothesis, surfaces on which ligands are distributed either uniformly or in aggregates of 1 nm to 30 nm in size, with spacings of 20 nm to 500 nm between clusters were prepared, giving us simultaneous control over ligand density and spatial distribution (see Chapters 3 - 5). In NR6 cells, it is estimated that there are approximately 100 integrin receptors per μm^2 in contact with the surface. It is difficult to estimate *a priori* the number of ligands that will be required per receptor, hence the surfaces prepared spanned the range of RGD densities, from 1,000 to 200,000 RGD molecules/μm^2, expected to encompass poorly cell-adhesive to highly adhesive conditions.

6.2 Experimental design

The objectives of the cell-based assays performed in this chapter were to determine (i) whether cells interact with tethered RGD on the star PEO-RGD surfaces, (ii) whether observed interactions are integrin-specific, and (iii) whether the presentation of ligands in a clustered format affected a cell's response to a material for a given *average* ligand density.

The first evidence of a cell-substrate interaction is usually the cells' ability to adhere and spread on its substrate [31], [30]. This basic response was assessed in a qualitative fashion with several cell types: NR6 fibroblasts, Chinese Hamster Ovary (CHO) cells, Bovine Aortic Endothelial (BAE) cells and BAF/3 cells (an embryonic stem cell line).

Two assays for the integrin specificity of the interaction were performed. First, an inactive form of the RGD peptide was tethered to the substrates, and the cell substrate interaction observed. Second, cells were allowed to attach to the tethered RGD, then an active RGD peptide was added in soluble form to the culture medium. If adhesion to the substrate is integrin-mediated, then soluble RGD should competitively bind to the substrate-bound integrins, lessening the degree of adhesion to the substrate, and causing the cells to visibly round or even to detach from the substrate [15], [30].

More sensitive and quantitative assays for the effects of clustering on cell response were also carried out. The spread area achieved by cells after 24 hours of adhesion was measured on clustered RGD surfaces and on surfaces on which the RGD distribution was uniform. This is a good indicator of the extent of interaction with the substrate, relatively high spread areas suggesting a strong adhesive interaction with the substrate [126]. Finally, the effect of the presentation of ligands in a clustered format on the adhesion and

migration behaviour of cells was examined in collaboration with Gargi Maheshwari of the Department of Chemical Engineering at MIT.

6.3 Materials and Methods

6.3.1 Cell culture

The four cell types used in these assays, NR6, BAE, BAF/3 and CHO-LA were cultured as described in Appendix C. Most cell types were removed from culture dishes by trypsinization, then the action of the trypsin was stopped by the addition of a small amount of the culture medium. CHO-LA cells were removed from culture dishes by the action of EDTA.

6.3.2 Surface preparation

Crosslinked PEO hydrogels were prepared on 18 mm, PEG silane-grafted glass coverslips by irradiation of 5 % (w/v) bis(polyoxyethylene (bis) amine) with a 2 MRad electron beam, as described in Chapter 3. The chain ends end of star PEO 460 were modified from hydroxyl to carboxyl, then the PEO was conjugated with the peptide Tyr-Gly-Arg(Pmc)-Gly-Asp(tBu) in aqueous MES buffer, as described in Chapter 4. Star PEO-RGD conjugates were coupled to hydrogel substrates from solutions containing a mixture of unmodified and RGD-modified star PEO, then the RGD peptide was deprotected. Due to the relatively large number of chemicals with which these surfaces come into contact during this preparation, it was not considered practical to maintain sterility during the process. Therefore, immediately prior to seeding of cells on these substrates they were sterilized by light spraying with a 70% solution of ethanol in water, and rinsing in sterile PBS.

6.3.3 Initial screen of cell adhesion

An initial, qualitative screen for cell adhesion was performed. The four cell types were seeded on substrates having a relatively high RGD density, prepared by immobilizing 9-RGD clusters on hydrogels from solutions containing 5 % (w/v) of PEO-RGD conjugate (previously determined to present an average of 1.2 x 10^5 ligands/μm^2, see Chapter 4). Approximately 8,000 cells were seeded per well in serum-containing medium, and three surfaces were tested for each cell type. As a control, cells were also seeded on tissue culture-treated polystyrene, to which human fibronectin (Sigma) had been adsorbed from a 1 µg/ml solution in PBS. The fibronectin concentration was selected because it is believed to give a sufficiently high fibronectin density on the substrate to saturate all integrin receptors. Cells were incubated for 24 hours at 37 °C, then the surfaces were gently rinsed with PBS to remove nonadherent cells. Attached cells were fixed in a 3.7% solution of glutaraldehyde in water for 20 minutes, then rinsed three times in PBS. Cells were then photographed using a phase contrast microscope.

6.3.4 Test for specificity of cell-substrate interaction

A: Inhibition by soluble RGD peptide

Receptor-ligand interactions are reversible in nature, that is, a receptor can bind to a ligand, unbind, then bind to a different ligand [4]. The introduction of an integrin-binding soluble RGD peptide to the culture medium after cells have specifically attached to a substrate should reduce that attachment, since at equilibrium, the occupied receptors will be distributed between surface-bound fibronectin and soluble peptide Such reversal of

attachment is observed when the soluble peptide GRGDSP (2 mM, Gibco) is added to NR6 cells attached to FN substrates in serum-free medium.

NR6 cells were therefore allowed to attach to substrates having 1.2 x 10^5 RGD peptide molecules per μm^2, for 24 hours, as described above. Then the culture medium was changed to a serum free MEM-α, containing 2 mM dissolved GRGDSP (Gibco). The cells were incubated for 20 minutes at 37 °C, then examined under a phase contrast microscope.

B: Adhesion to inactive RGD peptide

An inactive peptide, one that does not undergo specific interaction with integrin receptors, will not reverse binding- we found that a GRGDY peptide synthesized in-house failed to reverse binding at 2 mM and could thus be considered inactive. the GRGDY peptide was thus used to create control substrates which were chemically similar to those bearing the active YGRGD peptide. 125I-labeled GRGDY was conjugated to star PEO 704 (f = 64, M(arm) = 11,000), and the conjugates were covalently grafted on PEO hydrogels. Radiolabeling of the peptide with ^{125}I enabled average cluster size and RGD density to be determined as described in Chapter 4. PEO-RGD conjugates were coupled from solution in MES buffer, at concentrations of 0.1 %, 0.5 % and 1 % (w/v). Unmodified star PEO was not added to the coupling solution. Cells were seeded on these substrates in serum-containing medium, left to attach for 24 hours, and examined under a phase contrast microscope.

6.3.5 Influence of RGD density and distribution on cell behaviours

A: Cell spread area

Star RGD conjugates were coupled to substrates from 5 % (w/v) solutions containing 100 %, 20 %, 10%, 5 % and 2.5% RGD-modified stars. NR6 cells were seeded on star PEO-RGD surfaces (cluster sizes of 1 and 9) in serum-free medium. After 24 hours surfaces were rinsed gently with PBS to remove unattached cells. Remaining cells were fixed for 20 minutes with 3.7 % paraformaldehyde in PBS, then photographed. Cell outlines were obtained by tracing images of at least 30 isolated cells in the phase contrast micrographs; from these outlines the cell spread areas determined using Scion Image 1.49 software.

B: Clustering effects on adhesion and migration

Quantitative studies of the effects of ligand clustering on adhesion and migration were performed by Gargi Maheshwari. Cells used in these studies were wild-type NR6 cells, cultured as described in Appendix C. The cell culture and assay procedures have been described elsewhere in detail [127].

The strength of adhesion of NR6 cells to star PEO-RGD surfaces was quantified by a centrifugation assay [128], [127]. Substrates were glued into the wells of a 12-well culture dish. Cells were seeded on these substrates in serum-free conditions for 12 hours at a density of 12,000 per well. Medium was then changed to MEM-α with 25 mM HEPES containing 1 % dialysed fetal bovine serum (FBS), and incubated in a humid environment at 37 °C for 8 hours. Plates were inverted, and centrifuged in a swing bucket SH-3000 rotor in a benchtop centrifuge (Sorvall) for 10 minutes at 25 °C at 800 g. As a control, one

plate at the highest RGD density (1.2×10^5 molecules/μm^2) was kept at 1 g at 25 °C. After centrifugation, the cell number was measured by manually counting the cells in a well-defined area. At least 3 wells were seeded at each condition, with 4 fields examined per well, and each experiment was performed three times. The average cell number in the experimental wells was normalized to that in the control wells to obtain the fraction of adherent cells remaining after centrifugation.

In migration experiments, star PEO-RGD surfaces were glued to the bottom of 35 mm culture dishes using an optically clear adhesive. 30,000 cells were seeded in each dish in serum-free medium and incubated at 37 °C. After 12 hours, the medium was changed to MEM-α with 25 mM HEPES containing 1 % dialysed fetal bovine serum (FBS), and incubated in a humid environment at 37 °C for 8 hours. The culture dish was inserted into a temperature-controlled, motorized stage (Ludl 99S008) on a Zeiss Axiovert 35 microscope, and cell locomotion was recorded using time-lapse videomicroscopy of single cells. The x- and y-co-ordinates of the cell centroids were determined every 15 minutes, using image processing software (Engineering Technology Center, Mystic CT), and single cell speeds were determined by measuring the centroid displacement divided by the tracking time.

6.4 Results and Discussion

6.4.1 Cell interactions with tethered RGD surfaces

The underlying hydrogel substrates are completely non-adhesive to the four cell types investigated for at least 24 hours under serum-containing conditions (Chapter 3). Substrates derivatized with unmodified star PEO molecules (no RGD) are also completely

resistant to cell adhesion. Therefore any adhesion observed in these assays was attributed to the recognition and ligation of the tethered RGD peptide by integrin receptors.

Phase contrast micrographs of cells on the star PEO-RGD substrates are displayed in Figure 6.1. As can be seen from the photographs, the NR6, CHO and BAE cells adhered and spread, both on the RGD surfaces (1.2×10^5 RGD molecules/μm^2) and on fibronectin controls (adsorbed from a 1 μg/ml solution). These data demonstrate that a bioinert surface, covalently derivatized with RGD has been achieved, and supports adhesion and spreading for most cell types in a manner similar to that seen on adsorbed fibronectin, a common "standard" used in studies of adhesion phenomena. This has typically not been achieved in studies of RGD-mediated adhesion: many studies on covalently grafted surfaces are done over much shorter time periods (2 hours [14], [129] compared with 24 hours in this study), while experiments in which the inertness of the unmodified substrate was proven over a 24 hour period have usually been performed on non-covalent surfaces [30], [31]. In addition, the results suggest that the substrates present the RGD peptide to cells in a conformation and an orientation which they are able to recognize, and that the tethered RGD peptide is active.

BAF/3 (stem) cells were unable to attach to RGD surfaces, although they adhered to fibronectin. A possible explanation for this observation may again involve the cell-type specificity of adhesion behaviour. Stem cells are known to go through various stages of development, and their interactions with fibronectin have been found to change according to their stage of differentiation [130]. Primitive stem cells lack many of the surface antigens found on more mature cells; upon maturation and differentiation that these cells appear to express new types of receptors. It has been suggested that primitive stem cells do not express the $\alpha_5\beta_1$ receptor, adhering to fibronectin instead by the $\alpha_4\beta_1$ integrin [131],

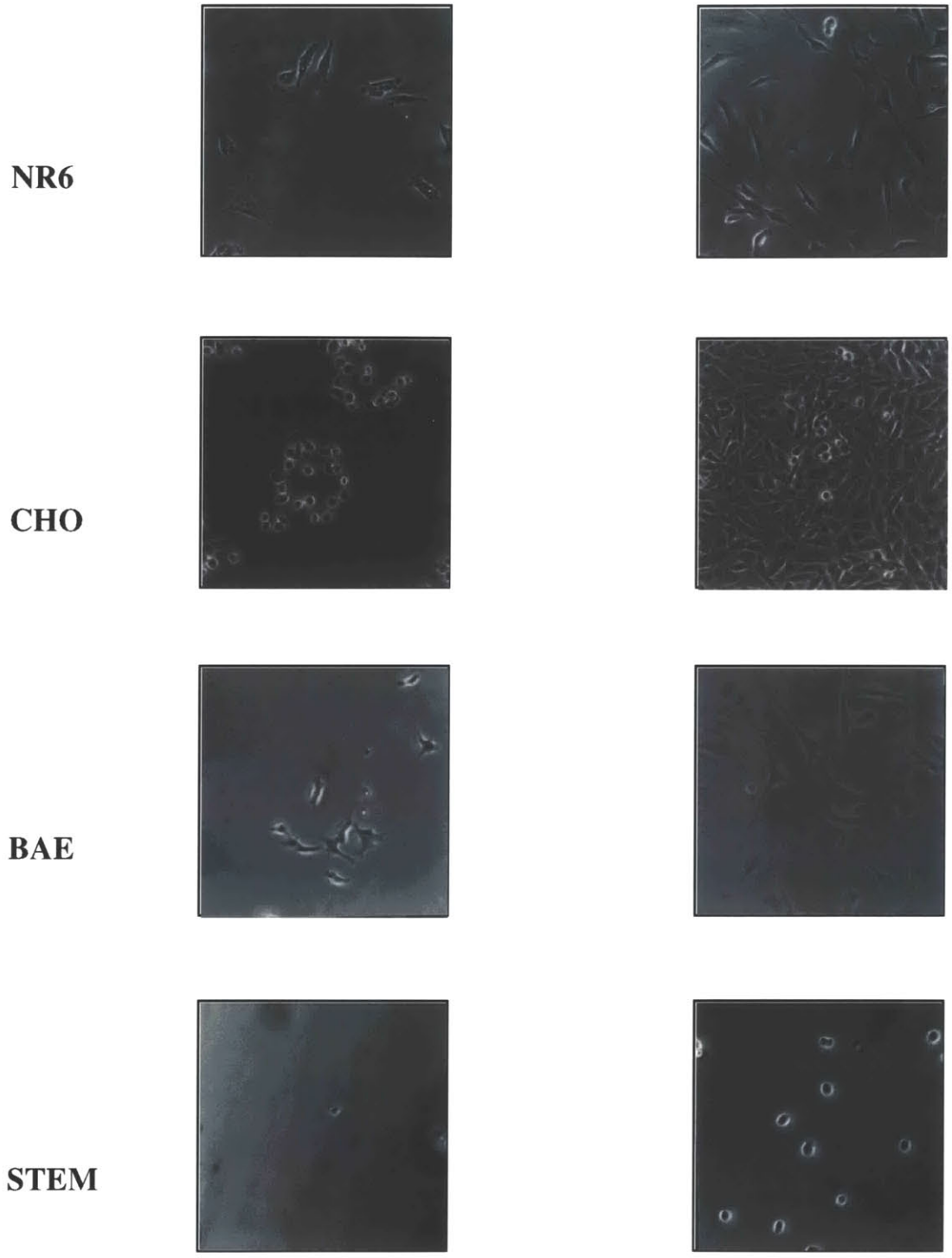

Figure 6.1: Cell responses to star PEO-RGD and fibronectin surfaces after 24 hours

[130], which binds to the heparin-binding fragment of fibronectin which contains the amino acid sequence LDV [132]. The binding of primitive stem cells to fibronectin can therefore take place in an RGD-independent fashion [133]. BAF/3 cells are a murine bone marrow-derived cell-line, and have been characterized as primitive or immature [134], [135]. Hence, it is possible that BAF/3 cells either do not express, or express very low levels of the fibronectin receptor $\alpha_5\beta_1$, adhering to fibronectin instead by the $\alpha_4\beta_1$ receptor. If that is the case, then the cells would not be expected to adhere to an RGD surface.

All other cell types used in this investigation express at least one of the types of receptor known to bind to the RGD sequence (either $\alpha_5\beta_1$ or $\alpha_v\beta_3$), and adhered and spread on the star PEO-RGD surfaces. This gives the first suggestion that the binding of cells to the PEO-RGD surfaces is specific: only those cells whose receptors recognize the RGD sequence are able to attach.

6.4.2 Inhibition of attachment and spreading by soluble RGD peptide

A: Inhibition of attachment and spreading by soluble RGD peptide

Figure 6.2 contains photographs of NR6 cells on RGD substrates, before and after the addition of 2 mM soluble GRGDSP. Significant rounding of the cells occurred within 20 minutes of the addition of soluble peptide; when the RGD peptide-containing medium was replaced with serum-free medium, the cells resumed their well spread morphologies.

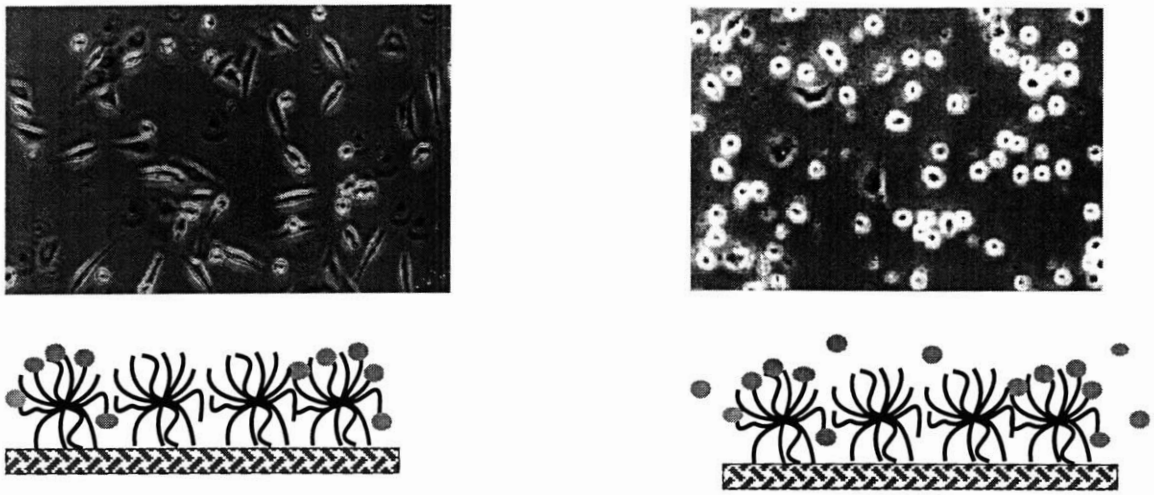

Figure 6.2: NR6 fibroblasts after (a) 24 hours' adhesion to star PEO-RGD surfaces, followed by (b) addition of 2 mM soluble GRGDSP peptide

Similar results were seen on fibronectin surfaces, suggesting that the NR6 cells are attached to the RGD surfaces via the same receptor responsible for binding to fibronectin; when soluble RGD peptide, is added to the culture medium, it competitively binds the same integrin receptors, reducing the degree of attachment and spreading of the cells on the substrate. The NR6 cells adherent on other PEO-RGD surfaces are therefore presumed to be interacting specifically with the peptide.

B: NR6 interactions with a tethered inactive peptide

The second test for specificity involved the conjugation of an inactive peptide to star PEO molecules, then coupling those conjugates to hydrogel substrates. Figure 6.3 shows the RGD densities obtained by immobilizing star PEO-nonsense peptide conjugates on hydrogels. As in Chapter 4, a range of average RGD densities was obtained. However, NR6 cells were completely unable to attach and spread on these surfaces- after 24 hours no cells had adhered to these surfaces. The results suggest that the PEO hydrogel surfaces

modified with active RGD are not supporting cell adhesion merely by providing hydrophobic or electrically charged surface sites for the adsorption of serum or endogenous proteins. The NR6 cells adherent on other PEO-RGD surfaces are therefore interacting specifically with the peptide.

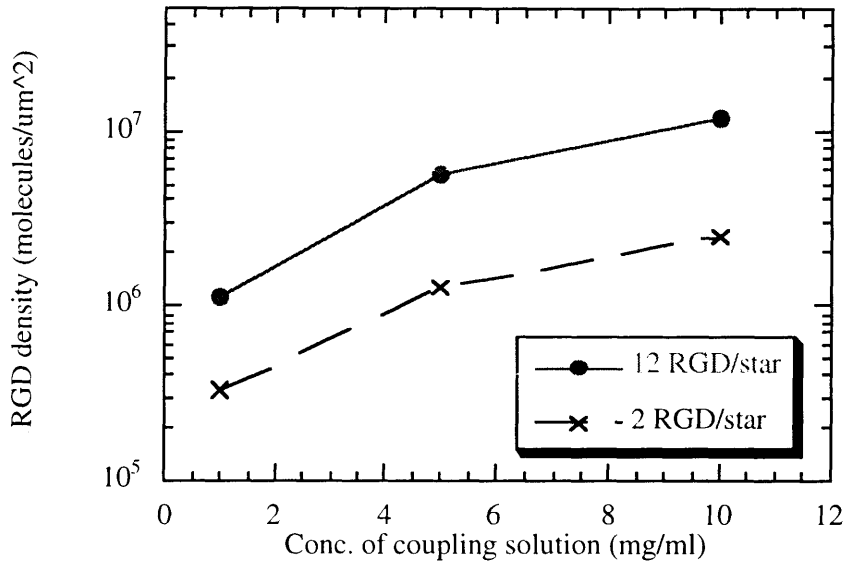

Figure 6.3: Average densities of (inactive) GRGDY peptide achieved by coupling star PEO-RGD conjugates to hydrogel substrates from 1, 5 and 10 mg/ml solutions

In other systems, in which RGD is immobilized on a substrate which itself supports matrix deposition and remodeling, experimental results are confounded by the interactions of integrins with other proteins than those specifically bound, and are possibly also confounded by the interactions of other integrins which are not involved in binding to RGD

[30]. The achievement of a surface which can be shown to support *only* specific interactions over relatively long periods of time is therefore an important one for the quantitative model studies which are intended.

6.4.3 Adhesion to RGD compared with fibronectin

Star PEO-RGD surfaces appear to support cell attachment and spreading in a manner similar to that seen on fibronectin. However, the surfaces fabricated for this thesis are significantly different from typical fibronectin surfaces, usually prepared by adsorbing fibronectin on the surface of a culture dish, and therefore will not give exactly the same results. For example, the attachment of NR6 fibroblasts to PEO-RGD surfaces was observed to be significantly slower than that seen on fibronectin (unpublished data). One explanation for this could involve the lower affinity of integrins for RGD than fibronectin [114]. Streeter et al. showed that cells on RGD surfaces showed slower spreading kinetics, and required higher RGD densities to get to the same level of attachment and spreading as on FN [43]. It is also quite possible that the presence of the non-adhesive PEO substrate, as well as the star PEO tethers, has the effect of reducing the frequency of encounters between receptor and ligand, thereby reducing the rate of adhesion. Furthermore, Roberts et al. observed that fibronectin surfaces support matrix deposition, while mixed SAMs of $(EG)_3OH$- and $(EG)_6OGRGD$-terminated alkanethiolates were resistant to the non-specific adsorption of proteins [30]. If cells are able to deposit proteins on the surface during our experiments which either assist or hinder their adhesion and migration, then their response to these PEO-RGD substrates which support only specific interactions will be different from that observed on fibronectin. This should be taken into consideration in investigations of the PEO-RGD system, where fibronectin is used as a "standard. One possible future study could therefore involve a comparison of the kinetics of cell adhesion to the two substrates.

6.4.4 Density dependence and effects of clustering

The remaining cell assays were quantitative in nature, that is, the *magnitude* of the cells' response was measured as a function of RGD density and lateral distribution. Ward and Hammer proposed a theoretical model of focal contact formation in terms of (i) the binding of a receptor to its extracellular ligand (affinity constant = K_D), (ii) the binding of a receptor its cytoskeletal component (affinity constant = K_c), and (iii) the self-association of receptor-ligand-cytoskeletal protein complexes (affinity constant = K_p) into focal contacts, as represented below in Figure 6.4.

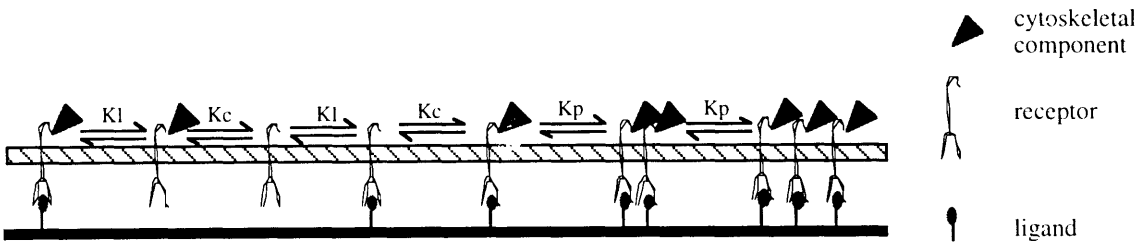

Figure 6.4 Schematic representation of the interactions of receptors with exrtracellular ligands and with intracellular cytoskeletal proteins, and their assembly into clusters. Adapted from Ward and Hammer [18].

They concluded that at low ligand density ([ligand] < [receptor]), clustering is limited by the availability of ligand, while at high ligand density ([ligand] > [receptor]), clustering is limited by the availability of cytoskeletal proteins. They also showed that the most significant parameter affecting clustering of cell surface receptors is the ability of the cytoskeletal elements to associate, or "polymerize", which occurs only when receptors are bound to their extracellular ligands. The affinity of ligand-receptor-cytoskeletal complexes

for each other, K_p, appears to increase with increasing ligand concentration [18]. This finding was supported in part by the experiments of Massia et al. who found a minimum density of immobilized RGD (60 molecules/μm^2, uniformly distributed) below which focal contacts are unable to form in fibroblasts [16]. We therefore hypothesized presenting ligands in a clustered format might promote the polymerization of ligand-receptor-cytoskeletal complexes by constraining the receptors to be in close proximity when they bind to their extracellular ligands.

In addition to those previously seen effects of ligand density, we expected to observe a simultaneous effect of ligand spatial distribution on cell behaviour. We hypothesized that the presentation of ligands in a clustered format would provide a more physiological environment for adhesion and adhesion-related events, possibly allowing cell behaviours previously seen only at relatively high (uniform) densities to be observed at lower average densities.

A: Cell spread area

The cell spread area gives an indication of the number of receptors involved in bond formation, and therefore the number of receptors available for clustering into focal contacts [126]. Figure 6.5 shows the variation in cell spread area on substrates with evenly distributed and clustered peptides. These substrates were prepared from 9-RGD and 0.8-RGD clusters, as described in Chapter 4. The spread area on uniformly distributed, adsorbed fibronectin (420 molecules/μm^2) was also measured for comparison purposes. Several interesting features are evident in these data. First, when clustered RGD surfaces are compared with those having a uniform RGD distribution (9 vs. 0.8 RGD molecules per star), it can be seen that surfaces having the uniform ligand distribution are unable to

support cell spreading to the same extent as clustered ligand surfaces *at the same average ligand density*. These results provide our first evidence that not only ligand density, but also its spatial presentation, can affect a cell's response to its environment.

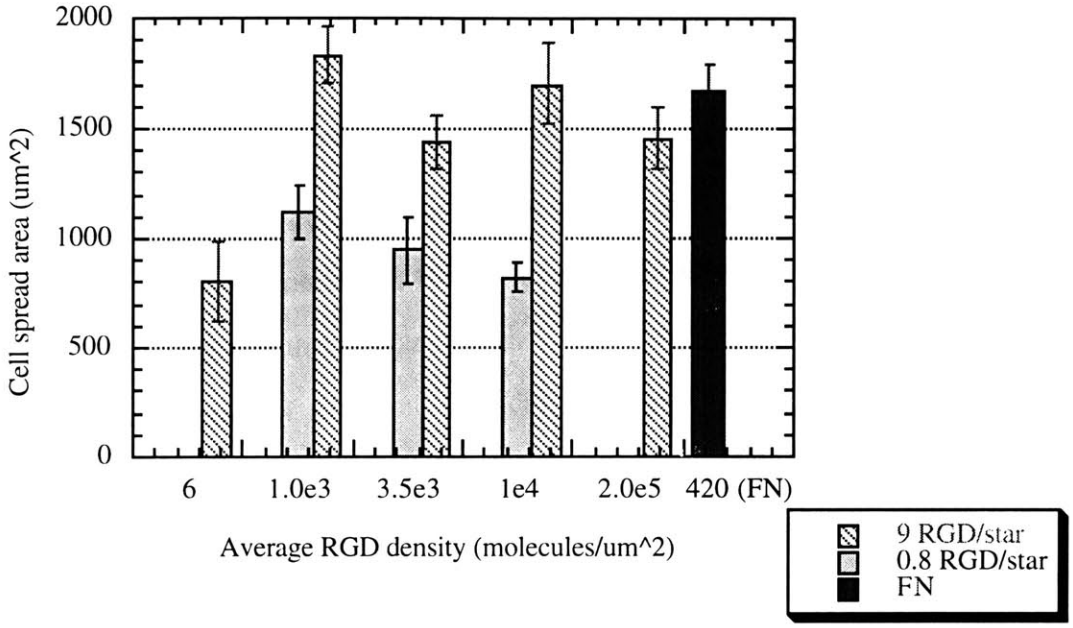

Figure 6.5: NR6 cell spread areas on clustered and uniform RGD surfaces after 24 hours

The 9 RGD/ star substrates support cell spreading in a density-dependent manner, as has been seen previously on uniform RGD surfaces [16], [30], [82] and on adsorbed fibronectin [127]. At high average ligand densities (1,000 to 200,000 molecules/μm^2), the clustered surfaces appear to promote spreading to the same extent as 420 molecules/μm^2 of fibronectin (spread areas ~ 1600 μm^2), while at the lowest RGD density tested, the spread

area achieved was significantly lower (~ 1000 μm^2). This probably indicates that at very low densities, not enough RGD peptide molecules have been bound by the cell at equilibrium to enable the processes of spreading and cytoskeletal organization to occur.

The densities of uniformly distributed RGD (1 per star) achieved on the surface (1,000 to 10,000 molecules/μm^2) are significantly higher than the density of fibronectin, and higher than the estimated density of receptors at the cell surface (~ 100/μm^2) yet adhesion and spreading occurred did not occur to the same extent as on FN. Since the affinity of the fibronectin receptor for fibronectin is 10-100 times higher than its affinity for RGD [114], it has also been suggested that relatively high levels of immobilized RGD are required to achieve the same degrees of adhesion, spreading and cytoskeletal organization as are seen on fibronectin, to compensate for the lower affinity of receptor for ligand. The RGD densities achieved on the 1 RGD/star surfaces are also significantly higher than the minimum reported by Massia et al. [16], who found that an RGD average density of only 60 molecules/μm^2 was sufficient for cell attachment and spreading. That the RGD peptide in most other studies is immobilized on a substrate which itself supports matrix deposition has already been discussed [14]; it is likely that the cell adhesion and spreading observed at such low RGD densities is facilitated in part by non-specifically adsorbed proteins. In addition, however, the RGD peptide in the present studies is tethered to the hydrogel substrate via star PEO molecules, and is probably not completely available to cell surface receptors, depending on whether the peptide molecule points downward towards the substrate our outward into solution when the star molecule is coupled. Only some fraction of the tethered RGD (possibly 50 - 70%) is expected to be accessible to receptors for binding. The RGD densities measured by radiolabeling may therefore be higher than the density of accessible peptide on the surface.

B: Clustering effects on adhesion and migration

The strength of adhesion of NR6 cells to clustered ligand surfaces was determined by a centrifugation assay. Cells are first allowed to attach to the star PEO-RGD surfaces, then subjected to a centrifugal force; cells which have adhered more strongly to the substrate are more resistant to detachment than those which are weakly adhered. Figure 6.6 shows the fraction of cells remaining after the centrifugation in each case, indicative of their adhesivity.

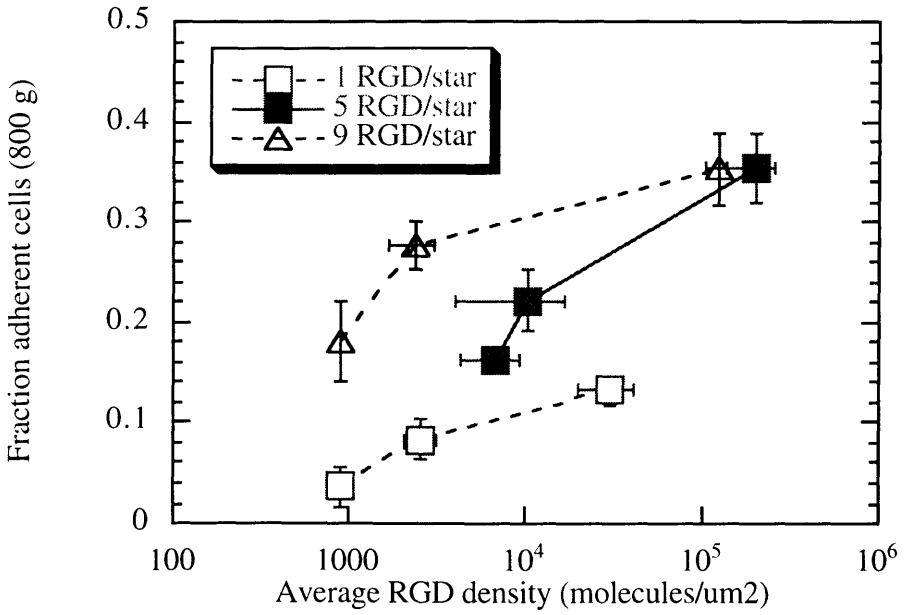

Figure 6.6 Fraction of adherent cells remaining after 10 min. centrifugation (at 800 g) of cells attached to RGD surfaces (relative to control at 1 g)

Similar to results obtained previously on (uniform) fibronectin surfaces [127], the adhesion strength generally increases with increasing average RGD density, indicating that higher average RGD densities promote higher densities of receptor-ligand complexes at equilibrium, so that more force is required to break the receptor-ligand bonds and detach cells from the surface. The figure also shows that for a given average RGD density, the presentation of RGD in clusters instead of at a uniform distribution causes cells to adhere more strongly. Furthermore, increasing the RGD cluster size (from 5 to 9) leads to higher adhesion strength.

Roughly 50% of adherent cells remained on fibronectin surfaces after centrifugation under the same conditions [127], suggesting that cells adhere more strongly at a lower average density of fibronectin than at any density of RGD. This may point to the existence of a synergistic site on the fibronectin molecule, which many authors have suggested is crucial to exactly reproducing cell response to fibronectin [136], [137], [12]. The presence of this synergistic site, separated from the RGD sequence by 100 amino acid residues probably serves to improve the efficiency of the cell-fibronectin interaction; when RGD is immobilized alone, the observed trends are therefore the same, however the magnitudes of the measured adhesion strengths are lower.

A second possible reason for the lower adhesion strengths on star PEO-RGD surfaces, may again be found in the results of Roberts [30] which suggest that fibronectin surfaces, after 24 hours may adsorb matrix proteins non-specifically, and may even form additional adhesions using other receptors than those for RGD.

To ensure that the difference in adhesivity was not due to the inability of cells on star PEO-RGD surfaces to form focal contacts, fixed NR6 cells were permeabilized and stained for

F-actin with rhodamine-phalloidin (Molecular Probes), according to the protocol in Appendix A, and photographed using a fluorescence microscope. The images are displayed in Figure 6.7. The figure shows that at the highest RGD cluster size and density

(9 RGD/cluster, 200,000 RGD molecules/μm^2), the cells undergo the same type of cytoskeletal organization as they do on the adsorbed fibronectin surface. This presence of actin stress fibers is often taken as an indicator of focal contact formation. Stress fibers form on the RGD surfaces at high cluster sizes and average densities, which, together with the high cell spread area and adhesion data indicates that the adhesive bond is relatively strong. On the other hand, at the high cluster size, but low average density, the cytoskeletal organization which is usually indicative of strong adhesion is absent (Figure 6.6). This is consistent with the experimental observation that the cells on surfaces of low density are relatively weakly adhered; in the absence of focal adhesions a large percentage of the cells will become detached from the surface during centrifugation. From these data it may be inferred that the presentation of ligand in a clustered format is promoting stronger adhesive interactions than surfaces on which ligands are uniformly distributed.

The effect of RGD density and distribution on measured migration speeds is plotted in Figure 6.8. Here again, several of our observations match our predictions. Most importantly, the presentation of ligands in clusters leads to an increase in migration speeds over those obtained on uniform surfaces at a constant average ligand density. Furthermore, as the cluster size is increased (from 5 to 9 RGD/star) at constant ligand density, the speed is increased, indicating that it is not just the fact that ligands are clustered, but also the *size* of the clusters that is important.

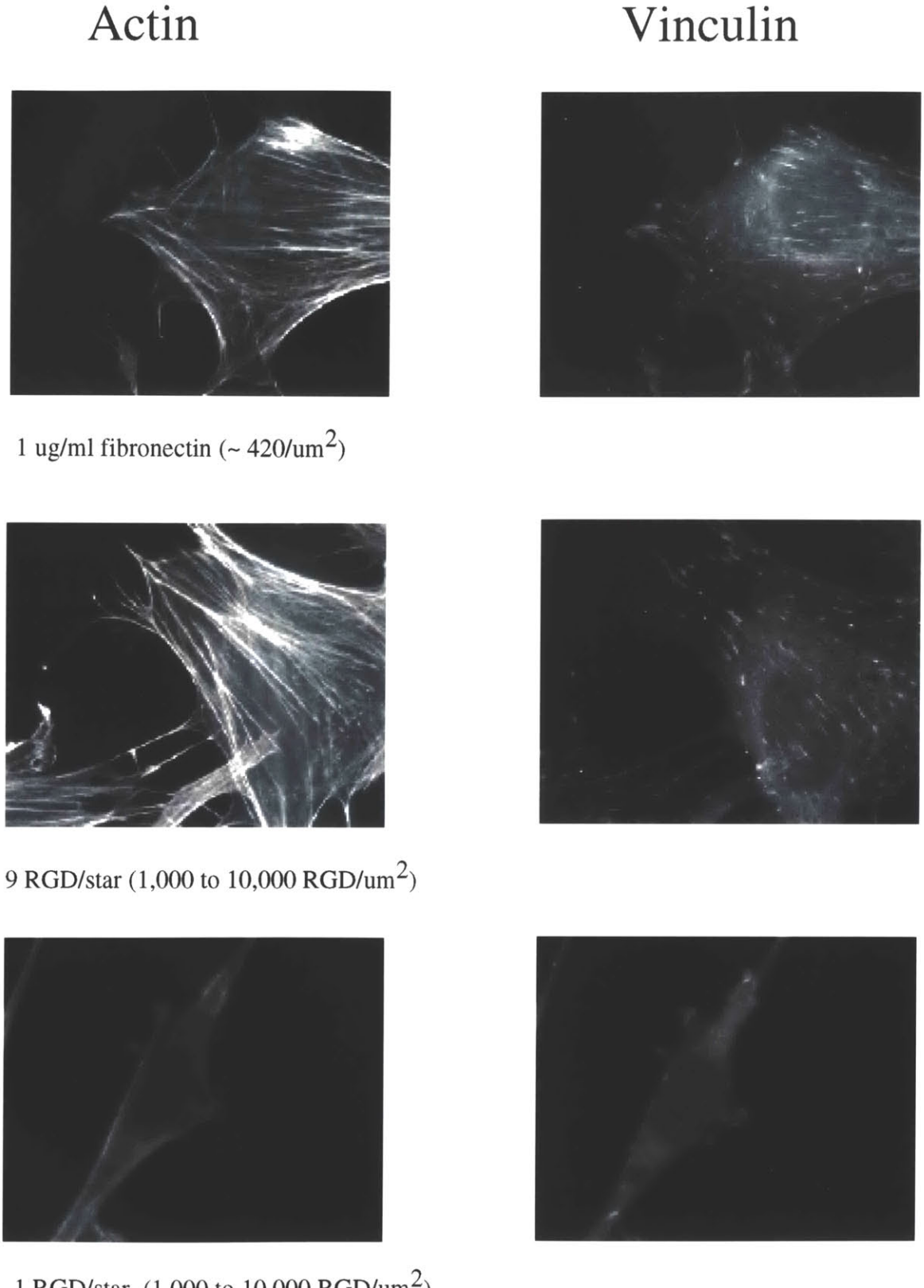

Figure 6.7 Actin stress fiber formation on star PEO-RGD surfaces and fibronectin

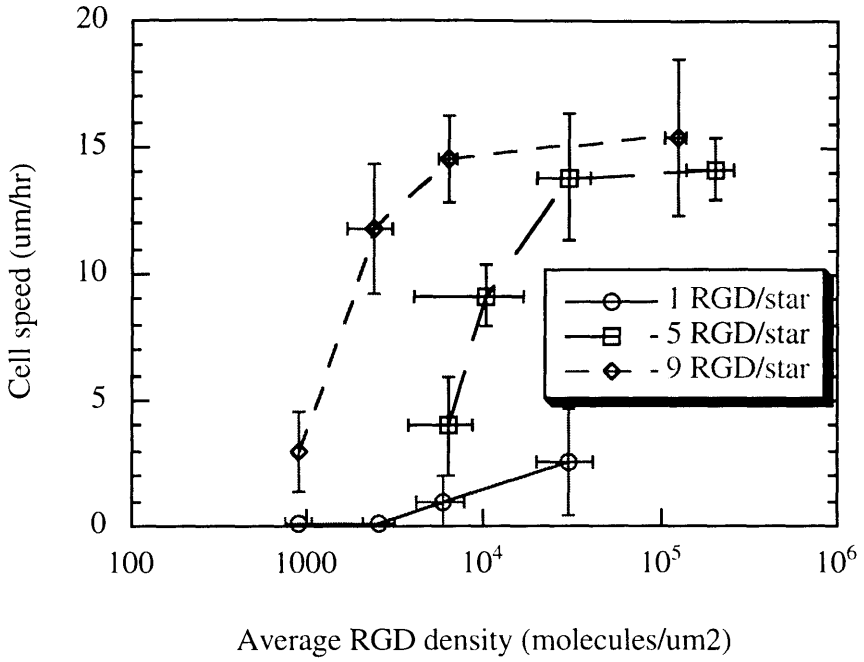

Figure 6.8 Variation in cell speed as a function of average RGD density, at three different cluster sizes.

At every cluster size, an increase in the average RGD density also resulted in an increase in migration speed. Unlike the results of other authors [Palecek, 1996 #207], [127], the speed did not vary with density in a biphasic manner. Instead, for the clustered surfaces, the cell speed showed an initial increase with RGD density, then reached a plateau, perhaps indicating that the cells never achieved such high adhesion strengths that they were unable to break their cell-substratum bonds during migration [138]. It is not clear whether the biphasic relationship would be observed if the average RGD density could be increased beyond the maximum of 2×10^5 achieved in these studies.

Cells attain significantly higher migration speeds on clustered than on uniformly distributed RGD surfaces. When the ligands are presented in clusters (of 5 or 9 RGD/star), and the average RGD densities are increased, we see that cells approach the migration speeds reported by Maheshwari for uniform fibronectin surfaces: 16 - 18 μm/hr on fibronectin surfaces (regardless of fibronectin density). On surfaces bearing only one RGD peptide per star, adhesion was so poor that no migration was observed until the average ligand density approached $10^4/\mu m^2$. Migration speeds of NR6 cells on uniform RGD surfaces were significantly lower than those measured on fibronectin by Maheshwari [127], 2 μm/hr on uniform RGD surfaces. Again, the effect of adhesivity of the substrate appears to have an effect on cell behaviour: as the adhesion of cells to the uniform RGD surfaces is significantly weaker than their adhesion to fibronectin, the cells on RGD are probably adhered too weakly to be able to generate sufficient traction for locomotion.

Finally, in Figure 6.9, migration speed is plotted as a function of adhesivity, eliminating the average RGD density as a variable. It has previously been shown by Palecek that the variation in migration speed of CHO cells with ECM surface density is due to a variation in cell-substratum adhesion [Palecek, 1996 #207]. The figure shows that at each cluster size, the cell speed increases with adhesivity. In addition, we can see from the figure that the plots of speed versus adhesivity at different cluster sizes appear to collapse to a single relationship, as was found by Palecek. This indicates that cell speed in this system is regulated solely be the adhesivity, which in turn is controlled by the presentation of the ligand to cells in clusters.

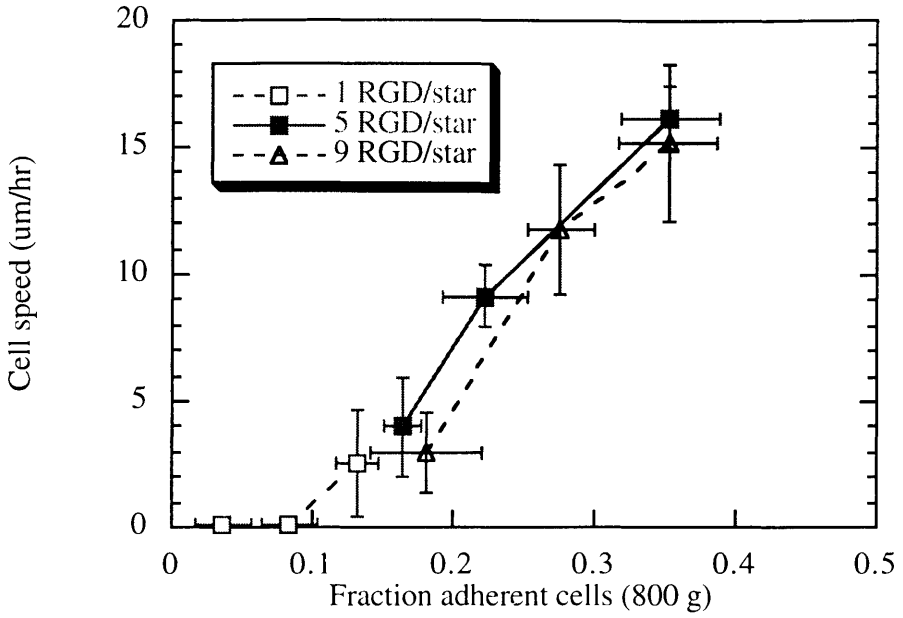

Figure 6.9 Variation in migration speed with adhesivity of cells

6.4.5 Physical effect of clustered ligand presentation on cell behaviour

There are at least two possible explanations for the observed effects of ligand clustering on cell behaviour. The first possible explanation is that by confining the ligands to small (~ 30 nm) domains, we are constraining the integrin receptors to bind within those domains, essentially forcing them into clusters. Once they bind to the RGD ligand, the receptor-ligand complexes are close enough to each other for their cytoskeletal components to polymerize, so that the process of focal contact formation described previously is facilitated. Focal contacts therefore appear to form more easily on clustered ligand substrates than on uniform RGD surfaces at the same ligand density, as evidenced in our system by stronger adhesion. The observed results are reasonable consistent with the

predictions by Ward and Hammer: an increase in the average ligand density apparently promotes focal contact formation [18].

A second explanation, however, can be arrived at by consideration of the biophysical process of receptor-ligand binding. Cell surface receptors bind to their respective ligand according to its concentration, and while in most models of receptor-ligand interactions the ligand concentration is assumed constant and uniform, any local deviation of the ligand concentration from its mean value may cause deviations from the expected number of bound receptors at equilibrium [4]. Tranquillo derived an expression for the fluctuation in the equilibrium number of receptor-ligand complexes due to random fluctuations in the ligand concentration in the vicinity of a receptor [139]:

$$\frac{\delta C_{eq}}{C_{eq}} = \left[1 + \left(\frac{L}{K_D}\right)\right]^{-1} \frac{\delta L}{L} \qquad (1)$$

where:

L	=	the average ligand concentration
δL	=	the standard deviation in the value of L due to local fluctuations in ligand concentration
C_{eq}	=	mean number of receptor-ligand complexes at equilibrium
δC_{eq}	=	standard deviation in the value of C_{eq} due to local deviations in ligand density from the average value

From Equation (1), the extent to which local fluctuations in ligand density affect the distribution of receptor-ligand complexes is determined by the ratio of K_D to L. If we assume a value of K_D for RGD as $5 \times 10^{11} cm^{-2}$ [18], then at a typical average ligand density

of 10,000 μm^{-2} (or 1 x 10^{12} cm^{-2}), we find that a local increase in ligand concentration of 25 % above the mean causes a 8.3 % increase in the number of receptor-ligand complexes. The deviation of the local RGD from the mean would be expected to increase as the cluster size is increased from 1 to 5 to 9. Hence, in addition to constraining receptors to bind only at small domains on the surface, it is also possible that at equilibrium, the *number* of receptor-ligand complexes formed at these local domains of high ligand concentration is increased.

6.5 Conclusions

A variety of cell-based experiments have indicated that (a) star PEO-RGD surfaces support adhesion and spreading of various cell types, (b) we have been successful at creating a minimalistic matrix analogue which interacts specifically with receptors which recognize the RGD sequence, and (iii) cells interact with these substrates in a density-dependent and spatial distribution-dependent manner. With these results, the fundamental aims of this thesis, the synthesis and characterization of clustered ligand surfaces has been successfully completed, and the hypothesis which provided the driving force for the work has been strongly supported by the results of the spread area measurements, and adhesion and migration assays. The clustering of receptors into focal adhesions is apparently enhanced by the presentation of ligand in a clustered format. Having observed this, later work may be aimed at controlling fundamental cell behaviours by controlling receptor-ligand interactions on this scale.

CHAPTER 7. CONCLUSIONS

7.1 Summary

The first objective of this thesis was the design and fabrication of a series of model bioactive substrates which would present ligands to cells in domains of high concentration, or clusters, and which would specifically support cell adhesion by integrin-mediated interactions only. That objective has been accomplished by tethering the well known minimal adhesion sequence, Arg-Gly-Asp to surfaces via star PEO molecules. Taking advantage of the high density of chain ends of star polymers, control over ligand cluster size was achieved by conjugating RGD with PEO in varying proportions. Clusters containing approximately 1 to 10 RGD peptides were synthesized in this way.

Surfaces were prepared by immobilizing ligands on a crosslinked PEO hydrogel substrate which is absolutely inert to non-specific interactions for at least 24 hours. Control over ligand cluster spacing was achieved by the "dilution" of RGD-modified star molecules with unmodified star PEO. Radioactive labeling of the RGD peptide enabled the quantitation of average ligand density, and the percentage of stars immobilized on the surface which were modified with RGD inferred. A model of competitive adsorption was derived, which fits the observations well; star molecules modified with larger amounts of ligand appear to be less reactive than those modified to a lesser extent or not at all.

The second objective of this thesis was the development of characterization techniques to enable the location of ligand on the surface. This was accomplished by immobilizing biotin as the ligand, and labeling it with an anti-biotin antibody adsorbed on a colloidal gold marker. The technique was used in the preparation of PEO-biotin conjugates for low voltage SEM studies, which gave strong indications of clustering on star PEO-biotin

surfaces, as shown by the Kolmogorov test, frequently used to demonstate the occurrence of clustering, and by the examining the distributions of nearest neighbour distances on star-tethered and linear-tethered biotin surfaces.

Finally, some cell-based assays were performed to assess the ability of the prepared surfaces to specifically bind integrin receptors, and to look for evidence of an effect of presenting ligands in a clustered format. Data suggest that presentation of ligands to cells in clustered format is an effective way of achieving strong adhesion and focal contact formation at relatively low average ligand densities. This system is now being used to study a variety of cell behaviours, including adhesion, migration and proliferation.

7.2 Recommendations

Although the materials used for this thesis allowed for the effective proof of the underlying concept, quantitation and characterization would be made much easier if the quality of the star molecules was improved. The star PEO used in this thesis had a polydispersity index of > 9, precision which could therefore be achieved in this system was therefore dramatically reduced. A star polymer with a narrower molecular weight distribution, or a PEO molecule of a different architecture is recommended for future experiments.

Future studies of this system should include the development of techniques for assessing the bioavailability of the ligand when tethered. When star molecules attach to a substrate, the orientation of the attached RGD molecules is at present uncertain. The ability of receptors to bind RGD ligands will likely be dependent on their accessibility.

Finally, the kinetics of binding of receptors to RGD, and of anti-biotin to biotin, when immobilized against a dense, PEO background, should be investigated. Experiments

performed for this thesis indicated that binding of receptor to ligands immobilized on these surfaces is significantly slower than is seen on other surfaces. It is possible that steric repulsions caused by the PEO hinder the ligation; this would be an interesting topic to study in more depth.

The PEO-RGD surfaces prepared for this work were used in studies of specific receptor-mediated phenomena. However, the RGD peptide, does not display cell selectivity, and binds many cell types, including fibroblasts and platelets. For tissue engineering applications, the basic lessons learned from these surfaces may be applied to the design of systems intended for the targeting of specific cells, for example, endothelial cells using the peptide sequence REDV [40].

Although the surfaces designed and fabricated for this thesis were intended for fundamental studies of cell behaviour, the principles applied have widespread application in many other biomedical and biotechnological endeavours. The elimination of non-specific interactions, molecular recognition and spatial control of the presentation of ligands are common challenges in the field of bioengineering. For example, the presentation of biomolecules in the correct orientation and at the correct densities for specific binding of analytes is a common problem in biosensors research [140]. Another emerging technology is that of point-of-care diagnostics, in which the fouling of microfluidic channels in which blood or other body fluids is analysed is currently a significant challenge. The patterning of well-defined substrates with oligonucleotides is receiving a great deal of attention in genomics and drug discovery research. Finally, many researchers are investigating the encapsulation of cells such as islets of Langerhans, in immuno-friendly, semipermeable hydrogels [141].

REFERENCES

1. Peppas, N. and R. Langer, *New challenges in biomaterials.* Science, 1994. **263**: p. 1715.
2. Ratner, B., *New ideas in biomaterials science- a path to engineered biomaterials.* Journal fo Biomedical Materials Research, 1993. **27**: p. 837.
3. Horbett, T. and J. Brash, *Proteins at Interfaces: Current Issues and Future Prospects,* in *ACS Symposium Series.* 1987. p. 1.
4. Lauffenburger, D.A. and J.J. Linderman, *Receptors: Models for Binding, Trafficking and Signaling.* 1993, New York: Oxford University Press.
5. Bell, G.I., *Models for the Specific Adhesion of Cells to Cells.* Science, 1978. **200**: p. 618-627.
6. Alberts, B., *et al.*, *Essential Cell Biology.* 1998, New York: Garland Publishing, Inc.
7. Hynes, R.O., *Integrins: versatility, modulation and signaling in cell adhesion.* Cell, 1992. **69**: p. 11.
8. Hynes, R.O., Cell, 1987. **48**: p. 549-554.
9. Pierschbacher, M.D. and E Ruoslahti, *Cell attachment activity of fibronectin can be duplicated by small synthetic fragments of the molecule.* Nature, 1984. **309**: p. 30-33.
10. Ruoslahti, E. and M. Pierschbacher, *Arg-Gly-Asp: A versatile cell recognition signal.* Cell, 1986. **44**: p. 517.
11. Ruoslahti, E. and M. Pierschbacher, *New perspectives in cell adhesion: RGD and integrins.* Science, 1987. **23**: p. 491.
12. Ruoslahti, E., *RGD and Other Recognition Sequences for Integrins.* Annual Review of Cell and Developmental Biology, 1996. **12**: p. 697-715.
13. Yamada, Y. and H.K. Kleinman, *Functional domains of cell adhesion molecules.* Current Biology, 1992. **4**: p. 819-823.
14. Massia, S.P. and J.A. Hubbell, *Covalent Surface Immobilization of Arg-Gly-Asp and Tyr-Ile-Gly-Ser-Arg-Containing Peptides to Obtain Well-Defined Cell-Adhesive Substrates.* Analytical Biochemistry, 1990. **187**: p. 292.
15. Singer, I.I., *et al.*, *The Fibronectin Cell Attachment Sequence Arg-Gly-Asp-Ser Promotes Focal Contact Formation during Early Fibroblast Attachment and Spreading.* Journal of Cell Biology, 1987. **104**: p. 573-584.

16. Massia, S.P. and J.A. Hubbell, *An RGD Spacing of 440 nm is Sufficient for Integrin α-v β-3-mediated Fibroblast Spreading and 140 nm for Focal Contact and Stress Fiber Formation.* Journal of Cell Biology, 1991. **114**: p. 1089.

17. Hautanen, A., *et al., Effects of Modifications of the RGD Sequence and Its Context on Recognition by the Fibronectin Receptor.* Journal of Biological Chemistry, 1989. **264**(3): p. 1437-1442.

18. Ward, M.D. and D.A. Hammer, *Focal contact assembly through cytoskeletal polymerization: steady state analysis.* Journal of Mathematical Biology, 1994. **32**: p. 677-704.

19. Burridge, K., *et al., Focal Adhesions: Transmembrane junctions between the extracellular matrix and the cytoskeleton.* Annual Review of Cell Biology, 1988. **4**: p. 487-525.

20. Jockusch, B.M., *et al., The Molecular Architecture of Focal Adhesions.* Annual Review of Cell and Developmental biology, 1995. **11**: p. 379-416.

21. Rees, D.A., C.W. Lloyd, and D. Thom, *Control of grip and stick in cell adhesion through lateral relationships of membrane glycoproteins.* Nature, 1977. **267**: p. 124-128.

22. Wang, N., J.P. Butler, and D.E. Ingber, *Mechanotransduction Across the cell Surface and Through the Cytoskeleton.* Science, 1993. **260**: p. 1124-1127.

23. Ezzell, R.M., *et al., Vinculin Promotes Cell Spreading by Mechanically Coupling Integrins to the Cytoskeleton.* Experimental Cell Research, 1997. **231**: p. 14-26.

24. Juliano, R.L. and S. Haskill, *Signal transduction from the extracellular matrix.* Journal of Cell Biology, 1993. **120**: p. 577.

25. Kornberg, L.J., *et al., Signal transduction by integrins: Increased protein tyrosine phosphorylation caused by clustering of beta-1 integrins.* Proceedings of the National Academy of Science of the United States of America, 1991. **88**: p. 8392.

26. Kornberg, L., *et al., Cell Adhesion or Integrin Clustering Increases Phosphorylation of a Focal Adhesion-associated Tyrosine Kinase.* Journal of Biological Chemistry, 1992. **267**(33): p. 23439-23442.

27. Gombotz, W.R., *et al., Protein adsorption to poly(ethylene oxide) surfaces.* Journal of Biomedical Materials Research, 1991. **25**: p. 1547-1562.

28. Drumheller, P.D. and J.A. Hubbell, *Densely crosslinked polymer networks of poly(ethylene glycol) in trimethylolpropane triacrylate for cell-adhesion-resistant surfaces.* Journal of Biomedical Materials Research, 1995. **29**: p. 207-215.

29. Prime, K.L. and G.M. Whitesides, *Adsorption of proteins onto surfaces containing end-attached oligoethylene oxide: a model system using self-assembled monolayers.* Journal of the American Chemical Society, 1993. **115**: p. 10714.

30. Roberts, C., *et al.*, *Using Mixed Self-Assembled Monolayers Presenting RGD and $(EG)_3OH$ Groups To Characterize Long-Term Attachment of Bovine Capillary Endothelial Cells to Surfaces.* Journal of the American Chemical Society, 1998. **120**: p. 6548-6555.

31. Neff, J.A., K.D. Caldwell, and P.A. Tresco, *A novel method for surface modification to promote cell attachment to hydrophobic substrates.* Journal of Biomedical Materials Research, 1998. **40**: p. 511-519.

32. Glass, J., *et al.*, *Cell Attachment and Motility on Materials Modified by Surface-Active RGD-Containing Peptides.* Annals of the New York Academy of Sciences, 1994. **745**: p. 177.

33. Harris, J.M., ed. *Poly(Ethylene Glycol) Chemistry: Biotechnical and Biomedical Applications.* . 1992, Plenum Press: New York.

34. Mori, Y., *et al.*, *A new antithrombogenic material with long polyethylene oxide chains.* Transactions of the American Society for Artificial Internal Organs, 1982. **27**: p. 459.

35. Morra, M., E. Occhiello, and F. Garbassi, *Surface Modification of Blood Contacting Polymers by Poly(ethylene Oxide).* Clinical Materials, 1993. **14**: p. 255.

36. Jeon, S., *et al.*, *Protein-surface interactions in the presence of poly(ethylene oxide) I. Simplified theory.* Journal of Colloid and Interface Science, 1991. **142**: p. 159.

37. Jeon, S. and J. Andrade, *Protein-surface interactions in the presence of poly(ethylene oxide) II. Effect of protein size.* Journal of Colloid and Interface Science, 1991. **142**: p. 149-158.

38. Szleifer, I., *Protein adsorption on surfaces with grafted polymers: A theoretical approach.* Biophysical Journal, 1997. **72**: p. 595-612.

39. Van Delden, C.J., *et al.*, *Poly(ethylene oxide)-modified carboxylated polystyrene latices- immobilization chemistry and protein adsorption.* journal of Biomaterials Science-Polymer Edition, 1996. **8**(4): p. 251-268.

40. Hubbell, J.A., *et al.*, *Endothelial cell-selective materials for tissue engineering in the vascular graft via a new receptor.* Bio/Technology, 1991. **9**: p. 568.

41. Massia, S.P. and J.A. Hubbell, *Immobilized Amines and Basic Amino Acids as Mimetic Heparin-binding Domains for Cell Surface Proteoglycan-mediated Adhesion.* Journal of Biological Chemistry, 1992. **267**(14): p. 10133-10141.

42. Woods, A., S. Johansson, and M. Hook, *Fibronectin Fibril Formation Involves Cell Interactions with Two Fibronectin Domains.* Experimental Cell Research, 1988. **177**: p. 272-283.

43. Streeter, H.B. and D.A. Rees, *Fibroblast Adhesion to RGDS Shows Novel Features Compared with Fibronectin.* Journal of Cell Biology, 1987. **105**: p. 507-515.

44. McPherson, T.B., S.J. Lee, and K. Park, *Analysis of the Prevention of Protein Adsorption by Steric Repulsion Theory*, in *Proteins at Interfaces II.* 1995, American Chemical Society. p. 395-404.

45. Desai, N.P. and J.A. Hubbell, *Biological responses to polyethylene oxide modified polyethylene terephthalate surfaces.* Journal of Biomedical Materials research, 1991. **25**: p. 829.

46. Daoud, M. and J.P. Cotton, *Star shaped polymers: a model for the conformation and its concentration dependence.* Le Journal de Physique, 1982. **43**: p. 531-538.

47. Irvine, D.J., *et al.*, *Comparison of tethered star and linear poly(ethylene oxide) for control of biomaterials surface properties.* Journal of Biomedical Materials Research, 1998. **40**: p. 498-509.

48. Sofia, S.J., V. Premnath, and E.W. Merrill, *Poly(ethylene oxide) Grafted to Silicon Surfaces: Grafting Density and Protein Adsorption.* Macromolecules, 1998. **31**: p. 5059-5070.

49. Pale-Grosdemange, C., *et al.*, *Formation of Self-Assembled Monolayers by Chemisorption of Derivatives of Oligo(ethylene glycol) of Structure* $HS(CH_2)_{11}(OCH_2CH_2)_mOH$ *on Gold.* Lournal of the American Chemical Society, 1991. **113**: p. 12-20.

50. Mrksich, M., G.B. Sigal, and G.M. Whitesides, *Surface plasmon resonance permits in situ measurement of protein adsorption on self-assembled monolayers of alkanethiolates on gold.* Langmuir, 1995. **11**: p. 4383-4385.

51. Chen, C.S., *et al.*, *Micropatterned Surfaces for Control of Cell Shape, Position and Function.* BIotechnology Progress, 1998. **14**: p. 356-363.

52. Singhvi, R., *et al.*, *Engineering Cell Shape and Function.* Science, 1994. **264**: p. 696-698.

53. Lee, S.-W. and P.E. Laibinis, *Protein-resistant coatings for glass and metal oxide surfaces derived from oligo(ethylene glycol)-terminated alkyltrichlorosilanes.* Biomaterials, 1998. **19**(18): p. 1669-1675.

54. Ulman, A., *Formation and Structure of Self-Assembled Monolayers.* Chemical Reviews, 1996. **96**: p. 1533-1554.

55. Mrksich, M. and G.M. Whitesides, *Using self-assembled monolayers to understand the interactions of man-made structures with proteins and cells.* Annual Review of Biophysics and Biomolecular Structure, 1996. **25**: p. 55-78.

56. Lee, J.H., J. Kopecek, and J.D. Andrade, *Protein resistant surfaces prepared by PEO-containing block copolymer surfactants.* Journal of Biomedical Materials Research, 1989. **23**: p. 351.

57. Bearinger, J.P., *et al.*, *P(AAm-co-EG) Interpenetrating Polymer Networks Grafted to Oxide Surfaces: Surface Characterization, Protein Adsorption, and Cell Detachment Studies.* Langmuir, 1997. **13**: p. 5175-5183.

58. Kamath, K.R., *et al.*, *Platelet interactions with plasma-polymerized ethylene oxide and N-vinyl-2-pyrrolidone films and linear poly(ethylene oxide) layer.* Journal of Biomaterials Science, Polymer Edition, 1996. **7**(11): p. 977-988.

59. Royer, G.P. and G.M. Anantharmaiah, *Peptide Synthesis in Water and the Use of Immobilized Carboxypeptidase Y for Deprotection.* Journal of the American Chemical Society, 1979. **101**(12): p. 3394-3396.

60. Stenger, D.A., *et al.*, *Coplanar molecular assemblies of amino- and perfluorinated alkylsilanes: characterization and geometric definition of mammalian cell adhesion and growth.* Journal of the American Chemical Society, 1992. **114**: p. 8435-8442.

61. Laibinis, P.E., C.D. Bain, and G.M. Whitesides, *Attenuation of Photoelectrons in Monolayers of n-Alkanethiols Adsorbed on Copper, Silver and Gold.* Journal of Physical Chemistry, 1991. **95**: p. 7017-7021.

62. De Gennes, P.G., *Conformations of polymers attached to an interface.* Macromolecules, 1980. **13**: p. 1069-1075.

63. Zhulina, E.B., *et al.*, Macromolecules, 1995. **28**: p. 8612.

64. Drumheller, P.D. and J.A. Hubbell, *Surface Immobilization of Adhesion Ligands for Investigations of Cell-Substrate Interactions*, in *CRC Handbook of Biomedical Engineering*. 1995, CRC Press. p. 1583.

65. Massia, S.P. and J.A. Hubbell, *Human endothelial cell interactions with surface-coupled peptides on a non-adhesive glass substrate and two polymeric biomaterials.* Journal of Biomedical Materials Research, 1991. **25**: p. 223.

66. Milner, S.T., *Competitive adsorption kinetics of end-adsorbing polymers.* Macromolecules, 1992. **25**: p. 5487-5494.

67. Harder, P., *et al.*, *Molecular conformation in oligo(ethylene glycol)-terminated self-assembled monolayers on gold and silver surfaces determines their ability to resist protein adsorption.* Journal of Physical Chemistry B, 1998. **102**: p. 426-436.

68. Lopina, S.T., *et al.*, *Hepatocyte culture on carbohydrate-modified star polyethylene oxide hydrogels.* Biomaterials, 1996. **17**: p. 559-569.

69. Lopina, S.T. and L.G. Cima, *Network structures of radiation-crosslinked hydrogels.* Macromolecules, 1995. **28**: p. 6787.

70. Dennison, K.A., *Radiation Crosslinked Poly(ethylene oxide) Hydrogel Membranes*, in *Chemical Engineering*. 1986, Massachusetts Institute of Technology: Cambridge, MA. p. 367.

71. Minkova, L., *et al.*, *Structural Studies of Radiation-crosslinked Poly(ethylene oxide).* Journal of Polymer Science: Part B: Polymer Physics, 1989. **27**: p. 621-642.

72. Allgor, S.J.S., *Linear and Star-Shaped Poly(Ethylene Oxide) Grafted Surfaces: Grafting Density and Protein Adsorption*, in *Chemical Engineering*. 1996, Massachusetts Institute of Technology: Cambridge, MA.

73. McPherson, T.B., H.S. Shim, and K. Park, *Grafting of PEO to Glass, Nitinol and Pyrolytic Carbon Surfaces by γ Irradiation.* Journal of Biomedical Materials Research (Applied Biomaterials), 1997. **38**(289-302).

74. Suzuki, A., M. Yamazaki, and Y. Kobiki, *Direct observation of polymer gel surfaces by atomic force microscopy.* Journal of Chemical Physics, 1996. **104**(4): p. 1751-1757.

75. Matsuo, E.S., *et al.*, *Origin of Structural Inhomogeneities in Polymer Gels.* Macromolecules, 1994. **27**: p. 6791-6796.

76. Canal, T. and N.A. Peppas, *Correlation between mesh size and equilibrium degree of swelling of polymeric networks.* Journal of Biomedical Materials research, 1989. **23**: p. 1183-1193.

77. Bray, J.C. and E.W. Merrill, *Poly(vinyl Alcohol) Hydrogels. Formation by Electron Beam Irradiation of Aqueous Solutions and Subsequent Crystallization.* Journal of Applied Polymer Science, 1973. **17**: p. 3779-3794.

78. Flory, P.J., *Principles of Polymer Chemistry.* 1953, Ithaca, N.Y.: Cornell University Press.

79. Lopina, S.T., *Carbohydrate-Derivatized Poly(Ethylene Oxide) Hydrogels For Hepatocyte Adhesion*, in *Chemical Engineering*. 1996, Massachuseetts Institute of technology: Cambridge, MA. p. 167.

80. Williams, E.C., *et al.*, *Conformational states of fibronectin- effects of pH, ionic strength and collagen binding.* Journal of Biological Chemistry, 1982. **257**: p. 4973-4978.

81. Tweden, K.S., *et al.*, *Accelerated Healing of Cardiovascular Textiles Promoted by an RGD Peptide.* Journal of Heart Valve Diseaase, 1995. **4 (Suppl. I)**: p. S90-S97.

82. Lin, H., *et al.*, *Synthesis, surface and cell-adhesion properties of polyurethanes containing covalently grafted RGD-peptides.* Journal of Biomedical Materials Research, 1994. **28**: p. 329.

83. Chen, C.S., D.E. Ingber, and G.M. Whitesides, *Geometric Control of Cell Life and Death.* Science, 1997. **276**: p. 1425.

84. Staros, J.V., R.W. Wright, and D.M. Swingle, *Enhancement by N-Hydroxysulfosuccinimide of Water-Soluble Carbodiimide-Mediated Coupling Reactions.* Analytical Biochemistry, 1986. **156**: p. 220-222.

85. Rein, D., P. Rempp, and P.J. Lutz, *Recent developments in the field of star-shaped polymers.* Macrocolecular Symposia, 1993. **67**: p. 237.

86. Gnanou, Y., P. Lutz, and P. Rempp, *Synthesis of star-shaped poly(ethylene oxide).* Makromoleculare Chemie, 1988. **189**: p. 2885.

87. Markwell, M.A.K., *A new solid state reagent to iodinate proteins: conditions for the efficient labelling of antiserum.* Analytical Biochemistry, 1982. **125**: p. 427.

88. Knoche, H.W., *Radioisotopic Methods for Biological and Medical Research.* 1991, New York: Oxford.

89. King, D.S., C.G. Fields, and G.B. Fields, *A cleavage method which minimizes side reactions following Fmoc solid phase peptide synthesis.* International Journal of Peptide and Protein research, 1990. **36**: p. 255-266.

90. Yen, D.R., *Synthesis and Characterization of Poly(ethylene oxide) Star Molecules for Biological and Medical Applications*, in *Chemical Engineering*. 1998, Massachusetts Institute of Technology: Cambridge, MA. p. 127.

91. Yen, D.R., S. Raghavan, and E.W. Merrill, *Fractional Precipitation of Star Poly(ethylene Oxide).* Macromolecules, 1996. **29**: p. 8977-8978.

92. Bauer, B.J., *et al.*, *Chain Dimensions in Dilute Polymer Solutions: A Light Scattering and Viscometric Study of Multiarmed Polyisoprene stars in Good and Theta Solvents.* Macromolecules, 1989. **22**: p. 2337-2347.

93. Grabarek, Z. and J. Gergely, *Zero-Length Crosslinking Procedure with the Use of Active Esters.* Analytical Biochemistry, 1990. **185**: p. 131-135.

94. Masel, R.I., *Principles of Adsorptoin and Reaction on Solid Surfaces.* Wiley Series in Chemical Engineering. 1996, New York, NY: john Wiley and Sons, Inc.

95. Hoffman, A., *A Commentary on the Advantages and Limitations of Synthetic Polymer-Biomolecule Conjugates*, in *Biorelated Polymers and Gels- Controlled release and Applications in Biomedical Engineering*, T. Okano, Editor. 1998, Academic Press: San Diego, CA. p. 231-248.

96. Roovers, J., *et al.*, *Regular star polymers with 64 and 128 arms. Models for polymeric micelles.* Macromolecules, 1993. **26**: p. 4324.

97. Watt, I.M., *The principles and practice of electron microscopy.* 2nd edition ed. 1997, Cambridge, U.K.: Cambridge University Press.

98. Vezie, D.L., E.L. Thomas, and W.W. Adams, *Low-voltage, high-resoluition scanning electron microscopy: a new characterization technique for polymer morphology.* Polymer, 1995. **36**(9): p. 1761.

99. Noy, A., D.V. Vezenov, and C.M. Lieber, *Chemical Force Microscopy.* Annual Review of Materials Science, 1997. **27**: p. 381-421.

100. Akari, S., *et al.*, *Chemical Imaging by Scanning Force Microscopy.* Advanced Materials, 1995. **7**(6): p. 549-551.

101. Frisbie, C.D., *et al.*, *Functional Group Imaging by Chemical Force Microscopy.* Science, 1994. **265**: p. 2071-2074.

102. van der Vegte, E.W. and G. Hadziioannou, *Scanning Force Microscopy with Chemical Specificity: An Extensive Study of Chemically Specific Tip-Surface Interactions and the Chemical Imaging of Surface Functional Groups.* Langmuir, 1997. **13**(16): p. 4357-4368.

103. Noy, A., *et al.*, *Chemical Force Microscopy: Exploiting Chemically-Modified Tips to Quantify Adhesion, Friction and Functional Group Distributions in Molecular Assemblies.* Journal of the American Chemical Society, 1995. **117**: p. 7943.

104. Eppell, S.J., F.R. Zypman, and R.E. Marchant, *Probing the Resolution Limits and Tip Interactions of Atomic Force microscopy in the Study of Globular Proteins.* Langmuir, 1993. **9**: p. 2281-2288.

105. Griffith, J.E. and D.A. Grigg, *Dimensional metrology with scanning probe microscopes.* Journal of Applied Physics, 1993. **74**(9): p. R83-R108.

106. Grabar, K.C., *et al.*, *Nanoscale Characterization of Gold Colloid Monolayers: A Comparison of Four Techniques.* Analytical Chemistry, 1997. **69**: p. 471-477.

107. Mulvaney, P. and M. Giersig, *Imaging nanosized gold colloids by atomic force microscopy: A direct comparison with transmission electron microscopy.* Journal of the Chemiocal Society, Faraday Transactions, 1996: p. 3137-3143.

108. Eppell, S.J., *et al.*, *Cell-Surface Receptors and Proteins on Platelet Membranes Imaged by Surface Force Microscopy and Immunogold Contrast Enhancement.* 68, 1995: p. 671-680.

109. Hisano, S. and s. Daikoku, *Electron Microscopic Immunocytochemistry- Major Visualization Techniques- Colloidal Gold Methods*, in *Electron Microscopic Cytochemistry*

and Immunocytochemistry in Biomedicine, K. Ogawa and T. Barka, Editors. 1993, CRC Press, Inc.

110. Hodges, G.M., J. Southgate, and E.C. Toulson, *Colloidal gold- a powerful tool in scanning electron microscope immunocytochemistry: an overview of bioapplications.* Scanning Microscopy, 1987. **1**: p. 301-318.

111. Putnam, C.A.J., *et al.*, *Immunogold labels: cell-surface markers in atomic force microscopy.* Ultramicroscopy, 1993. **48**: p. 177-182.

112. Wilchek, M. and E.A. Bayer, *The Avidin-Biotin Complex in Bioanalytical Applications.* Analytical Biochemistry, 1988. **171**: p. 1-32.

113. Green, N.M., ed. *Avidin and Streptavidin.* Methods in Enzymology. Vol. 184. 1990. 51-67.

114. Akiyama, S.K., K. Nagata, and K.M. Yamada, *Cell surface receptors for extracellular matrix components.* Biochimica et Biophysica Acta, 1990. **1301**: p. 91-110.

115. Wilchek, M. and E.A. Bayer, eds. *Biotin-Containing Reagents.* Methods in Enzymology. Vol. 184. 1990. 123-138.

116. Vincent, P. and D. Samuel, *A comparison of the binding of biotin and biotinylated macromolecular ligands to an anti-biotin monoclonal antibody and to streptavidin.* Journal of Immunological Methods, 1993. **165**: p. 177-182.

117. Spinke, J., *et al.*, *Molecular recognition at self-assembled monolayers: Optimization of surface functionalization.* Journal of Chemical Physics, 1993. **99**(9): p. 7012-7019.

118. Rao, S.V., K.W. Anderson, and L.G. Bachas, *Determination of the Extent of Protein Biotinylation by Fluorescence Binding Assay.* Bioconjugate Chemistry, 1997. **8**: p. 94-98.

119. Diggle, P.J., *Statistical analysis of spatial point patterns.* Mathematics in Biology, ed. R. Sibson and J.E. Cohen. 1983, London: Academic Press.

120. Lindgren, B.W., *Basic Ideas of Statistics.* 1975, New York: Macmillan Publishing Co., Inc.

121. Zar, J.H., *Biostatistical Analysis.* 1996: Prentice-Hall, Inc.

122. Van Der Smissen, P., P.J. Courtoy, and P. Baudhin, *Quantitative analysis of clustering on biological membranes: methodology and application to ligand-induced asialoglycoprotein receptor redistribution on rat hepatocytes.* European Journal of Cell Biology, 1996. **69**: p. 45-54.

123. Park, K., S.R. Simmons, and R.M. Albrecht, *Surface characterization of biomaterials by immunogold staining- quantitative analysis.* Scanning Microscopy, 1987. **1**(1): p. 339-350.

124. Grabar, K.C., *et al.*, *Kinetic Control of Interparticle Spacing in Au Colloid-Based Surfaces: Rational Nanometer-Scale Architecture.* Journal of the American Chemical Society, 1996. **118**: p. 1148-1153.

125. Wong, J.Y., *et al.*, *Direct Measurement of a Tethered Ligand-Receptor Interaction Potential.* Science, 1997. **275**: p. 820-822.

126. Xiao, Y. and G.A. Truskey, *Effect of Receptor-Ligand Affinity om the Strength of Endothelial Cell Adhesion.* Biophysical Journal, 1996. **71**: p. 2869-2884.

127. Maheshwari, G., *et al.*, *Biophysical Integration of Effects of Epidermal Growth Factor and Fibronectin on Fibroblast Migration.* Biophysical Journal (in press), 1999.

128. Chu, L., *et al.*, *Centrifugation assay of IgE-mediated cell adhesion to antigen-coated gels.* AIChE Journal, 1994. **40**: p. 692-703.

129. Olbrich, K.C., *et al.*, *Surfaces modified with covalently-immobilized adhesive peptides affect fibroblast motility.* Biomaterials, 1996. **17**: p. 759-764.

130. Verfaillie, C.M., J.B. McCarthy, and P.B. McGlave, *Differentiation of Primitive Human Multipotent Hematopoietic Progenitors into Single Lineage Clonogenic Progenitors Is Accompanied by Alterations in Their Interaction with Fibronectin.* Jouranl of Experimental Medicine, 1991. **174**: p. 693-703.

131. Elices, M.J., *et al.*, *VCAM-1 on Activated Endothelium Interacts with the Leucocyte Integrin VLA-4 at a Site Distince from the VLA-4/Fibronectin Binding Site.* Cell, 1990. **60**: p. 577-584.

132. Hemler, M.E., *VLA proteins in the integrin family: structures, functions, and their role on leucocytes*, in *Annual Review of Immunology*, W.E. Paul, Editor. 1990, Annual Reviews, Inc.: Palo Alto, CA. p. 365-400.

133. McCarthy, J.B., *et al.*, *RGD-independent cell adhesion to the carboxy terminal heparin binding fragment of fibronectin involves heparin-dependent and -independent activities.* Journal of Cell Biology, 1990. **110**: p. 777-791.

134. Daley, G.Q. and D. Baltimore, *Transformation of an interleukin 3-dependent hematopeitic cell line by the chronic myelogenous leukemia-specific $P210^{bcr/abl}$ protein.* Proceedings of the National Academy of Science (USA), 1988. **85**: p. 9312-9316.

135. Bazzoni, G., *et al.*, *Bcr/Abl Expression Stimulates Integrin Function in Hematopoetic Cell Lines.* Journal of Clinical Investigation, 1996. **98**(2): p. 521-528.

136. Obara, M., M.S. Kang, and K.M. Yamada, *Site-Directed Mutagenesis of the Cell-Binding Domain of Human Fibronectin: Separable, Synergistic Sites Mediate Adhesive Function.* Cell, 1988. **53**: p. 649-657.

137. Dufour, S., *et al., Attachment, spreading and locomotion of avian neural crest cells are mediated by multiple adhsesion sites on fibronectin molecules.* EMBO, 1988. **7**(9): p. 2661-2671.

138. DiMilla, P.A., *et al., Maximal migration of human smooth muscle cells on fibronectin and type IV collagen occurs at an intermediate attachment strength.* Journal of Cell Biology, 1993. **122**: p. 729-737.

139. Tranquillo, R.T., *Theories and models of gradient perception*, in *Biology of the Chemotactic Response*, J.P. Armitage and J.M. Lackei, Editors. 1990, Cambridge University Press: Cambridge, U.K.

140. Zhao, S. and W.M. Reichert, *Influence of Biotin Lipid Surface Density and Accessibility on Avidin Binding to the Tip of an Optical Fiber Sensor.* langmuir, 1992. **8**: p. 2785-2791.

141. Cruise, G.M., D.S. Scharp, and J.A. Hubbell, *Characterization of permeability and network structure of interfacially photopolymerized poly(ethylene glycol) diacrylate hydrogels.* Biomaterials, 1998. **19**: p. 1287-1294.

APPENDIX A: PROTOCOLS

A1: Carboxylation of star PEO

The following procedure is used to convert PEO terminal groups from hydroxyl (as-received) to carboxyl, and was adapted from that described by Royer [59]. The method was selected for its simplicity (it can be carried out in a sealed flask, and an atmosphere of dry argon or nitrogen is not required), and for the high yields of polymer and high degrees of conversion obtained.

A1.1 Materials

1 g star PEO 460 (Shearwater polymers)
1.0 M potassium *t*-butoxide solution in *t*-butyl alcohol (Aldrich)
Bromoethyl acetate (Aldrich)
Dialysis cassettes, M.W. cutoff = 10,000 (Sigma)
Dried glassware: 100 ml round-bottomed flask, 500 ml conical flask

1.0 M $NaHCO_3$, pH = 9
1.0 M hydrochloric acid

A1.2 Method

1. Dissolve 1g star-704 in 30 ml KOBu/t-BuOH in 100 ml r.b. flask, sealed with rubber septum cap. Stir at 45 °C to dissolve.
2. Add 0.67 ml BrEtAc dropwise, via syringe, over 10 min. Stir, 4 hours
3. Precipitate PEO in 200 ml cold ether in 500 ml flask at 4 °C (overnight).
4. Collect precipitate by centrifugation, wash three times in ether, dry.
5. Dissolve in 15 ml carbonate buffer, pH = 9. Stir, 90 min. at room temperature.
6. Acidify to pH = 3, using 1.0 M HCl.
7. Dialyze against a large amount (~ 10 liter) of pure water, 36 hours, using Pierce dialysis cassettes, changing the water four times.
8.. Freeze, then lyophilize.

A2: Iodination of YGRGD peptide

This protocol may be used to label an RGD peptide possessing a tyrosine residue with radioactive iodine for quantitation purposes. The procedure is adapted from Massia [14], and uses the Iodobead™ method.

A2.1 Materials

10 µl, 1 mg/ml RGD peptide
2 mCi $Na^{125}I$ (New England Nuclear)
~50 ml PBS
Chase solution: 20 ml PBS
1 xtl KI
on ice
12 mg/ml sodium metabisulfite/PBS,
mixed fresh on day of use
Iodobeads (Pierce)
C_{18} Reverse phase cartridge (Waters)
Microfuge tubes: screw cap
snap cap
no cap
Empty centrifuge tubes (2, 30 ml)
Disposable syringe (10 cc)
Pipetman and tips
Spare lead pigs
Radioactivity tape
Gamma counters
Racks
Latex gloves
Bench paper

A2.2 Solutions for purification of labeled peptide

1. 10 ml 80:10:1 (MeOH:H2O:TFA)
2. 10 ml PBS

3. 5 ml 99:1 (H2O:TFA)
4. 2 ml 10:89:1
5. 2 ml 20:79:1
6. 2 ml 30:69:1
7. 2 ml 40:59:1
8. 2 ml 50:49:1
9. 2 ml 60:39:1
10. 2 ml 70:29:1
11. 2 ml 80:19:1 as before

A2.3 Procedure

1. Prepare column: 10 ml soln #1
   10 ml soln #2
2. Iodobead in microfuge tube
3. Rinse 1x with 1 ml PBS, discard PBS
4. Add 80 µl PBS
   2 mCi ^{125}I-I
5. Leave for 5 min.
6. Add 10 µl RGD- save tip and tube
7. Leave for 15 min.
8. Use RGD tip to transfer reaction liquid back to RGD tube.
   Save tip.
9. Add 80 µl Na-bisulfite to reaction tube, swirl gently (reduces I+).
   Transfer to RGD tube and discard tip.
10. Add 80 µl chase solution to reaction tube, swirl gently (competes off labeled protein). Transfer to RGD tube and discard tip.
11. Vortex, centrifuge if necessary.
12. Load cartridge.
13. Add 5 ml soln #3
14. Add other solns in order
15. Collect 1 ml fractions

A3: Deprotection protocol

This protocol uses a mixture of trifluoroacetic acid and scavengers to cleave the protecting groups from the side chains of the RGD peptide. Note: the mixture has a strong odour and is highly toxic, therefore it should be prepared and used in the hood.

A3.1 Materials

PEO-RGD, immobilized on coverslips
70% ethanol solution in water

Deprotection solution, Reagent "K" [89]:

8.25 ml trifluoroacetic acid
0.5 ml water
0.5 g phenol
0.5 ml thioanisole
0.25 ml ethanedithiol

A3.2 Method

1. Transfer coverslips to GLASS petri dishes
2. Gently pour in enough 70% ethanol to cover, soak for ~ 5 minutes
3. Remove 70% ethanol, immerse coverslips in Reagent "K", let stand for 60 minutes
4. Remove and dispose of deprotection solution, add 70 % ethanol again, soak for ~ 5 minutes
5. Remove 70% ethanol and rinse THOROUGHLY in water (~ 10 litres)
6. Store under PBS
7. Spray gently with 70% ethanol to sterilize before use

A4: Staining for actin stress fibres

A3.1 Materials

3.7 % paraformaldehyde in water, pH = 7
0.1 % Triton-X™
Methanol

A3.2 Method

1. Seed cells on substrates in the wells of a 6-well plate. Allow to attach for 24 hours
2. Remove media, wash gently with PBS to remove unattached cells
3. Add paraformaldehyde solution to cover coverslips. Leave for 12 minutes
4. Immerse in PBS for 10 minutes, remove and repeat
5. Add Triton-X™ for 3.5 minutes
7. Immerse in PBS for 10 minutes, remove and repeat
8. Evaporate methanol off of rhodamine-phalloidin (Rh-Ph) solution using a gentle stream of air. Dilute to 1:20 ratio, that is, 20 times the initial measured volume.
9. Place a 200 µl droplet of the Rh-Ph stain on a glass microscope slide bordered by coverslips. Invert coverslips with cells on the droplet of the stain. Stain for 60 minutes, keep in the dark
10. Transfer to 6-well plates, sample side up
11. Immerse in PBS for 10 minutes, remove and repeat. Keep in the dark
12. Wash the back of the coverslip with water

APPENDIX B: ESTIMATION OF EFFICIENCY OF CARBOXYLATION

The following procedure was used to obtain an estimate of the fraction of star PEO arms converted from OH-terminated to COOH-terminated (see Appendix A). The technique uses a linear carboxyl-terminated PEO (Sigma) as a standard. The molecular weight was determined to be approximately 3,300 by GPC, with a narrow molecular weight distribution. The polymer was activated with EDC and Sulfo NHS, and reacted overnight with a 10-fold molar excess of ethylene diamine (EDA) over PEO chain ends. Reacting the PEO with an excess of EDA enables us to assume that the bifunctional EDA is not crosslinking the polymer, but that each molecule is coupling with at most one PEO molecule.

The reaction product was purified by dialysis (Pierce dialysis cassettes, MWCO = 2,000), frozen and lyophilized. Solutions of various known concentrations of polymer were prepared in deionized distilled water, the concentration of the primary amine groups present in solution measured using o-phthaldiadehyde (OPA) reagent. The extent of conversion of chain ends from carboxyl-terminated to amine-terminated is unknown, however, from fluorescence measurements of amine measurements, a standard curve was constructed (see below). The curve which showed a linear relationship between the concentration of PEO chain ends, either converted (NH_2-terminated) or unconverted (COOH-terminated), with the measured fluorescence due to the amine terminal groups on the polymer. Note that this fluorescence technique does not measure directly the concentration of carboxylated PEO chain ends, rather, it measures the concentration of chain ends converted to amine. As the fluorescence signal increases linearly with PEO concentration, it is assumed that the concentration of PEO chain ends converted to amine also increases with total PEO concentration in solution; this test was therefore deemed reasonable to estimate number of PEO chain ends converted to amine by coupling with EDA.

To measure the extent of modification (hydroxyl to carboxyl) of star molecules, carboxylated star PEO was similarly activated with EDC and Sulfo NHS, and reacted with ethylene diamine overnight (10 fold molar excess of ethylene diamine over total star PEO chain ends). The star PEO molecules were purified by size exclusion chromatography, frozen and lyophilized. A star PEO solution of a known concentration was prepared, and the fluorescence of the amine terminated ends was measured using the OPA reagent, as before.

To gain an *estimate* of the percentage of carboxyl-converted star PEO chain ends, the assumption was made that the reactivity of carboxylated star PEO chain ends towards ethylene diamine was similar to that of carboxylated linear PEO. Then the fluorescence reading can be related to an amine concentration using the standard curve, and that concentration may be expressed as a fraction of carboxylated PEO chain ends in a solution of known concentration.

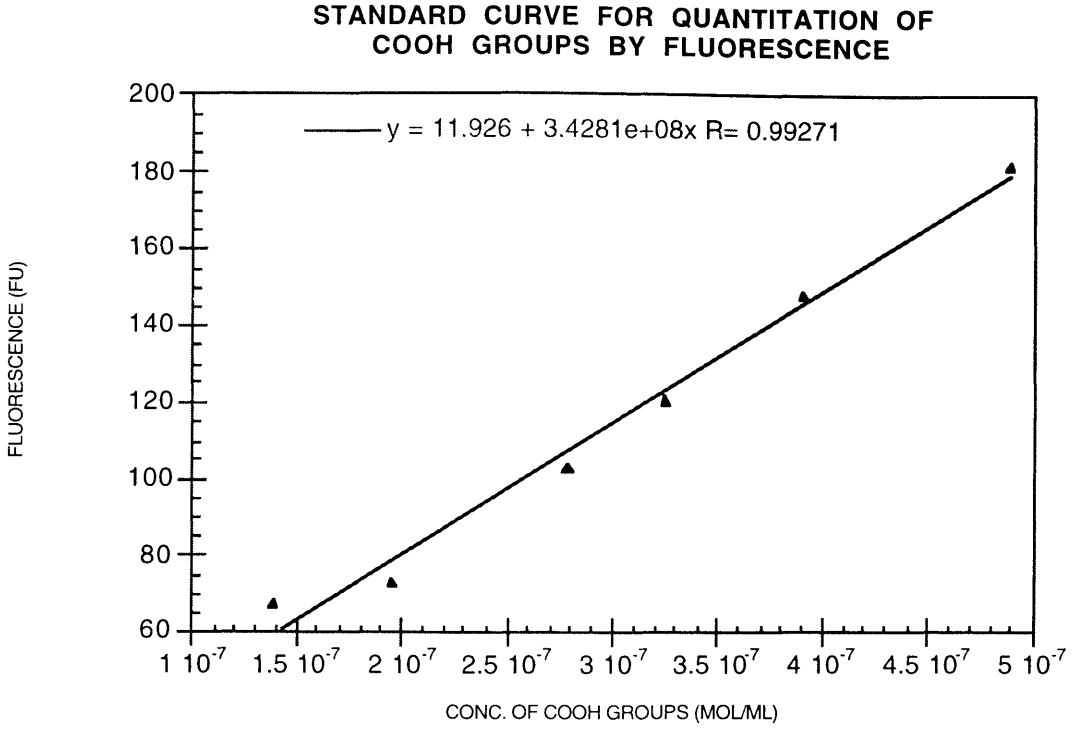

APPENDIX C: CELL CULTURE TECHNIQUES

C1: NR6 fibroblast cell culture

WT NR6 cells were obtained from Gargi Maheshwari. Cells are cultured in MEM-α medium, supplemented with 7.5 % fetal bovine serum, 100 U/ml penicillin, 200 mg/ml streptomycin, 2 mM glutamine, 1 mM sodium pyruvate, 1 mM non-essential amino acids and 350 μg/ml G418. For experiments described in the text as performed in serum-containing medium, the above medium was also used.

For experiments performed under serum-free conditions, the medium used contained MEM-α with 25 mM HEPES buffer, 1 g/l bovine serum albumin, 1 % dialyzed fetal bovine serum, 100 U/ml penicillin, 200 mg/ml streptomycin, 2 mM glutamine, 1 mM sodium pyruvate, 1 mM non-essential amino acids and 350 μg/ml G418. Cells are cultured at 37 °C (90% humidity and 5% CO_2).

C2: Rat lung microvascular and bovine aortic endothelial cell culture

RLMECs and BAEs were obtained from Mark Powers. Both cell lines are cultured in Dulbecco's Modified Eagle's Medium (D-MEM) to which 10% fetal bovine serum, 1% glutamine and 1% penicillin-streptomycin had been added. This medium is also used for experiments performed in serum-containing medium. Cells are cultured at 37 °C, 90% humidity and 5% CO_2.

For experiments in serum-free medium, fetal bovine serum was omitted from the above mixture.

C3: Chinese hamster ovary cell culture

CHO-LA were obtained from Jennifer Fujii. Cells are cultured in D-MEM containing 10% fetal bovine serum, with 2 mM glutamine, 100 U/ml penicillin and 200 mg/ml streptomycin at 37 °C, with 90% humidity and 10% CO_2.

C4: BAF/3 (murine) stem cell culture

BAF/3 cells were provided by Philip Mahdjoob. BAF/3 cells were cultured in RPMI medium, containing 10 % fetal bovine serum, 5 % WEHI, and 1 % penicilin-streptomycin-glutamine. Cells are cultured at 37 °C, 90% humidity and 10% CO_2.